UNIVERSITY OF CALIFORNIA
RIVERSIDE

Instrument Development and Measurements of the Atmospheric Pollutants Sulfur Dioxide, Nitrate Radical, and Nitrous Acid by Cavity Ring-down Spectroscopy and Cavity Enhanced Absorption Spectroscopy

A Dissertation submitted in partial satisfaction
of the requirements for the degree of

Doctor of Philosophy

in

Chemistry

by

David Salvador Medina

June 2011

Dissertation Committee:
Dr. Jingsong Zhang, Chairperson
Dr. Ryan Julian
Dr. Jason Cheng

The Dissertation of David Salvador Medina is approved:

_____

_____

_____

Committee Chairperson

University of California, Riverside

ACKNOWLEDGEMENTS

I would like to thank my Ph. D. advisor Dr. Jingsong Zhang for giving me the opportunity to do research in his laboratory and for his help and support over the years. This would not have been possible without his direction. I would also like to thank my fellow lab members that I have had the pleasure to work with and have assisted me on research projects: Dr. James Hargrove, Yingdi Liu, Dr. Rodrigo Morales-Cueto, Kevin Weber, Jessy Lemieux, Yu Song, and Mary Castro.

I would also like to thank Dr. Don Blake at UC Irvine for inspiring me to enter the field of chemistry. I would like to thank the people at CE-CERT, especially Dr. Cocker for the use of the environmental chamber used in the study of BBCEAS measurements of NO_3. Also, I would like to thank the CNAS machine shop, electronics shop, and glass shop for their assistance in the development of materials that were essential for my research. I would like to thank Dr. Kevin Simpson. It was a pleasure to work with Dr. Simpson over the years working in the general chemistry labs and discussion sections.

I would like to thank my close friends at UCR, Dr. Arun Agarwal and Dr. Andrew Rice for their help and camaraderie. Finally, I would like to thank my family, Anthony, Michael, Lanisa, and most of all my parents for their love and support.

DEDICATION

This dissertation is dedicated to my parents.

ABSTRACT OF THE DISSERTATION

Instrument Development and Measurements of the Atmospheric Pollutants Sulfur Dioxide, Nitrate Radical, and Nitrous Acid by Cavity Ring-down Spectroscopy and Cavity Enhanced Absorption Spectroscopy

by

David Salvador Medina

Doctor of Philosophy, Graduate Program in Chemistry
University of California, Riverside, June 2011
Dr. Jingsong Zhang, Chairperson

Sulfur dioxide (SO_2), nitrate radical (NO_3), and nitrous acid (HONO) play important roles in the atmosphere. SO_2 is associated with the combustion of fossil fuels and contributes to acidification of the ecosystem, particulate sulfate formation and SO_2 is an EPA regulated species. NO_3 is the major oxidation species at night often reacting with biogenic volatile organic hydrocarbons emitted during the nighttime air, which lead to peroxyl radical and nitric acid formation. HONO is a major source of hydroxyl radical (OH) in the early morning. All of these three pollutants exhibit strong absorptions in the UV and visible region and their absorption bands are exploited for measurements using the ultrasensitive absorption spectroscopy techniques, cavity ring-down spectroscopy (CRDS) and broadband cavity enhanced absorption spectroscopy (BBCEAS). SO_2 is

measured by CRDS near 308 nm in the UV region with a limit of detection of 3.5 ppb/10 seconds (S/N = 2) and ambient measurements are attempted. Instruments based on light emitting diode (LED) based BBCEAS are developed for measurements of NO_3 and HONO. NO_3 is monitored using the 662 nm absorption feature with a limit of detection of 10 ppt/2 minutes (1σ) and the technique is demonstrated by sampling from an environmental chamber. HONO is measured in the UV region using the 368 nm absorption with a limit of detection of 10 ppb/2 minutes (1σ).

Table of Contents

LIST OF FIGURES

CHAPTER 5:

CHAPTER 6:

Chapter 1

Introduction

1.1 The Atmosphere, Pollution, and Methods of Detection

Earth is enveloped by a thin layer of gases held in place by Earth's gravitational forces. This thin layer of gases is what we refer to as the atmosphere. The main components of our atmosphere (by volume) include nitrogen (78.1 %) and oxygen (21.0 %) while minor components include argon (0.9 %), water vapor, and carbon dioxide (0.03 %). In addition to these components there are trace atmospheric gases which are emitted into the atmosphere naturally and anthropogenically. It is the anthropogenic species that are of interest due to their contribution to pollution (smog) in the atmosphere. Typically these smog episodes occur under atmospheric conditions known as temperature inversions where a cold air mass is trapped beneath warmer air, thereby trapping the pollutants and posing a health risk to the local region. Some of these pollutants include oxides of carbon, sulfur containing compounds, non-methane hydrocarbons, and nitrogen oxides.

Of the sulfur containing species, sulfur dioxide (SO_2) from the combustion of coal has been a significant component of smog and has been responsible for the deadly smog episodes of the 20^{th} century. SO_2 has also been a major source of acid rain and increased acidity of the ecosystem particularly in the eastern United States. It has been responsible for not only damaging the local landscape but historical buildings and national

monuments until the passing of the Clean Air Act of 1990, which focused on reducing SO_2 emissions. However, the continued trend of burning fossil fuels for the generation of electricity in developing countries is still a source of global SO_2 emissions.

In addition to smog from SO_2, major urban areas have experienced pollution from the formation of tropospheric ozone through photochemical reactions. Non-methane hydrocarbons (NMHC) or volatile organic compounds (VOC) play an important role in the formation of tropospheric ozone because of their formation of peroxyl radicals (RO_2), which convert NO to NO_2:

$$HO_2 + NO \rightarrow OH + NO_2$$

$$RO_2 + NO \rightarrow RO + NO_2$$

NO_2 is then photolyzed by sunlight to yield a single oxygen atom, which recombines with a molecular oxygen to produce ozone (O_3):

$$NO_2 + h\nu \rightarrow NO + O\left(^3P\right)$$

$$O\left(^3P\right) + O_2 \xrightarrow{M} O_3$$

An important oxidant that initiates peroxyl radical formation from NMHC's and drives daytime chemistry in the atmosphere is the hydroxyl radical (OH) and a major source of the OH radical is the photodissociation of nitrous acid (HONO) in the early morning:

$$HONO + h\nu \rightarrow OH + NO$$

Similarly, the major oxidation species of hydrocarbons, typically alkenes, at night is the nitrate radical (NO_3)[1]. NO_3 is formed by the reaction of NO_2 and ozone:

$$NO_2 + O_3 \rightarrow NO_3 + O_2$$

NO_3 can in turn react with NO_2 present at night and undergo formation of dinitrogen pentoxide:

$$NO_3 + NO_2 \xleftrightarrow{M} N_2O_5$$

Measurements of trace gas pollutants in the atmosphere require the use of instrumentation capable of detecting the pollutants at levels as low as parts per trillion (ppt) to several parts per billion (ppb) to elucidate on key mechanisms of the atmospheric processes. Early atmospheric measurement techniques included collection and wet chemical analysis of atmospheric compounds but suffered from interfering species and long sampling times. Advances in instrumentation methods have pushed the limits of detection down to the ppt and ppb level. For instance, trace levels of volatile organic compounds (VOC) are commonly measured using gas chromatography (GC) and gas chromatography/mass spectrometry (GC/MS)[2]. In addition to organics, many important trace gases of atmospheric interest (O_3, NO_2, HONO, SO_2, NO_3) possess strong absorption cross sections in the ultraviolet (UV) and visible region. As a result spectroscopic methods have been developed to measure atmospheric pollutants in real time and continue to be the most commonly used and most reliable techniques for atmospheric measurements. Spectroscopic instruments used in atmospheric

measurements include absorption spectroscopy, fluorescence, chemiluminescence, and infrared spectroscopy[1]. Absorption spectroscopy is an ideal method to employ because of the large absorption cross sections of pollutants in the UV-visible region and the simplicity of the technique. Long path absorption methods such as differential absorption spectroscopy (DOAS) have measured nitrogen dioxide (NO_2), nitrate radical (NO_3), nitrous acid (HONO), and sulfur dioxide (SO_2)[3]. Recently, new absorption spectroscopy methods based on cavity ring-down spectroscopy (CRDS)[4-6] and broadband cavity enhanced absorption (BBCEAS)[7], have been implemented for the measurement of pollutants in the atmosphere. In this thesis I will discuss the development of instrumentation based on cavity ring-down spectroscopy (CRDS) and broadband cavity enhanced absorption spectroscopy (BBCEAS) for measurements of the inorganic pollutants sulfur dioxide (SO_2), nitrate radical (NO_3), and nitrous acid (HONO).

1.2 References

1. Finlayson-Pitts, B. J.; Pitts, J. N., *Chemistry of The Upper and Lower Atmosphere*. Academic Press: 2000.

2. Sipin, M. F.; Guazzotti, S. A.; Prather, K. A., Recent advances and some remaining challenges in analytical chemistry of the atmosphere. *Anal. Chem.* **2003,** *75*, 2929-2940.

3. Sigrist, M. W., *Air monitoring by spectroscopic techniques*. Wiley: New York, 1994.

4. Berden, G.; Engeln, R., *Cavity ring-down spectroscopy: techniques and applications*. Wiley: 2009.

5. Hargrove, J.; Wang, L.; Muyskens, K.; Muyskens, M.; Medina, D.; Zaide, S.; Zhang, J., Cavity ring-down spectroscopy of ambient NO_2 with quantification and elimination of interferences. *Environ. Sci. Technol.* **2006,** *40* (24), 7868-7873.

6. Brown, S. S., Absorption spectroscopy in high-finesse cavities for atmospheric studies *Chem. Rev.* **2003,** *103* (12), 5219-5239.

7. Langridge, J. M.; Ball, S. M.; Shillings, A. J. L.; Jones, R. L., A broadband absorption spectrometer using light emitting diodes for ultrasensitive, in situ trace gas detection. *Rev. Sci. Instrum* **2008,** *79* (12), 14.

Chapter 2

Cavity Ring-down Spectroscopy (CRDS)

2.1 Abstract

Cavity ring-down spectroscopy (CRDS) is an ultrasensitive absorption spectroscopy technique. The advantage of the technique is a long effective absorption pathlength in a compact setup due to a multipass cell composed of two highly reflective mirrors. Measurements are based on the rate of decay of light within the cavity. Analytical applications of CRDS range from measurements of atmospheric pollutants, kinetic studies, and biological applications. In this chapter, a detailed description of the technique is provided. For this thesis, CRDS is used for laboratory measurements of sulfur dioxide (SO_2).

2.2 Introduction

Absorption spectroscopy is the study of the absorption of electromagnetic radiation at a certain frequency by matter (molecules). As radiation passes through the molecules they are promoted to an excited state. The amount of radiation that is absorbed is proportional to the amount of absorbing molecules present in the medium. Absorption is dependent on the thickness or length of the absorbing medium and the number density of the molecules present in the medium. Traditional or conventional absorption spectroscopy follows the Beer-Lambert law:

$$I = I_0 \exp(-\sigma N l) \qquad \textbf{[2.1]}$$

where, I_0, is the incident light through an absorbing medium and decreases exponentially as it travels through the absorber occupying a column having a distance, l, with the absorber having a cross section, σ, and a number density, N, resulting in transmitted light, I, that is lower in intensity than the incident light. In terms of absorbance, this concept can be expressed as:

$$Abs = -\ln\left(\frac{I}{I_0}\right) = \varepsilon c l = \sigma l N = \alpha l \qquad \textbf{[2.2]}$$

where ε, is the molar exctinction coefficient, *c*, is the concentration, *l*, is the pathlength, σ, is the cross section, *N*, is the number density, and α, is the absorption coefficient. If the path length and the absorbance cross section of the absorbing medium are known and the absorbance is measured, the concentration can be extracted. The limitation to conventional absorption spectroscopy comes when trying to detect either low concentrations of absorber or an absorber with a small absorbing cross section. The path lengths are typically small and when the incident light travels through the absorbing medium the absorption of light is undetectable compared to the fluctuations of the initial incident light, which results in lower sensitivity. One method of increasing the sensitivity of absorption spectroscopy is to use long path absorption techniques such as differential optical absorption spectroscopy (DOAS)[1], however the fluctuating light intensity and background remain a problem. This is why fluorescence techniques are preferred when measuring trace species since it is typically considered to be background free compared to traditional absorption spectroscopy. However, fluorescence is not absolute and requires calibration.

Cavity ring-down spectroscopy (CRDS) is a unique and sensitive absorption technique developed by O'Keefe and Deacon[2] in 1988 which demonstrated that forbidden transition of the oxygen molecule could be observed. The technique was derived from methods originally intended for the characterization of highly reflective mirrors.[3] CRDS is based on measurements of the rate of light absorption through a sample rather than the magnitude, which minimizes the effects of light source fluctuation. In a typical CRDS set up using a pulsed laser, light is injected into an optical cavity

composed of two highly reflective mirrors (R > 99.9 %) and is reflected between the mirrors making multiple round trips. A small percentage of the light exits the cavity after each round trip, and the signal exiting from the pulse of light is in the form of a first-order exponential decay. The time required for the light in the cavity to decay to 1/e of the initial output is the ring-down time (τ) and $1/\tau_0$ is the decay rate:

$$\frac{1}{\tau_0} = \frac{c}{L}\left[(1-R)\right] \qquad \textbf{[2.3]}$$

where, c, is the speed of light, L, is the distance separating the high reflective mirrors, and, R, is the mirror reflectivity. The principle of CRDS is shown in Figure 2.1. In the presence of an absorber, the additional loss causes a faster rate of decay, $1/\tau$, given by the equation:

$$\frac{1}{\tau} = \frac{c}{L}\left[(1-R)+\alpha l_s\right] \qquad \textbf{[2.4]}$$

where, α, is the absorption coefficient of the absorber present within the cell and, l_s, is the sample path length, which must be taken into account if the length is different from L, typically when a buffer gas is used to protect the mirrors from degradation. Using equations **2.3** and **2.4** to solve for the absorption coefficient, α, yields the new equation:

$$\alpha = \frac{L}{l_s c}\left(\frac{1}{\tau} - \frac{1}{\tau_o}\right) = \sigma n \qquad \textbf{[2.5]}$$

where, $1/\tau_o$ is the decay rate without sample present in the cavity, $1/\tau$, the decay rate with sample present, c, the speed of light, L, the length of the cavity, l_s, the sample path length,

σ, the cross section of the absorber, and n, the number density of the absorbing sample. Thus, if the cross section of the absorbing medium is known, concentration information can be extracted from the absorption coefficient. Its multipass nature provides a long effective absorption path length (~km) in a compact setup (~m). For a cell having a length of 110 cm and a typical mirror reflectivity of R = 99.98 % the expected ring-down time is ~20μs corresponding to 2500 round trips within the cell or ~5 km effective pathlength. A typical ring-down signal is shown in Figure 2.2. Spectra of molecules can be obtained by scanning the frequency of the laser. It is important to consider that all absorbers in the region of the spectrum being probed will contribute to the decrease of the ring down time. CRDS can be applied for wavelengths from the deep ultraviolet to the mid infrared regions.

In addition to mirror transmission and absorption of light through a medium, the ring down time is influenced by Rayleigh scattering of light by molecules in the air. In terms of the losses from Rayleigh scattering in the air the cross section for Rayleigh scattering can be calculated using[4]:

$$\sigma_{Rayleigh}(\lambda) = \frac{8\pi^3}{3}\left[\frac{\left(n^2-1\right)^2}{N^2\lambda^4}\right] \qquad \textbf{[2.6]}$$

where n is the refractive index of air, N, the number density of air molecules, and λ, the wavelength of light. Shorter wavelengths of light will be influenced more by scattering than longer wavelengths and the effect of scattering on the ring-down time is that using shorter wavelengths as the probe light means that the ring down time that can be achieved is significantly smaller than ring-down times from longer wavelengths assuming similar mirror reflectivities.[5] However, the main limitation to achieving long ring-down times in the UV region is the mirror reflectivity. Mirror reflectivity in the UV region is typically lower (R ~ 0.999) than in the visible. Thus, probing species in the ultraviolet region becomes significantly more difficult to measure due to the decreased workable ring down signal.

Measurements are typically made using a pulsed laser (10 Hz to 1 KHz) injecting light into the cavity and then the light exits the second mirror and is detected using a PMT, and the signal is then digitized from an oscilloscope and the exponential decay is curve fitted to a first order exponential. The fitted ring-down curves are then averaged and the 1/e value is extracted to provide the ring-down time. The two important factors that provide the best sensitivity for CRDS are the mirrors and the digitization of the ring-down curve. Having higher reflective mirrors typically provides a longer ring-down signal. Using a high resolution digital oscilloscope or digitizer on the ring down curve will result in having more points to be digitized, thus providing a better fit of the ring down curve and reducing the residual noise from the curve fit. Although CRDS is insensitive to shot to shot fluctuations from the pulsing light source there is a compromise from having mirrors that have a reflectivity that is too high which does not allow enough

light from coupling into the ring down cell. This results in having a low intensity ring-down decay that will be difficult to curve fit with the digitization software. Conversely, low quality mirrors would provide an intense ring down signal but a short decay or ring down time.

2.3 High Reflective Mirrors

The sensitivity is largely based on the reflectivity of the mirrors. The higher the reflectivity of the mirrors means that there will be more passes or reflections within the cavity, thus increasing the effective path length. In addition, as mentioned above, higher reflective mirrors provide longer ring down times. The mirrors employed in cavity ring down are made of multiple layers of metal oxide coating on a highly polished substrate, which allows for a negligible loss of light through the mirrors[3]. The mirrors have a radius of curvature that is typically the same as the length of the CRDS cell allowing for a stable cavity. Because of the high reflectivity of the mirrors, most of the light is lost when the light from the pulsed laser is injected into the cavity. Only a small percentage of the light is transmitted to within the cell. As the light exits the second mirror and into the detector, most of the light will be reflected back into the cavity. The majority of the light will continue to resonate back and forth only if the laser beam is aligned normal to the incident light entering the cell and if the cell forms a stable cavity. The wavelength region that the mirrors can function depends on the type of coating along the substrate. Thus, losses from the spectrometer occur from absorbance and scattering. The mirrors

typically have a range with high reflectivity of a few tens of nanometers with the mirror reflectivity tapering off significantly. Thus, when performing a frequency scan of an absorbing molecule, the mirror reflectivity curve must be taken into account to correct for the ring-down time change due to mirror reflectivity.

2.4 Cavity Modes

The optical cavity composed of the two mirrors has mode effects similar to that observed inside a cavity of a laser. One requirement of CRDS is that the bandwidth of the light coupled into the cavity overlaps with multiple cavity modes. The cavity modes are separated by:

$$\Delta\nu = \frac{1}{\tau} = \frac{c}{(2l \cdot n\cos\theta)} \qquad \textbf{[2.7]}$$

$\Delta\nu$ is defined as the free spectral range (FSR), in units of Hz, τ , is the cavity round trip time. The angle, θ, is defined as the angle at which the light is injected, which is 0 and n is the refractive medium of the substrate of the mirrors. The equation can be simplified to:

$$\Delta\nu = \frac{1}{\tau} = \frac{c}{2l} \qquad \textbf{[2.8]}$$

These evenly spaced cavity modes are shown in Figure 2.3. If the laser line width is sharper or close to the FSR, no ring-down will be observed. The cavity modes are

activated when the incident laser having a TEM_{00} mode is on the same longitudinal axis as the cavity modes. When there is overlap of the modes this allows for a ring down. The pulse of the laser must also be taken into consideration. The pulse of light is usually shorter than the cavity round trip time. Misalignment or having an "unstable" cavity does not allow for activation of the modes within the optical cavity. In certain instances, having a mis-aligned cavity will activate transverse cavity modes, which results in having a multi exponential decay. Additionally, it is important to have a laser linewidth that is narrower than the absorption[6]. In instances where the laser linewidth is broader than the absorption features, the result can be a multi exponential curve. Although several methods have been formulated to account for these descrepencies in the ring down multi exponential curve fitting, in most instances the first order decay assumption is used to maintain the simplicity of the CRDS technique.

2.5 Analytical Chemistry Applications of CRDS

Applications of CRDS include molecular spectroscopy, kinetics, and atmospheric and environmental monitoring in addition to many recent applications of the technique including liquid and solid studies. The technique has seen great potential as an analytical tool in the field of environmental monitoring because of its simplicity, fast response time, and sensitivity during field campaigns. Environmental applications include the direct measurement of NO_2[7-9]and NO_3[10] in the atmosphere with great sensitivity (ppb level). In addition to the direct measurement of these species, thermal dissociation and chemical

conversion (chemical amplification) allow for the indirect measurement of alkyl nitrates/peroxy acyl nitrates and peroxyl radicals through the measurement as NO_2.[11, 12] Measurements of nitrous acid (HONO) in the lab have also been demonstrated using CRDS[13]. CRDS has also been useful to study cold PAH cations, which are important components found in interstellar dust[14, 15].

Although CRDS is primarily a gas phase detection technique, it has been extended to liquids, solids and surface adsorbed species. One such method is evanescent wave CRDS, which uses the exponentially decaying evanescent wave from light undergoing total internal reflection through a prism or waveguide to probe surface adsorbed species[16]. CRDS has been used to probe the SPR of the adsorption of nitro containing compounds on gold nanoparticle films acting as potential detectors for explosives.[17, 18] The measurement of thin films or substrates aligned using a Brewster's angle configuration has also been used, known as Brewster's angle CRDS (BA-CRDS). BA-CRDS has been used for the measurement of thin borosilicate subtrates coated with oxazine dyes aligned at Brewster's angle.[19] Kinetic studies of the nitrate radical with terpenes in solution have also been used with a modified cuvette set at Brewster's angle.[20] CRDS has shown the potential to extend to solid film studies or surface studies to measure absorbances that would normally be difficult to measure using conventional absorption spectroscopy. High performance liquid chrmomatography (HPLC) has also benefitied from the sensitivity provided by replacing traditional absorption methods as the detector and using CRDS by coupling a liquid flow cell between the two HR mirrors at Brewster's angle improving detection sensitivities by 50 fold.[21]

There is also pontential for CRDS to extend to biological applications. The detection of breast cancer cells at the single-cell level have also been demonstrated using an optical fiber coupled between the cavity is coated with the biological species, where the losses from scattering of the evanescent field are measured.[22] CRDS has also been used as a breath biomarker analysis tool.[23] One target molecule is acetone as a biomarker for blood glucose levels in diabetic patients.[24] CRDS in the UV region (266 nm) is capable of monitoring acetone on diabetic patients with little interference of water which correlates to their blood glucose levels. Additionally, gases such as ammonia, which is associated with asthma, and carbon dioxide, associated with oxidative stress, have also been measured in breath samples using CRDS in the near IR region.[23]

2.6 Conclusion

Cavity ring-down spectroscopy is an ultrasensitive absorption technique that provides a long effective pathlength (~km) in a compact setup. The advantages of the technique include, it is a direct absorption method and does not need to be calibrated, and is free of intensity fluctuations. The technique is also non invasive and non destructive. Because of the technique's ability for sensitive measurements, it has been extensively applied in ultratrace detection of species in the atmosphere. Although the technique has been demonstrated on important atmospheric pollutants such as NO_2 and NO_3, it has not been used to measure sulfur dioxide (SO_2) in the atmosphere. SO_2 is a component of smog in regions where large amounts of fossil fuels undergo combustion. Once in the

atmosphere they can be oxidized to sulfate particles, and can increase acidification of the environment upon deposition. New methods of measuring ambient SO_2 to compete with traditional methods, namely the pulsed fluorescent analyzer (PFA), are desired. In the next chapter, the CRDS technique is extended to SO_2 laboratory measurements and ambient measurements are attempted.

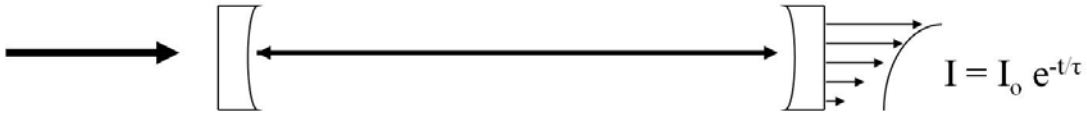

Figure 2.1: Principle of the CRDS technique. Light is injected into the cell composed of two high reflective mirrors. Light resonates between the two mirrors and as light exits the cell, the signal is in the form of a first order exponential decay.

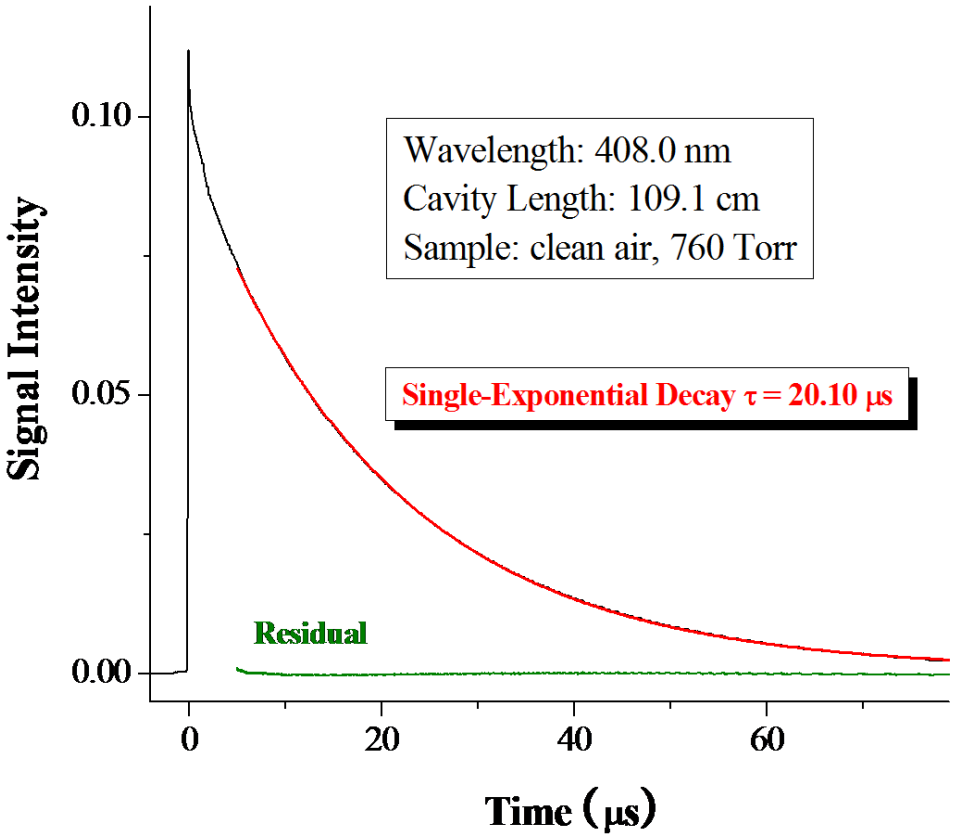

Figure 2.2: Sample of a typical cavity ring-down signal. A mirror reflectivity of 99.98 % with a length of 110 cm will have a ringdown time of ~20 μs.

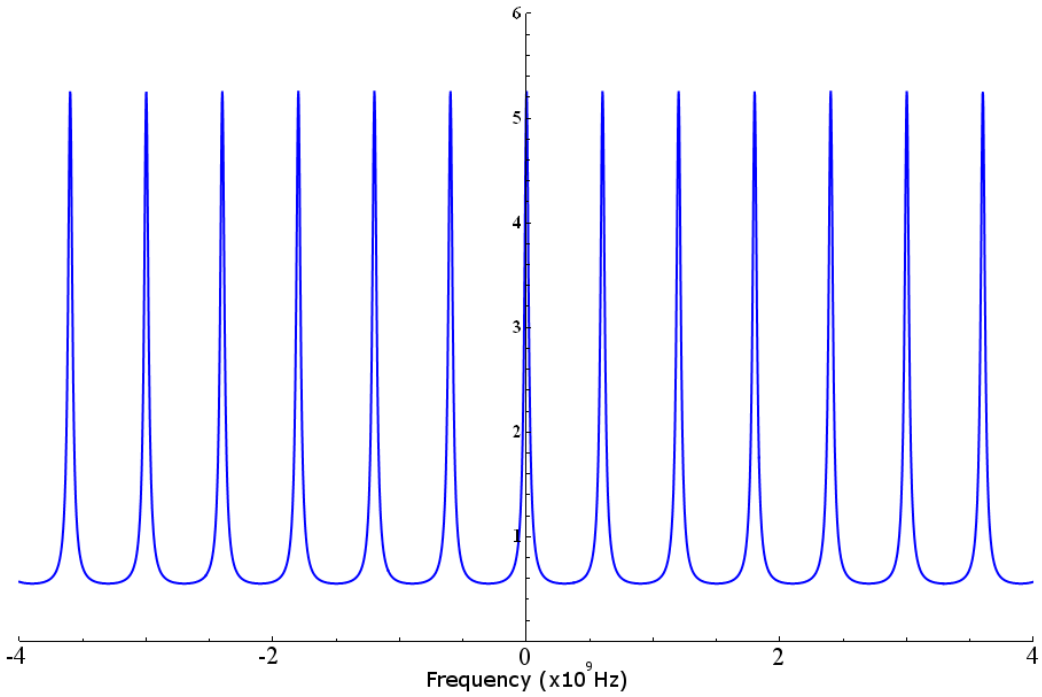

Figure 2.3: Cavity modes for a cavity having a length of 0.25 meters and a reflectivity of R = 0.9.

2.7 References

1. Sigrist, M., W., *Chemical Analysis*. 1994; Vol. 127.

2. Okeefe, A.; Deacon, D. A. G., Cavity ring-down optical spectrometer for absorption measurements using pulsed laser sources. *Rev. Sci. Instrum.* **1988,** *59* (12), 2544-2551.

3. Scherer, J. J.; Paul, J. B.; Okeefe, A.; Saykally, R. J., Cavity ringdown laser absorption spectroscopy: History, development, and application to pulsed molecular beams. *Chem. Rev.* **1997,** *97* (1), 25-51.

4. Sappey, A. D., Hill, E. S., Fixed-frequency cavity ringdown diagnostic for atmospheric particulate matter. *Optics Letters* **1998,** *23* (12), 954-956.

5. Kleine, D.; Murtz, M.; Lauterbach, J.; Dahnke, H.; Urban, W. G.; Hering, P.; Kleinermanns, K., Atmospheric trace gas analysis with cavity ring-down spectroscopy. *Isr. J. Chem.* **2001,** *41* (2), 111-116.

6. Zare, R. N., Yalin, A. P., Effect of Laser Lineshape on the Quantitative Analysis of Cavity Ring-Down Signals. *Laser Physics* **2002,** *12* (8), 1065-1072.

7. Hargrove, J.; Wang, L. M.; Muyskens, K.; Muyskens, M.; Medina, D.; Zaide, S.; Zhang, J. S., Cavity ring-down spectroscopy of ambient NO2 with quantification and elimination of interferences. *Environ. Sci. Technol.* **2006,** *40* (24), 7868-7873.

8. Wada, R.; Orr-Ewing, A. J., Continuous wave cavity ring-down spectroscopy measurement of NO2 mixing ratios in ambient air. *Analyst* **2005,** *130* (12), 1595-1600.

9. Osthoff, H. D.; Brown, S. S.; Ryerson, T. B.; Fortin, T. J.; Lerner, B. M.; Williams, E. J.; Pettersson, A.; Baynard, T.; Dube, W. P.; Ciciora, S. J.; Ravishankara, A. R., Measurement of atmospheric NO2 by pulsed cavity ring-down spectroscopy. *J. Geophys. Res.-Atmos.* **2006,** *111* (D12), 10.

10. Brown, S. S.; Stark, H.; Ravishankara, A. R., Cavity ring-down spectroscopy for atmospheric trace gas detection: application to the nitrate radical (NO3). *Appl. Phys. B-Lasers Opt.* **2002,** *75* (2-3), 173-182.

11. Hargrove, J.; Zhang, J. S., Measurements of NOx, acyl peroxynitrates, and NOy with automatic interference corrections using a NO2 analyzer and gas phase titration. *Rev. Sci. Instrum.* **2008,** *79* (4), 3.

12. Liu, Y. D.; Morales-Cueto, R.; Hargrove, J.; Medina, D.; Zhang, J. S., Measurements of Peroxy Radicals Using Chemical Amplification-Cavity Ringdown Spectroscopy. *Environ. Sci. Technol.* **2009,** *43* (20), 7791-7796.

13. Wang, L. M.; Zhang, J. S., Detection of nitrous acid by cavity ring down spectroscopy. *Environ. Sci. Technol.* **2000,** *34* (19), 4221-4227.

14. Romanini, D.; Biennier, L.; Salama, F.; Kachanov, A.; Allamandola, L. J.; Stoeckel, F., Jet-discharge cavity ring-down spectroscopy of ionized polycyclic aromatic hydrocarbons: progress in testing the PAH hypothesis for the diffuse interstellar band problem. *Chem. Phys. Lett.* **1999,** *303*, 165-170.

15. Biennier, L.; Salama, F.; Gupta, M.; O'Keefe, A., Multiplex integrated cavity output spectroscopy of cold PAH cations. *Chem. Phys. Lett.* **2004,** *387* (4-6), 287-294.

16. van der Sneppen, L.; Ariese, F.; Gooijer, C., Liquid-phase and evanescent-wave cavity ring-down spectroscopy in analytical chemistry. *Annual Review of Analytical Chemistry* **2009,** *2*, 13-35.

17. Pipino, A. C. R.; Woodward, J. T.; Meuse, C. W.; Silin, V., Surface-plasmon-resonance-enhanced cavity ring-down detection. *J. Chem. Phys.* **2004,** *120* (3), 1585-1593.

18. Pipino, A. C. R.; Silin, V., Gold nanoparticle response to nitro-compounds probed by cavity ring-down spectroscopy. *Chem. Phys. Lett.* **2005,** *404* (4-6), 361-364.

19. Muir, R. N.; Alexander, A. J., Structure of monolayer dye films studied by Brewster angle cavity ringdown spectroscopy. *Phys. Chem. Chem. Phys.* **2003,** *5* (6), 1279-1283.

20. Alexander, A. J., Reaction kinetics of nitrate radicals with terpenes in solution studied by cavity ring-down spectroscopy. *Chem. Phys. Lett.* **2004,** *393* (1-3), 138-142.

21. Bechtel, K. L.; Zare, R. N.; Kachanov, A. A.; Sanders, S. S.; Paldus, B. A., Moving beyond traditional UV-visible absorption detection: Cavity ring-down spectroscopy for HPLC. *Anal. Chem.* **2005,** *77* (4), 1177-1182.

22. Tarsa, P. B.; Wist, A. D.; Rabinowitz, P.; Lehmann, K. K., Single-cell detection by cavity ring-down spectroscopy. *Appl. Phys. Lett.* **2004,** *85* (19), 4523-4525.

23. Wang, C. J.; Sahay, P., Breath Analysis Using Laser Spectroscopic Techniques: Breath Biomarkers, Spectral Fingerprints, and Detection Limits. *Sensors* **2009,** *9* (10), 8230-8262.

24. Wang, C.; Surampudi, A. B., An acetone breath analyzer using cavity ringdown spectroscopy: an initial test with human subjects under various situations. *Meas. Sci. Technol.* **2008,** *19* (10), 10.

Chapter 3

Detection of Sulfur Dioxide by Cavity Ring-Down Spectroscopy

3.1 Abstract

Sulfur dioxide (SO_2) is a major air pollutant that can contribute to the production of particulate sulfate and increase the acidity in the environment. SO_2 is detected by cavity ring-down spectroscopy (CRDS) utilizing the SO_2 absorption in the 308 nm region. A ferrous sulfate scrubber and sodium carbonate annular denuder are used to reduce background interferences and to obtain quantitative values of SO_2. The method is characterized using SO_2 standards in the laboratory and compared to a commercial pulsed fluorescence analyzer (PFA). A limit of detection of 3.5 ppb/10 seconds (S/N=2) is demonstrated. Ambient measurements are attempted to demonstrate this technique.

3.2 Introduction

Sulfur dioxide (SO_2) is a major atmospheric pollutant. It is emitted into the atmosphere anthropogenically from combustion of fossil fuels, oil refineries, and power plants[1]. SO_2 is also released naturally from volcano emissions and oxidation of dimethylsulfide released from oceans[1]. Once in the atmosphere SO_2 is oxidized in the gas phase and on clouds to form H_2SO_4 and leads to the production of aerosol sulfate, which can contribute to a climate's net cooling effect. Deposition of sulfate also contributes to acidification of the surrounding ecosystem. Typical concentrations of SO_2 in the atmosphere range from tens to hundreds of ppt in remote locations to tens of ppb in cities and up to hundreds of ppb in the most polluted environments[1]. SO_2 emissions are regulated by the US Environmental Protection Agency (EPA) in order to maintain air quality standards; it is one of the criteria pollutants that the EPA uses to determine air quality, where the others include NO_2, ozone, CO_2, particulate matter, and lead. Consequently, analytical instruments that allow for fast, sensitive and accurate measurements of SO_2 are important for a better understanding of the sulfur budget in the atmosphere.

Many techniques have been developed to measure SO_2 in the atmosphere. The most commonly used one is pulsed fluorescence analyzer (PFA), which is based on exciting SO_2 by UV radiation in the 190-230 nm range and measuring the fluorescence of SO_2 between 240 and 420 nm (peaking at 320 nm). Commercial PFA's can reach sensitivities of 0.3-2.0 ppb/10 seconds and are used by monitoring agencies to report SO_2 concentrations. However, the PFA's are sensitive to potential interferences such as NO

and aromatic hydrocarbon compounds which can cause positive bias, while the fluorescence of the excited SO_2 could be quenched by oxygen and water causing negative bias. Several chemiluminescence techniques have also been used for the detection of SO_2[2-6] with detection limits as low as 30 ppt[6] but these techniques require chemical conversion, need to be calibrated and are often accompanied by interfering species. Absorption techniques used to measure SO_2 include long path and multi-axis differential optical absorption spectroscopy (DOAS)[7-9] and tunable diode laser absorption spectroscopy (TDLAS)[7, 10]. DOAS is based on UV absorption of SO_2 in the 300 nm region with sensitivities in the tens of ppt range and has been used to measure emission plumes from power plants[8] and volcanoes[9]. The disadvantage of these long path absorption techniques is that the measurements are taken as an average concentration through the entire path, and these instruments can be complex and cumbersome. TDLAS detection of SO_2 is based on the infrared absorption at 1360.7 cm^{-1} and has sensitivities of 500 ppt[1, 7]. Recently a tunable diode laser in the UV region has been applied for detection of SO_2 in the range of 20 ppm but lacks the sensitivity for ambient measurements[10]. Wet chemistry techniques such as denuders and/or passive samplers coated with sodium carbonate have also been used to measure SO_2 in the ppb range[11-13] by detection as sulfate using ion chromatography. The wet chemistry methods require long sampling times, and the measurements are an average in the total sampling time and are not suitable for real time monitoring.

Cavity ring-down spectroscopy (CRDS) is a sensitive absorption technique that is based on measurements of the rate of light absorption through a sample rather than the

magnitude[14, 15]. Its multipass nature provides a long effective absorption path length (~km) in a compact setup (~m). Light is injected into an optical cavity composed of two highly reflective mirrors (R>99.9 %) and is reflected between the mirrors making multiple round trips. A small percentage of the light exits the cavity after each round trip, and the signal exiting from one pulse of light is in the form of a first-order exponential decay. In the presence of an absorber, the additional loss causes a faster decay and the absorption coefficient, α, can be calculated from equation 3.1 below:

$$\alpha = \frac{L}{l_s c}\left(\frac{1}{\tau} - \frac{1}{\tau_o}\right) = \sigma n \qquad \textbf{[3.1]}$$

$1/\tau_o$ is the cavity ring-down decay rate without sample present in the cavity, $1/\tau$, the decay rate with sample present, c, the speed of light, L, the length of the cavity, l_s, the sample path length, σ, the cross section of the absorber, and n, the number density of the absorbing sample. Given accurate absorption cross sections, CRDS can provide fast, sensitive, and reliable measurements of trace gas species with little or no need of calibration.

CRDS has been demonstrated as a powerful technique for measuring atmospheric pollutants that absorb in the UV and visible regions. For examples, it has been used to monitor ambient NO_2[16-18] and NO_3[19, 20] with excellent sensitivities. A near-UV CRDS absorption spectrum of 7 ppm SO_2 in laboratory clean air was reported briefly before[21], although the detection sensitivity of SO_2 was not characterized and ambient

measurements were not attempted. In this study, CRDS is utilized for detection of SO_2 at concentrations of ppb to hundreds of ppb (in the range of urban pollution levels). The detection sensitivity is characterized, and potential background interferences in the ambient measurements of SO_2 and their removal are investigated. Ambient measurements of SO_2 are then carried out. The development of the CRDS technique to monitor SO_2 emissions could benefit areas where SO_2 is a major source of air pollution.

3.3 Experimental

The CRDS set-up used in this study has been described in detail before[17, 22] and is shown in Figure 3.1. The 532-nm output from a Nd:YAG laser (Continuum Surelite II) pumped a dye laser (Lambda Physik Scanmate II) to produce radiation near 616 nm, which was then doubled to ~308 nm (10 Hz repetition rate, 0.5-1 mJ/pulse, linewidth 0.2-0.3 cm^{-1}). The 308-nm laser radiation entered the cavity ring-down chamber and the output light was detected by a photomultiplier tube. The cavity mirrors were separated by 1.0 m and had a reflectivity of 99.9% at 308 nm (Los Gatos, diameter = 2.54 cm, radius of curvature (ROC) = 1.0 m). The ring-down signal was collected on a 14-bit 200 MS/s oscilloscope card; each ring-down curve was fitted with a fast algorithm in combination with the data collection software on National Instruments Labview. Figure 3.2 shows a typical ring-down curve for a cavity filled with zero air and the exponential fit. The typical ring-down time was ~3 μs was obtained at 308 nm with a cell filled with zero air. Although SO_2 has stronger absorption bands in the deep UV region than in the near-UV region (*1*), the currently available mirror reflectivity in the 308 nm region is

higher, and therefore the absorption of SO_2 near 308 nm is used for detection of SO_2. For the ambient measurements, a buffer gas was used in front of the mirrors to protect the mirror surfaces. The air sample length l_s was taken into account in the calculations.

The SO_2 standards of concentrations down to 10 ppb were obtained by dynamic dilution of SO_2 from a gas cylinder (Matheson, 10 ppm in zero air) with zero air and flowed at a total flow rate of ~1 L/min through a Teflon tubing to the inlet of the CRDS cell. As the SO_2 sample exited the cell it was subsequently introduced into a commercial SO_2 PFA (Thermo Electron Corporation, Model 43) where the SO_2 sample was measured again for intercomparison. The pressure in the CRDS cell was monitored using a pressure gauge (Cole-Parmer) and was in the range of 755 to 760 Torr.

3.4 Scrubber and Annular Denuder

In the 308 nm region, other species such as HONO, NO_2, and O_3 have absorption cross sections comparable to SO_2 and could potentially interfere in the ambient measurements of SO_2 (discussed below). A ferrous sulfate scrubber was used to selectively remove these interfering species. The scrubber was made out of a glass tube (1/2" o.d., 3/8" i.d., 8" in length; connected to the 1/4" tubing with reducing unions) packed with ferrous sulfate. The use of ferrous sulfate to selectively remove NO_2 and O_3 has been utilized with chemiluminescence analysis of SO_2[3, 23]. In this study, it was also shown that the ferrous sulfate scrubber could remove NO_2 efficiently and selectively without impeding the air flow and SO_2 level.

In order to quantify SO_2 in the ambient measurements, zero level of SO_2 should be obtained throughout the course of the CRDS measurements. One way to obtain the zero level is to replace the ambient sample with zero air. Another approach is to remove SO_2 in the ambient sample stream using a denuder, which also has the advantage of revealing any remaining background. A denuder has been coupled with CRDS for NO_2 detection before[17]. In this work, the annular denuder for SO_2 removal was composed of a 8" long, 1/8" diameter pyrex glass rod centered in a 3/8" o.d., ¼" i.d. glass tubing. For effective removal of SO_2, the inner walls of the denuder were coated with a saturated solution of sodium carbonate (Na_2CO_3) or 2% (w/w) Na_2CO_3/ 1% (w/w) glycerol in methanol solution[12]. The addition of glycerol as a binding agent to the Na_2CO_3 denuder material ensured high denuder efficiency and improved the loading capacity of SO_2 to Na_2CO_3[12, 24], although for our purpose the saturated solution of Na_2CO_3 was sufficient enough to remove SO_2 from the air sample. When the denuder was installed in line in the sample stream, SO_2 in the sample was removed by adsorption onto the denuding material, and the CRDS signal dropped to a baseline level (zero concentration). The denuder was then removed from the sample line for the SO_2 measurements; the net CRDS signal above the baseline level was due to the SO_2 absorption and allowed for real time, quantitative measurements of SO_2.

For the ambient measurements, the ferrous sulfate scrubber was installed all the time to remove background NO_2 and ozone, while the sodium carbonate denuder was used periodically to obtain the zero level for quantification of SO_2 in the air sample. It was necessary to place the ferrous sulfate scrubber in front of the sodium carbonate

denuder in the CRDS measurements, as the denuder could partially remove NO_2 and ozone and cause positive bias in the SO_2 level if used alone. To prevent the scrubber and denuder materials from entering the ring-down cell, a 0.45-μm Teflon filter (Savillex) was installed in front of the cell. No effect on the pressure was observed when the filter was placed in line with the denuder, and the Teflon filter passed SO_2 in the air sample through with no observable loss.

3.5 Results and Discussion

Figure 3.3 shows the CRDS absorption spectrum of SO_2 at a concentration of 500 ppb in zero air (1 atm. pressure). The reference absorption spectrum of neat SO_2 at a pressure of 6.9 Torr taken by Rufus et. al.[25] is also plotted for comparison. The CRDS absorption spectrum was taken at a resolution of ~0.3 cm^{-1}, which is a lower resolution than that in the Rufus spectrum (0.04 cm^{-1}). Our CRDS spectrum is comparable to a previous CRDS absorption spectrum of 7 ppm SO_2 in 1 atm. pressure air taken in the region of 308.6-317.5 nm with a 2 cm^{-1} resolution[21]. The main features in the high resolution spectrum of SO_2 by Rufus et. al. are well reproduced by the CRDS spectra. In the current work, the CRDS measurements of SO_2 were carried out at 308.712 nm near an absorption peak, with the absorption cross sections of 5.90×10^{-19} cm^2/molecule[25].

An intercomparison was performed between CRDS and the commercial PFA, using the diluted laboratory standard mixtures of SO_2 in zero air in the range of 10 to 300 ppb. Figure 3.4 demonstrates a good linearity between the two techniques from 10 to 300 ppb, with the PFA reading slightly higher than CRDS (with a slope of CRDS vs. PFA of

0.95 ± 0.03). The small difference between the PFA and CRDS readings is possibly due to the calibration of PFA, which is needed frequently, while the CRDS measurements rely on using literature cross sections of SO_2. The detection sensitivity of SO_2 by CRDS is demonstrated in the step dilution in Figure 3.5. As calculated as 2σ of the baseline noise, a detection sensitivity of 3.5 ppb with 10 seconds of averaging was obtained, while a sensitivity of 7 ppb (2σ)/10 sec can be more routinely achieved. The current detection sensitivity is largely limited by the mirror reflectivity in the current setup. As demonstrated in our previous study of NO_2[17], a mirror reflectivity of 99.985 % gave a typical ring-down time of ~25 μs and sensitivity of 150 ppt/10 seconds for NO_2. A higher reflectivity would increase the effective path length and ring-down time of the CRDS spectrometer by increasing the number of reflections of light within the cavity. These increases would enhance the signal to noise (S/N) ratio of the ring-down curve and reduce the minimum detectable absorption coefficient. It is expected that the detection sensitivity of SO_2 could be improved with the availability of higher reflectivity mirrors in the 308 nm region than those used in this experiment. Nevertheless, CRDS is shown here to be comparable to PFA in monitoring the standard mixtures of SO_2 and responds linearly to the concentrations of SO_2 in the range of 10-300 ppb.

3.6 Scrubber and Denuder in the Ambient Measurements

In the 308 nm region, there are other absorbers, such as formaldehyde, nitrous acid, nitrogen dioxide, ozone, and polycyclic aromatic hydrocarbons (PAHs), which could interfere in the ambient measurements of SO_2. The absorption cross sections of

SO_2 at 308.7 nm are ~6×10^{-19} cm^2/molecule, while the ambient concentrations range from hundreds of ppt in remote locations to tens of ppb in cities and up to hundreds of ppb in the most polluted area[1]. Formaldehyde has cross sections of ~2.2×10^{-20} cm^2/molecule near 308.7 nm (away from its absorption peaks), more than one order of magnitude smaller than those of SO_2 in addition to lower concentrations in the atmosphere (about 0.1 – 20 ppb)[1]. Since the absorbance is proportional to the cross sections and number density, the interference of formaldehyde in the ambient measurements of SO_2 by CRDS is negligible due to its low cross sections and modest concentrations. Other aldehydes and ketones have 308.7 nm cross sections comparable to or smaller than those of formaldehyde and lower concentrations[1], thus also negligible. The interference from HONO is negligible, due its smaller cross sections (1×10^{-20} cm^2/molecule near 308.7 nm) and ambient concentrations (0.1 - 15 ppb) than those of SO_2[1]; the same is true for PAN due to its much lower cross sections near 308 nm[1]. PAHs have absorption in the 308.7 nm region comparable to or lower than that of SO_2 (e.g., naphthalene ~ 3×10^{-20} cm^2/molecule at 308.7 nm (away from sharp absorption peaks)[26] and anthracene ~ 10×10^{-20} cm^2/molecule near 308.7 nm[27]), while their ambient concentrations are typically in the range of a few ppt (except for naphthalene of ~ tens of ppt to ~1 ppb)[1, 28, 29]. The combination of the small and modest cross sections and small ambient concentrations of PAHs renders their interference insignificant. On the other hand, NO_2 could potentially interfere in the ambient measurements of SO_2, as NO_2 has cross sections about 4 times smaller (1.7×10^{-19} cm^2/molecule near 308.7 nm) than those of SO_2 and concentrations in the range of a few ppb to 40 ppb (typical daily average in

Southern California). Ozone is another interfering species with cross sections about 6 times smaller (~1 × 10^{-19} cm^2/molecule near 308.7 nm) than those of SO_2 and concentrations in the range of 10-50 ppb (typical daily average in Southern California). Consequently, the ferrous sulfate scrubber was used to remove the NO_2 and ozone backgrounds.

The ferrous sulfate scrubber was shown to efficiently remove NO_2 from the sample stream without affecting the concentration of SO_2. The high transmission of SO_2 through the ferrous sulfate scrubber was tested. As shown in Figure 3.6, the scrubber did not remove any SO_2 in the air sample stream with an SO_2 concentration as high as ~500 ppb. The effectiveness of the scrubber to remove NO_2 was also characterized. As shown in Figure 3.7, NO_2 was introduced at a concentration of ~300 ppb (much higher than the typical ambient levels), and when the scrubber was inserted in the air stream, NO_2 was completely removed and the CRDS reading approached the "zero" air baseline. When the scrubber was removed from the sample line, the signal recovered back to the upscale value of NO_2. Ozone removal using ferrous sulfate was not tested in this study but has been demonstrated in other experiments using ferrous sulfate as a scrubbing material[3, 5, 23].

Following the scrubber which selectively removes NO_2 and ozone, the sodium carbonate denuder was used to remove SO_2 from the air stream to obtain a zero concentration level for quantification of SO_2 in the ambient measurements. The efficiency of the denuder was tested and is shown in Figure 3.8. Approximately 700 ppb of SO_2 in zero air was introduced into the CRDS cell, and when the denuder was placed in the sample line the signal dropped to the baseline, indicating a complete removal of

SO_2 (at a level as high as 700 ppb) from the sample stream. However, the sodium carbonate denuder used could also partially remove HONO, NO_2, and O_3 in the ambient air stream[12], causing a positive bias towards the SO_2 level if used alone. Consequently, it was necessary to install the ferrous sulfate scrubber, which selectively removes HONO, NO_2, and O_3, in front of the sodium carbonate denuder in the CRDS measurements.

The effectiveness of the ferrous sulfate scrubber and sodium carbonate denuder combination was demonstrated in a simulated SO_2 and NO_2 air sample in Figure 3.9. A mixture of ~200 ppb NO_2 and 160 ppb SO_2 in zero air was introduced into the ring-down cell. In order to observe the response of NO_2, which has absorption cross sections at 308.7 nm ~4 times smaller than SO_2, the concentration of NO_2 was much higher than normally measured in the ambient air. When the ferrous sulfate scrubber was placed in the sample stream there was a reduction in the signal indicating the removal of NO_2. The sodium carbonate denuder was then placed in series and behind the scrubber to remove SO_2 in the sample, with the signal dropping to the "zero" baseline level. The drop to the baseline allowed for quantification of SO_2 present in the sample. The signal due to SO_2 was consistent with the SO_2 concentration of ~160 ppb, while the signal due to NO_2 indicated a NO_2 concentration of ~200 ppb. The signal was then recovered by first removing the sodium carbonate denuder followed by the ferrous sulfate scrubber, showing the SO_2 contribution and the NO_2 contribution sequentially. Finally, the zero air level was reached by using zero air. Note that the efficiency of the scrubber and denuder are not affected by relative humidity, and the performance of the scrubber and denuder remain unchanged for weeks.

3.7 Ambient Sampling

Ambient measurements of SO_2 were attempted after the characterizations of the ferrous sulfate scrubber and sodium carbonate denuder in this study. The outdoor ambient air was sampled using 5 ft of 1/4" Teflon tubing through the window of the laboratory on University of California, Riverside campus. The ferrous sulfate scrubber and the sodium carbonate denuder were placed in series, followed by a 0.45-μm Teflon filter to prevent dust and particles from entering the ringdown cell. Zero air was initially used to establish an overall zero baseline level before sampling the ambient air. The CRDS measurements were taken every 10 seconds by averaging 100 ring-down decay rates.

The typical ambient level of SO_2 in the Southern California region is in the range of ~ ppb, and local measurements at Mount Rubidoux (approximately 6 km to the west of the sampling site at Riverside) by the California Air Resource Board (ARB) reported hourly average concentrations of ≤ 1 ppb throughout the days of our ambient measurements. At our sampling site, both the commercial PFA and CRDS reported the SO_2 levels essentially zero or below the current limits of detection of both instruments. Two sample ambient measurements on October 11 and 13, 2010 are shown in Figure 3.9. According to the ARB data, there were 15 ppb NO_2, 48 ppb ozone, and 0 ppb SO_2 present at the Mount Rubidoux site between 6 pm to 7 pm on October 11, 2010, and 8 ppb NO_2, 53 ppb ozone, and 0 ppb SO_2 between 3.10a), when the ferrous sulfate scrubber was in place there was a small drop from the ambient level equal to about 3 ppb of SO_2,

indicating removal of the contributions from NO_2 and O_3. The equivalent of SO_2 is lower than expected from the NO_2 and O_3 concentrations from the ARB data, possibly due to the different locations of these two sites. Once the NO_2 and ozone were scrubbed from the air, the sodium carbonate denuder was then introduced. The signal essentially stayed at the same level, indicating no detectable amount of SO_2. For the October 13 measurements (Figure 3.10b), the ambient levels with and without the scrubber indicated that there was no contribution from the NO_2 and O_3 background. The signal with the denuder in place showed again no detectable SO_2. Throughout the ambient measurements using CRDS in October, 2010, the SO_2 levels were essentially zero (below the detection limit of 3.5 ppb) and were consistent with the PFA readings (~ 0 ppb) and the ARB data. Note that in the ambient measurements, the ferrous sulfate scrubber should be in place at all times to remove NO_2 and O_3, which makes the CRDS measurements of SO_2 independent of the ambient NO_2 and O_3 background. The sodium carbonate denuder could then be used to obtain the baseline values periodically or frequently (in case of significant baseline drift) by implementing an automated valve cycle.

3.8 Conclusion

In this study, CRDS is demonstrated as an alternative method for measuring SO_2 in the atmosphere. The issues of potential inferences such as formaldehyde, PAHs, HONO, NO_2, and ozone are addressed. The use of a ferrous sulfate scrubber to remove the NO_2 and ozone background and a sodium carbonate denuder to zero the SO_2 level are

demonstrated as a viable solution to reduce interferences and obtain quantitative values of SO_2 in the CRDS measurements. A limit of detection of 3.5 ppb/10 seconds (S/N=2) is achieved. This sensitivity is slightly lower than the regular-model commercial PFA (e.g., 2.0 ppb/10 sec (2σ), Thermo Scientific 43*i*) and much poorer than the enhanced-model PFA (e.g., 0.3 ppb/10 sec (2σ), Thermo Scientific 43*i*-TLE). This proof-of-principle CRDS setup is currently best suited for more polluted environments with SO_2 in the tens of ppb or higher, but with some improvements it may compete with the current methods used to measure the ambient SO_2. Better mode matching of the laser light into the cavity and better detection system could improve the sensitivity to ~1 ppb/10s. The sensitivity could be significantly enhanced with better mirror reflectivity. For example, if the reflectivity is increased from 99.9% to 99.97% (possible with better coating and material techniques), the sensitivity could be further improved by ~ 15 times, possibly to ~ 0.1 ppb/10s. At this point, the selectivity of CRDS could also be improved by using differential cross sections of SO_2 or taking measurements at multiple wavelengths at several SO_2 absorption peaks near 308 nm. In addition, the CRDS has a faster response time than PFA's (a few seconds vs. 80 seconds). The predicted detection sensitivity of SO_2 by CRDS could be in a sub-ppb level in seconds of sampling time and become comparable to that of the best PFA's. Finally, alternative techniques such as broadband cavity enhanced absorption spectroscopy (BBCEAS) *(30)*, which utilizes UV light emitting diodes (LEDs) to replace the laser light source, can also be explored for sensitive detection of SO_2 and for more compact and economical SO_2 analyzers.

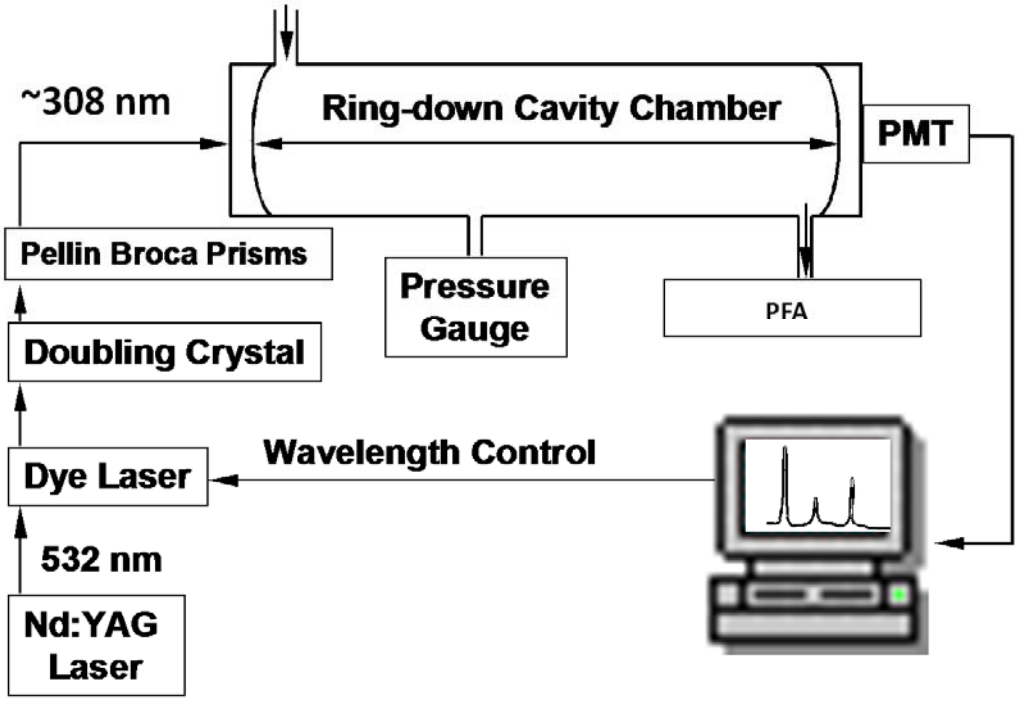

Figure 3.1: Experimental Setup of CRDS for SO2 analysis. The SO2 is introduced into the CRDS cell prior to analysis using PFA for intercomparison study.

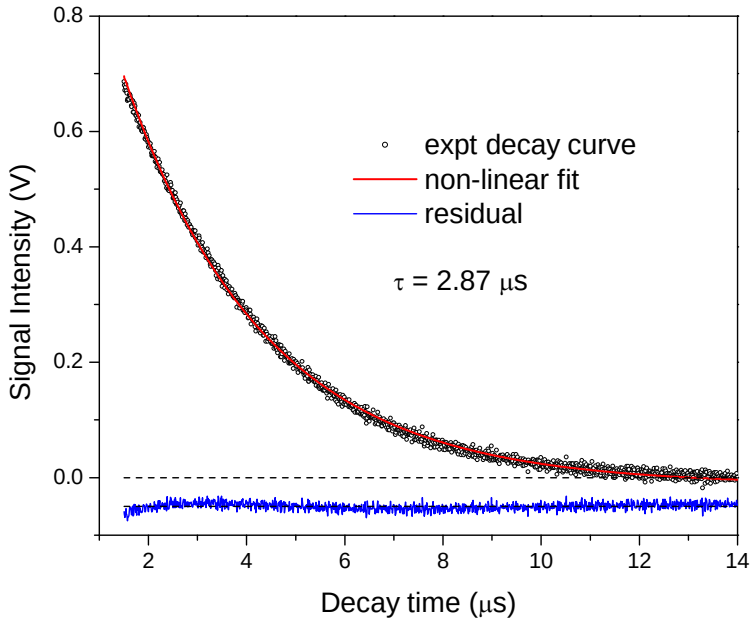

Figure 3.2. A typical experimental ring-down decay curve. The experimental data and the exponential fit are in the upper plot and the residual is shown in the lower plot.

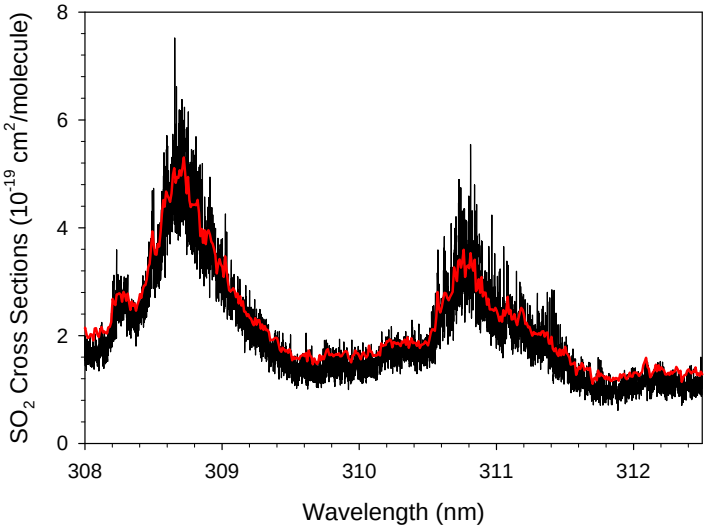

Figure 3.3: CRDS absorption spectrum of 500 ppb SO_2 in zero air (red) compared with high resolution spectrum of neat SO_2 at a pressure of 6.9 Torr (black, Rufus et. al., ref. 25). The comparison shows good agreements in the absorption cross sections and spectral features of SO_2 between the CRDS and traditional absorption spectroscopy and the greatly enhanced detection sensitivity in CRDS.

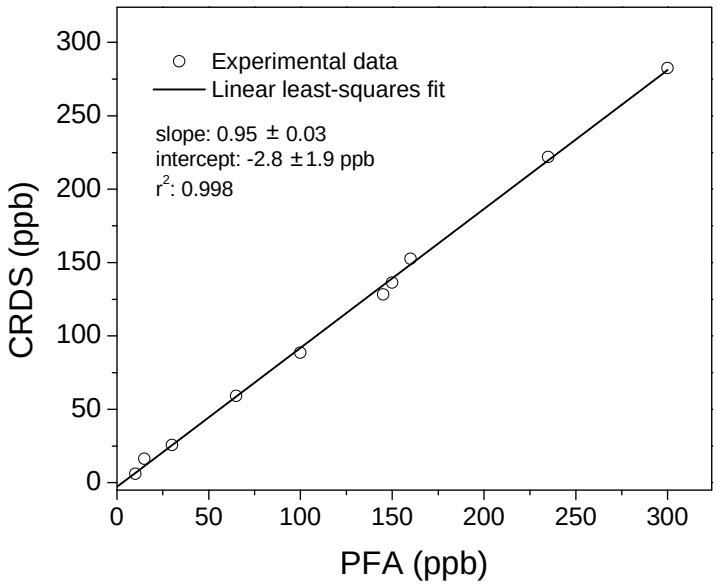

Figure 3.4: Intercomparison of the CRDS technique with a commercial PFA using SO_2 standards in zero air. The CRDS and PFA measurements have a good linear correlation in the range of 10-300 ppb. The small difference in the two measurements is likely due to the calibration of the PFA analyzer.

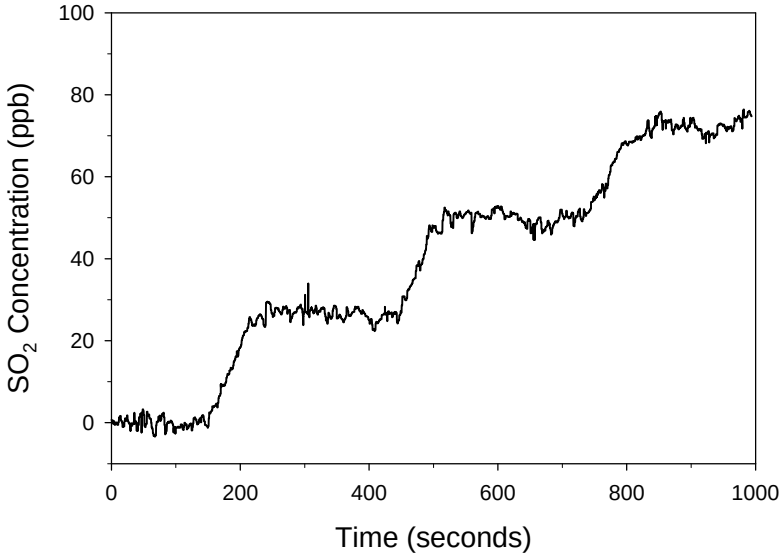

Figure 3.5: Step dilution of SO_2 ranging from 0 ppb (zero air) to 80 ppb. Measurements were taken at 308.7 nm. The sensitivity is calculated to be 5 ppb /10 sec (3σ) using the baseline (zero air) signal.

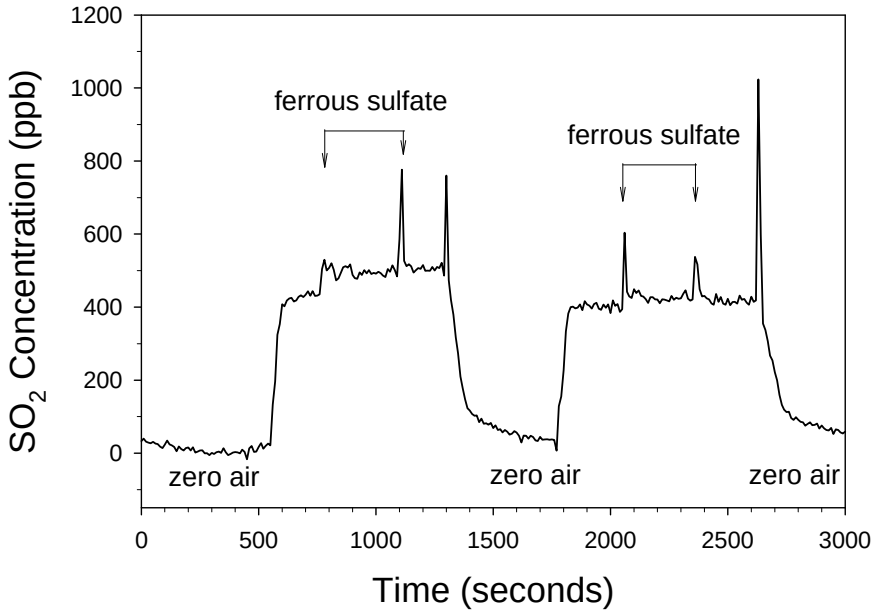

Figure 3.6: Transmission of SO_2 through the ferrous sulfate scrubber. The baseline signal represented zero air level, while the upscale values were from a standard of ~ 500 ppb SO_2 in zero air. The spikes indicated the time when the scrubber was placed in or removed from the sample line resulting in quick pressure spikes. When the scrubber was in place, no loss of SO_2 was observed.

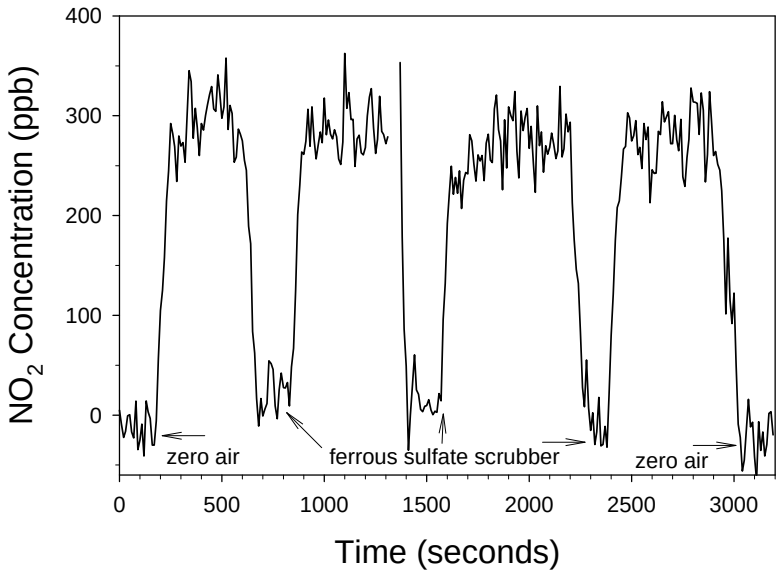

Figure 3.7: Removal efficiency of the ferrous sulfate scrubber. NO_2 was removed from the sample by using the ferrous sulfate scrubber at 750, 1500, and 2400 seconds. The baseline at 0 and 3000 seconds was from zero air.

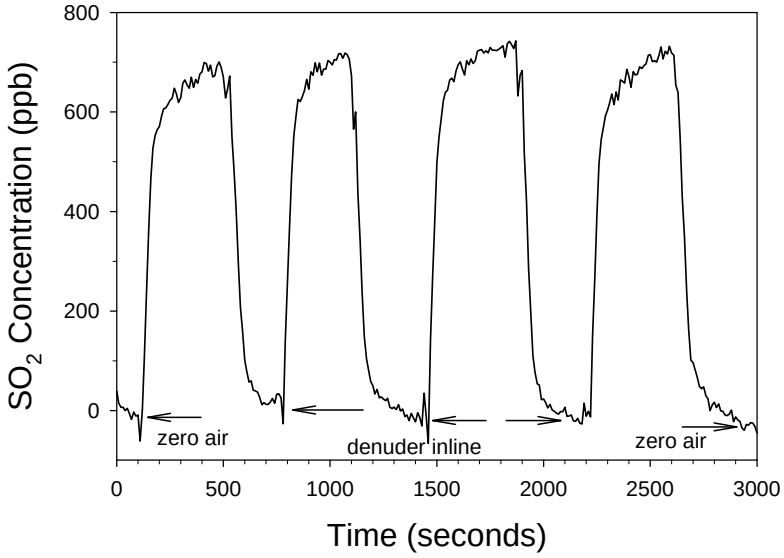

Figure 3.8: Removal efficiency of the sodium carbonate denuder. When the denuder was in line with the SO_2 in zero air sample stream, the signal of 700 ppb SO_2 dropped down to a baseline level of 0 ppb at 750, 1400, and 2000 seconds (comparable to the zero air baseline level at 0 and 3000 seconds). When the denuder was removed, the signal returned to the upscale value. There was a slight upward drift at the upscale values, possibly due to a slow uptake of SO_2 on the surface in the cell (which is not an issue for much lower ambient levels of SO_2).

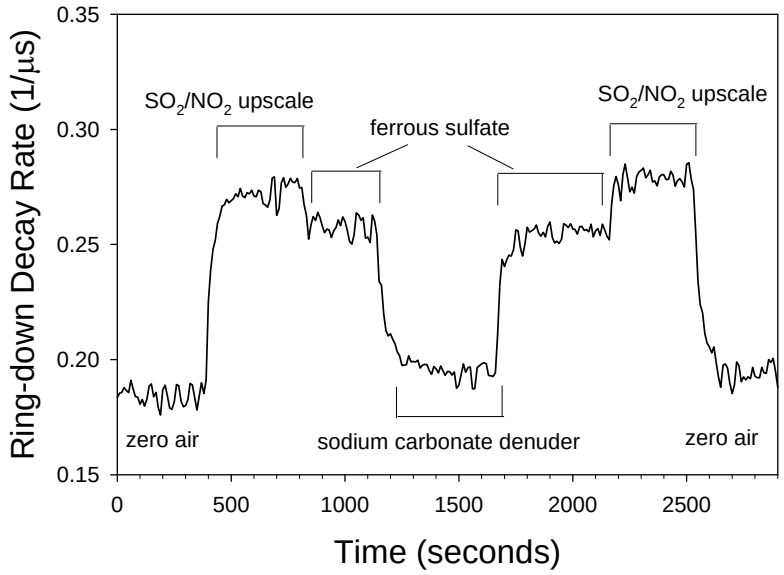

Figure 3.9: Test of a simulated ambient sample of 160 ppb of SO_2 and ~ 200 ppb of NO_2. At 800 seconds the ferrous sulfate scrubber was used to remove the NO_2 while the sodium carbonate denuder was placed in the sample stream at 1200 seconds to remove SO_2 and obtain a "zero" value and quantify the SO_2 level. The signal was recovered by first removing the sodium carbonate denuder and then the ferrous sulfate scrubber.

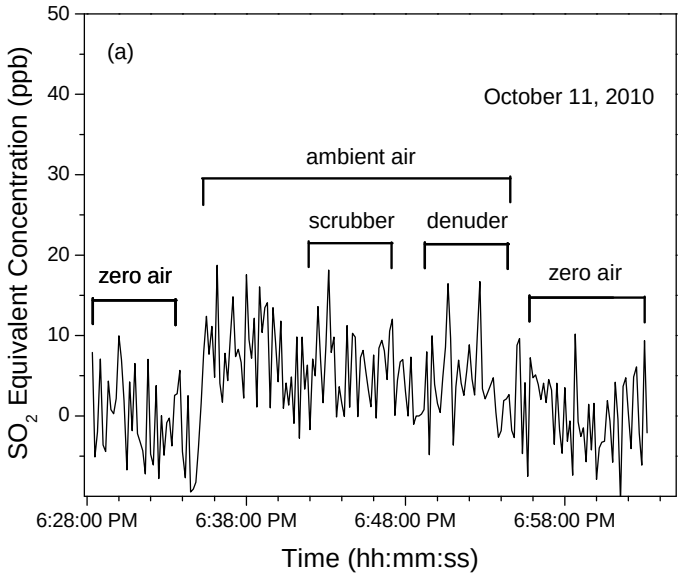

Figure 3.10 a. Ambient sample of air taken on October 11, 2010 is introduced and when the ferrous sulfate scrubber is placed before the gas enters the cell, most of the NO_2 is removed. The signal remains unchanged when the denuder is placed to remove SO_2, indicating the lack of SO_2 present in ambient air.

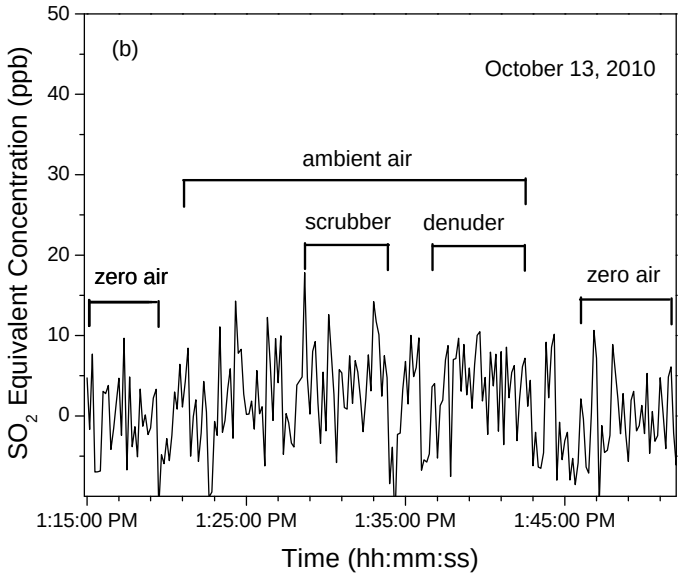

Figure 3.10 b. Ambient sample of air taken on October 13, 2010 is introduced and when the ferrous sulfate scrubber is placed before the gas enters the cell, most of the NO_2 is removed. The signal remains unchanged when the denuder is placed to remove SO_2, indicating the lack of SO_2 present in ambient air.

3.9 References

1. Finlayson-Pitts, B. J.; Pitts, J. N., *Chemistry of the upper and lower atmosphere : theory, experiments, and applications*. Academic Press: San Diego, Calif., 2000; p xxii, 969 p.

2. Kato, M.; Yamada, M.; Suzuki, S., Flavin mononucleotide sensitized and polyoxyethylene (20) sorbitan trioleate micelle-enhanced gas-solution chemi-luminescence for direct continuous monitoring of sulfur-dioxide in the atmosphere. *Analytical Chemistry* **1984,** *56* (13), 2529-2534.

3. Takenaka, N. M., M.; Munemori, M.; Zhang, D., Chemiluminescence method for the direct determination of sulfur dioxide. *Analyst* **1988,** *113* (1), 139-143.

4. Galan, G.; Navas, M. J.; Jimenez, A. M., Determination of sulfur compounds in air by chemiluminescence. *International Journal of Environmental Analytical Chemistry* **1997,** *68* (4), 497-510.

5. Zhang, D.; Maeda, Y.; Munemori, M., Chemiluminescence method for direct determination of sulfur dioxide in ambient air. *Analytical Chemistry* **1985,** *57* (13), 2552-2555.

6. Gregory, G. L.; Davis, D. D.; Beltz, N.; Bandy, A. R.; Ferek, R. J.; Thornton, D. C., An intercomparison of aircraft instrumentation for tropospheric measurements of sulfur-dioxide. *Journal of Geophysical Research-Atmospheres* **1993,** *98* (D12), 23325-23352.

7. Sigrist, M. W., *Air monitoring by spectroscopic techniques*. Wiley: New York, 1994.

8. Wang, P.; Richter, A.; Bruns, M.; Burrows, J. P.; Scheele, R.; Junkermann, W.; Heue, K. P.; Wagner, T.; Platt, U.; Pundt, I., Airborne multi-axis DOAS measurements of tropospheric SO_2 plumes in the Po-valley, Italy. *Atmospheric Chemistry and Physics* **2006,** *6*, 329-338.

9. Weibring, P.; Edner, H.; Svanberg, S.; Cecchi, G.; Pantani, L.; Ferrara, R.; Caltabiano, T., Monitoring of volcanic sulphur dioxide emissions using differential absorption lidar (DIAL), differential optical absorption spectroscopy (DOAS), and correlation spectroscopy (COSPEC). *Applied Physics B-Lasers and Optics* **1998,** *67* (4), 419-426.

10. Somesfalean, G.; Zhang, Z. G.; Sjoholm, M.; Svanberg, S., All-diode-laser ultraviolet absorption spectroscopy for sulfur dioxide detection. *Applied Physics B-Lasers and Optics* **2005,** *80* (8), 1021-1025.

11. Krochmal, D.; Kalina, A., A method of nitrogen dioxide and sulphur dioxide determination in ambient air by use of passive samplers and ion chromatography. *Atmospheric Environment* **1997,** *31* (20), 3473-3479.

12. Allegrini, I.; Desantis, F.; Dipalo, V.; Febo, A.; Perrino, C.; Possanzini, M.; Liberti, A., Annular denuder method for sampling reactive gases and aerosols in the atmosphere. *Science of the Total Environment* **1987,** *67* (1), 1-16.

13. Nishikawa, Y.; Taguchi, K., Ion chromatographic determination of nitrogen dioxide and sulfur dioxide in the atmosphere using triethanolamine potassium hydroxide - coated cartridges. *Journal of Chromatography* **1987,** *396*, 251-259.

14. Okeefe, A.; Deacon, D. A. G., Cavity ring-down optical spectrometer for absorption measurments using pulsed laser sources. *Rev. Sci. Instrum.* **1988,** *59* (12), 2544-2551.

15. Scherer, J. J.; Paul, J. B.; Okeefe, A.; Saykally, R. J., Cavity ringdown laser absorption spectroscopy: History, development, and application to pulsed molecular beams. *Chem. Rev.* **1997,** *97* (1), 25-51.

16. Wada, R.; Orr-Ewing, A. J., Continuous wave cavity ring-down spectroscopy measurement of NO_2 mixing ratios in ambient air. *Analyst* **2005,** *130* (12), 1595-1600.

17. Hargrove, J.; Wang, L. M.; Muyskens, K.; Muyskens, M.; Medina, D.; Zaide, S.; Zhang, J. S., Cavity ring-down spectroscopy of ambient NO_2 with quantification and elimination of interferences. *Environmental Science & Technology* **2006,** *40* (24), 7868-7873.

18. Osthoff, H. D.; Brown, S. S.; Ryerson, T. B.; Fortin, T. J.; Lerner, B. M.; Williams, E. J.; Pettersson, A.; Baynard, T.; Dube, W. P.; Ciciora, S. J.; Ravishankara, A. R., Measurement of atmospheric NO_2 by pulsed cavity ring-down spectroscopy. *Journal of Geophysical Research-Atmospheres* **2006,** *111* (D12), 10.

19. Brown, S. S.; Stark, H.; Ravishankara, A. R., Cavity ring-down spectroscopy for atmospheric trace gas detection: application to the nitrate radical (NO_3). *Applied Physics B-Lasers and Optics* **2002,** *75* (2-3), 173-182.

20. Ayers, J. D.; Apodaca, R. L.; Simpson, W. R.; Baer, D. S., Off-axis cavity ringdown spectroscopy: application to atmospheric nitrate radical detection. *Appl. Optics* **2005,** *44* (33), 7239-7242.

21. Kleine, D.; Murtz, M.; Lauterbach, J.; Dahnke, H.; Urban, W. G.; Hering, P.; Kleinermanns, K., Atmospheric trace gas analysis with cavity ring-down spectroscopy. *Israel Journal of Chemistry* **2001,** *41* (2), 111-116.

22. Wang, L. M.; Zhang, J. S., Detection of nitrous acid by cavity ring down spectroscopy. *Environmental Science & Technology* **2000,** *34* (19), 4221-4227.

23. Anderson, H. H.; Moyer, R. H.; Sibbett, D. J.; Sutherland, D. C. System and Method of Air Pollution Monitoring Utilizing Chemiluminescence Reactions. 1972.

24. Finn, D.; Rumburg, B.; Claiborn, C.; Bamesberger, L.; Siems, W. F.; Koenig, J.; Larson, T.; Norris, G., Sampling artifacts from the use of denuder tubes with glycerol based coatings in the measurement of atmospheric particulate matter. *Environmental Science & Technology* **2001,** *35* (1), 40-44.

25. Rufus, J.; Stark, G.; Smith, P. L.; Pickering, J. C.; Thorne, A. P., High-resolution photoabsorption cross section measurements of SO_2, 2: 220 to 325 nm at 295 K. *J. Geophys. Res.-Planets* **2003,** *108* (E2), 5.

26. Neuroth, R.; Dorn, H. P.; Platt, U., High resolution spectral features of a series of aromatic hydrocarbons and BrO: potential interferences in atmospheric OH-measurements. *Journal of Atmospheric Chemistry* **1991,** *12* (3), 287-298.

27. Ferguson, J.; Reeves, L. W.; Schneider, W. G., Vapor absorption spectra and oscillator strengths of naphthalene, anthracene, and pyrene. *Canadian Journal of Chemistry-Revue Canadienne De Chimie* **1957,** *35* (10), 1117-1123.

28. Martinez, M.; Harder, H.; Ren, X.; Lesher, R. L.; Brune, W. H., Measuring atmospheric naphthalene with laser-induced fluorescence. *Atmospheric Chemistry and Physics* **2004,** *4*, 563-569.

29. Brandenburger, U.; Brauers, T.; Dorn, H. P.; Hausmann, M.; Ehhalt, D. H., In-situ measurements of tropospheric hydroxyl radicals by folded long-path laser absorption during the field campaign POPCORN. *Journal of Atmospheric Chemistry* **1998,** *31* (1-2), 181-204.

30 Ball, S. M.; Jones, R. L., Broad-band cavity ring-down spectroscopy. *Chemical Reviews* **2003**, *103* (12), 5239-5262

Chapter 4

Broad-band Cavity Enhanced Absorption Spectroscopy (BBCEAS)

4.1 Abstract

Broadband cavity enhanced absorption spectroscopy (BBCEAS) is a simple absorption spectroscopy technique with high sensitivity and the potential for multiple component analysis having a long effective pathlength in a compact setup (~m). The absorption cell is composed of two highly reflective mirrors and the light introduced into the cell is provided by an incoherent light source from either a xenon arc lamp or a light emitting diode (LED). The technique has the advantage of being robust, portable, and inexpensive compared to other absorption techniques. Analytical chemistry applications include atmospheric measurements as well as liquid analysis.

4.2 Introduction

Conventional absorption spectroscopy is commonly used for the detection of trace atmospheric pollutants[1]. The absorption is expressed in terms of the Beer-Lambert law. From the Beer-Lambert law the sensitivity depends on the pathlength. This is the reason for employing long optical pathlengths[2] for sensitive measurements during field campaigns. In addition, when multiple compounds are to be measured simultaneously or measure species with broad absorption bands, wide spectral regions are preferred.

As was introduced in Chapter 1, cavity ring-down spectroscopy provides a long effective pathlength and is capable of measuring the absorbance of a trace species from the decay time of the laser pulse resonating within the cavity. This is only possible if the ring down time is obtained when there is no absorber present within the cavity. One way to do this is by introducing nitrogen gas or some other gas free of absorber. However, sometimes the region of interest has multiple absorbers that can pose as interfering species, thus simply using a zero gas background to obtain concentration information is not suitable in this situation. Background absorbers can contribute to positive interference, thus yielding higher concentration values of the analyte of interest. Since measurements are carried out at one wavelength and it is sometimes difficult to measure the absorbance of the analyte of interest if there are other absorbers in the same wavelength region, one way to get around this is by scanning the laser to a point on the absorbers spectrum where the cross section is a minimum and obtaining a differential absorption. Also, sometimes a denuder or titrant gas can be used to selectively remove the absorbing species and obtain the baseline ring-down time without absorber of interest.

An alternative is the technique incoherent broad-band cavity enhanced absorption spectroscopy. The technique stemmed from cavity enhanced absorption, which was introduced in 1988 by Englin, where a continuous wave laser is injected into a cavity, where the intensity reaches its limiting value and the time integrated intensity exiting the cavity is measured, and absorption spectra are obtained.[3] Having the limitation of small spectral regions from using a cw diode laser, when wide spectral regions are desired rather than high spectral resolution, the technique known as incoherent broad band cavity enhanced absorption (BBCEAS) was developed. Xenon-arc lamps, which provide incoherent light were initially used with the broad-band cavity enhanced absorption technique. The intensity is allowed to build up within the cavity and the absorption coefficient can be derived and the following equation is obtained.[4]

$$\alpha(\lambda) = \frac{1}{d}\left(\frac{I_0(\lambda)}{I(\lambda)} - 1\right)(1 - R(\lambda)) \qquad \textbf{[4.1]}$$

where α is the absorption coefficient, d is the length of the absorption path in the cavity, I_0 is the intensity of light exiting the cavity without any absorber present, I is the intensity of the cavity with absorber, and R is the reflectivity of the mirrors. It should be noted that all variables with the exception of the length of the cavity are wavelength dependent. Unlike CRDS, where the resolution is based on the bandwidth of the laser, the resolution is dictated by the optical characteristics of the light detection system (such as the slit

width and grating of the monochromator). If it is assumed that at small concentrations of absorber in the cavity $(I_0\text{-}I)/I_0 = (I_0\text{-}I)/I$, the minimum detectable absorption coefficient, α_{min} is:[4]

$$\alpha_{\min} = \frac{1}{d}\left(1 - \frac{I_{\min,\sin\, glepass}}{I_{0,\sin\, glepass}}\right) = \frac{1}{d}\left(1 - \frac{I_{\min}}{I_0}\right)(1 - R) \qquad \textbf{[4.2]}$$

This implies that the BBCEAS technique is $(1\text{-}R)^{-1}$ times more sensitive than the conventional absorption spectroscopy. Since the sensitivity is dependent on the mirror reflectivity, the mirror reflectivity should be characterized to provide the correct absorption coefficient. This is important considering the mirrors are wavelength dependent and typically have a region of peak high reflectivity of a few tens of nanometers before dramatically tailing off to a lower percent reflectivity. Also, the light is provided by a broadband light source which can vary in intensity at different wavelengths and when the broadband light is coupled with wavelength dependent mirror reflectivity, the resulting transmission signal is a factor of the two components. To obtain absolute concentration information of absorbers the mirror reflectivity must be known. Typical mirror reflectivities used range from R=0.999 to R=0.9999. Independent measurements of mirror reflectivity can be performed a few ways. One way is by using a calibration gas that is known to absorb in the region of interest such as NO_2 with a known concentration and extracting mirror reflectivity information by fitting the spectrum obtained with the literature spectrum of NO_2. Another method used to obtain mirror

reflectivity data is using the CRDS technique and measuring the reflectivity on a separate CRDS instrument. The mirror reflectivity is extracted from the wavelength dependent ring down time. The CRDS method of obtaining mirror reflectivity data typically yields higher reflectivity values because there are fewer losses of light within the cavity when a pulsed laser is used as opposed to the uncollimated light from an LED or xenon arc lamp. Therefore, the most reliable method of obtaining mirror reflectivity data is by using the calibration gas. One thing to consider with the mirror reflectivity is that using lower reflectivity mirrors will provide a higher transmission signal since more light is transmitted within the cavity. However, this also corresponds to a shorter effective pathlength since there will be fewer round trips of light within the cavity. In addition, lower reflectivity mirrors allow for a broader spectral region to be studied. The lower sensitivity from using low reflectivity mirrors can be overcome by increasing the length of the cell. To make a truly portable device, long pathlengths are not always possible. Thus, using higher reflectivity mirrors are preffered even though the signal intensity will be lower since the majority of the light will be cut off by the high reflectivity. The longer effective pathlength should overcome the decrease in transmission intensity. It should be noted that extremely high reflectivities are not desirable simply because the extremely low transmission intensity will be difficult to overcome due to increased noise in the signal. The selection of mirrors and their varying reflectivity become a compromise when it comes to the instrument design.

The transmission signal, or the intensity of light exiting the cell, when there are no absorbers present, I_0, must also be measured prior to measurements with an absorber

present in the cell. Also, unlike cavity ring-down, where the ring down time of the signal is not dependent on the stability of the light source, BBCEAS sensitivity can be affected by having a fluctuating light source. The high powered LEDs used tend to overheat with extended use and higher temperatures result in the spectral emission drifting to longer wavelengths. Therefore, it is important to maintain a stable source to minimize error from the fluctuation especially during long periods of sampling. This is achieved by mounting the light source to a Peltier cooler or thermo electric cooler (TEC) and a heat sink with a fan to provide additional cooling.

Similar to CRDS, BBCEAS provides the long pathlength that absorption spectroscopy can benefit from to improve sensitivity. BBCEAS also has the advantage of not requiring an expensive light source that is typically required for pulsed CRDS. The use of a high powered LED or xenon arc lamp is sufficient. BBCEAS has the potential for simultaneous analysis of multiple absorbers in the same spectal region.

4.3 Typical Experimental Setup

The typical setup of an BBCEAS instrument is shown in Figure 4.1. The incoherent light source can either be from a xenon arc lamp using a filter for wavelength selection or a high powered LED with a broad emission of a few tens of nanometers. A filter may or may not be needed depending on the LED. The light is coupled into the cavity using a lens to focus and couple the light into the spectrometer. More sophisticated setups may include the use of fiber optics to transfer the light from the LED

to the cell. The use of fiber optics is not required but can provide a more robust set up where the light source and detector can be housed separate from the optics. The length of the cell can vary from less than a meter to a few meters. The longer the cell length will offer longer effective pathlengths but it might be more difficult to keep the light in the cavity due to possible divergence of incoherent light. As the light exits the cavity, it is refocused using a lens. The focused light is imaged onto fiber optics that is typically mounted on an x-y translation stage for fine adjustment. The fiber optics steer the light into a monochromater, where it is then detected using a CCD.

4.4 Analytical Applications of BBCEAS

The first demonstration of BBCEAS used a xenon arc lamp as the light source and used a filter for wavelength selection and measurements were carried out on weak transitions in molecular oxygen and gaseous azulene.[4] Soon after the introduction of BBCEAS using a white light source from a xenon arc lamp, the use of light emitting diodes (LED) was incorporated in the cavity enhanced arrangement to measure trace atmospheric species (NO_3, NO_2, and I_2).[5] The introduction of high powered LEDs helped improve sensitivity for the atmospheric species NO_2 and NO_3[6-10]. NO_3 and nitrous acid (HONO) have also been measured using BBCEAS in the ultraviolet region.[11] In addition to the gas phase, BBCEAS has been applied to liquid samples by introducing two mirrors inside of a conventional UV-vis spectrometer to get enhancement and observe weak overtones of benzene in the visible region.[12] Another example of BBCEAS used for

analysis of liquids include the measurements of sudan black and methylene blue dissolved in acetonitrile using a 20 cm cavity where the solvent was in direct contact with mirrors having lower reflectivity mirrors of $R \geq 0.99$ having a wide spectral range and the use of a white LED[13]

4.5 Conclusion

BBCEAS is a simple absorption spectroscopy method using inexpensive LEDs as the light source and has the potential for measuring multiple absorbers simultaneously. In this thesis, two instruments based on BBCEAS are developed. One uses a red LED and measure NO_3 in the 662 nm region and is applied to the detection of the nitrate radical in an environmental chamber. The second device uses a high powered LED in the UV region and is developed for measurements of nitrous acid (HONO) and nitrogen dioxide (NO_2) simultaneously and can be potentially used for NO_2 heterogenous hydrolysis experiments.

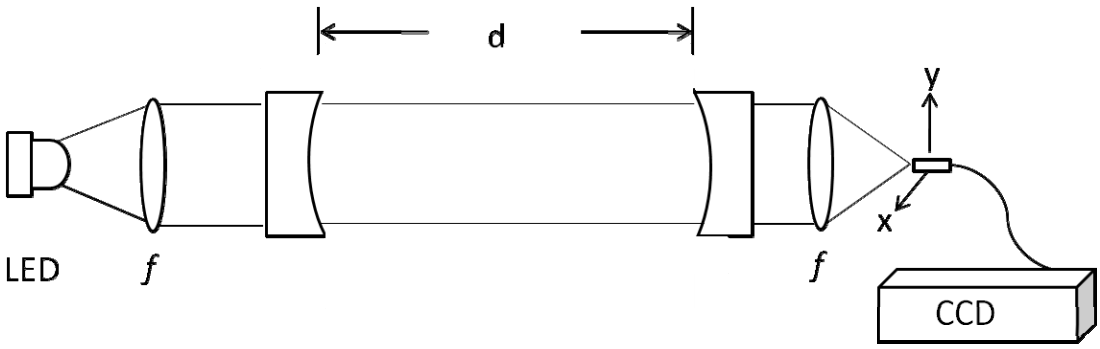

Figure 4.1: Typical BBCEAS arrangement. The light source used can either be a xenon arc lamp or an LED. A focusing lens is used to collimate the light and inject it into the cell composed of two high reflective mirrors (R>0.99). The high reflective mirrors are separated by a distance, d. The light exiting the cavity is focused using a focusing lens onto an x-y translational fiber optic cable leading to the CCD.

4.6 References

1. Finlayson-Pitts, B. J.; Pitts, J. N., *Chemistry of the upper and lower atmosphere: theory, experiments, and applications*. Academic Press: San Diego, CA, 2000.

2. Sigrist, M. W., *Air Monitoring by Spectroscopic Techniques*. Wiley: New York, 1994.

3. Engeln, R.; Berden, G.; Peeters, R.; Meijer, G., Cavity enhanced absorption and cavity enhanced magnetic rotation spectroscopy. *Rev. Sci. Instrum.* **1998,** *69* (11), 3763-3769.

4. Fiedler, S. E.; Hese, A.; Ruth, A. A., Incoherent broad-band cavity-enhanced absorption spectroscopy. *Chem. Phys. Lett.* **2003,** *371* (3-4), 284-294.

5. Ball, S. M.; Langridge, J. M.; Jones, R. L., Broadband cavity enhanced absorption spectroscopy using light emitting diodes. *Chem. Phys. Lett.* **2004,** *398* (1-3), 68-74.

6. Triki, M.; Cermak, P.; Mejean, G.; Romanini, D., Cavity-enhanced absorption spectroscopy with a red LED source for NO_x trace analysis. *Appl. Phys. B-Lasers Opt.* **2008,** *91* (1), 195-201.

7. Langridge, J. M.; Ball, S. M.; Jones, R. L., A compact broadband cavity enhanced absorption spectrometer for detection of atmospheric NO_2 using light emitting diodes. *Analyst* **2006,** *131* (8), 916-922.

8. Schuster, G.; Labazan, I.; Crowley, J. N., A cavity ring down/cavity enhanced absorption device for measurement of ambient NO_3 and N_2O_5. *Atmos. Meas. Tech.* **2009,** *2* (1), 1-13.

9. Langridge, J. M.; Ball, S. M.; Shillings, A. J. L.; Jones, R. L., A broadband absorption spectrometer using light emitting diodes for ultrasensitive, in situ trace gas detection. *Rev. Sci. Instrum.* **2008,** *79* (12), 14.

10. Heitmann, U.; Ruth, A. A.; Varma, R. M.; Venables, D. S. *Air pollution - trace radical absorption through cavity-enhanced spectroscopy (TRACES)*; 2008.

11. Gherman, T.; Venables, D. S.; Vaughan, S.; Orphal, J.; Ruth, A. A., Incoherent broadband cavity-enhanced absorption spectroscopy in the near-ultraviolet: Application to HONO and NO_2. *Environ. Sci. Technol.* **2008,** *42* (3), 890-895.

12. Fiedler, S. E.; Hese, A.; Ruth, A. A., Incoherent broad-band cavity-enhanced absorption spectroscopy of liquids. *Rev. Sci. Instrum.* **2005,** *76* (2), 7.

13. Seetohul, L. N.; Ali, Z.; Islam, M., Liquid-phase broadband cavity enhanced absorption spectroscopy (BBCEAS) studies in a 20 cm cell. *Analyst* **2009,** *134*, 1887-189

Chapter 5

Detection of Nitrate Radical (NO_3) by Broadband Cavity Enhanced Absorption Spectroscopy (BBCEAS)

5.1 Abstract

The nitrate radical (NO_3) is the major oxidation species in the night time troposphere. NO_3 is also believed to be involved in the production of secondary organic aersosols (SOA). Instrumentation for gaining more information on the role of NO_3 in the atmosphere is needed. Here, a portable, inexpensive LED instrument based on broadband cavity enhanced absorption spectroscopy (BBCEAS) is developed for the measurement of NO_3 in environmental chamber studies. In this chapter, the description of the cell construction and chamber measurements are presented to demonstrate the capability of the technique. The BBCEAS NO_3 instrument is demonstrated to have a sensitivity of 10 ppt/2 minutes.

5.2 Introduction

The nitrate radical (NO_3) plays a large role in the nitrogen oxide (NO_x) chemistry in the atmosphere. During the daytime, the main oxidant in the atmosphere is the hydroxyl radical (OH). However, at night when OH radical concentrations are low, NO_3 is considered to be the major oxidation species often reacting with biogenic volatile organic hydrocarbons (VOCs) emitted in the nighttime air. The primary source for NO_3 is the reaction of nitrogen dioxide, NO_2, with ozone, once the sun has set and NO_3 concentrations slowly rises throughout the night. The typical concentrations of NO_3 range from 10's of parts per trillion (ppt) in remote locations to 100's of ppt in more polluted environments[1]. The formation of nitric acid from NO_3 abstraction of a hydrogen atom from a hydrocarbon is considered a sink, which results in the hydrocarbon radical reacting with oxygen molecules to produce peroxyl radicals (RO_2) [1]. When NO_3 reacts with NO_2 present at night it forms dinitrogen pentaoxide (N_2O_5). The heterogeneous uptake of N_2O_5 on surfaces of particulates such as ammonium sulfate and ammonium bisulfate to form nitric acid has been measured in the troposphere and is another known sink for NO_x in the troposhere [2]. Additionally, the reaction of NO_3 with linear alkenes may contribute to secondary organic aerosol (SOA) formation [3, 4]. Much of the current research of NO_3 has involved its removal from the atmosphere through surface reactions of aerosol and its contribution to aerosol formation. However, measurements of NO_3 in the atmosphere as well as in the laboratories have been limited. Thus, instrumentation that is inexpensive, portable, as well as sensitive is needed to measure NO_3 to gain better insights into its removal pathways in the atmosphere. A sensitive and portable instrument

has been developed for the measurement of NO_3, Broadband Cavity Enhanced Absorption Spectroscopy (BBCEAS). BBCEAS has the advantage of a long effective absorption pathlength in a compact setup, and sensitivity (ppt level) and the use of an inexpensive light emitting diode as a broadband light source allows for the simultaneous analysis of multiple absorbers. Instrumentation that can provide insights into the reactions and variability of the nitrate radical during the nighttime atmosphere can shed light on the sinks, which are valuable to computer models that provide information on atmospheric pollutants and their sources and sinks. In this chapter, the focus will be on the development of an inexpensive portable NO_3 analyzer to conduct measurements in an environmental chamber for the purpose of gathering data in a controlled environment to provide data for atmospheric models.

The nitrate radical was first measured in the troposphere using long path differential absorption spectroscopy (DOAS) in the Los Angeles air basin [5]. The DOAS technique measured the nitrate radical at concentrations of around 355 ppt in polluted air using the strong absorption features at 623 and 662 nm. Sensitivities of DOAS measurements of NO_3 fall within the range of 0.2 to 10 ppt. Prior to spectroscopic techniques to directly measure NO_3, models were used to predict NO_3 concentrations in the atmosphere. Although the long path DOAS technique is capable of measuring NO_3, it requires a long optical path length. Often these path lengths are ~1 km (970 and 750 m) in length and the measured concentration is an average over the entire optical column sampled rather than a direct point source. The DOAS method is useful in terms of outdoor sampling but when measurements in an indoor environmental chamber are

desired, setting up the long path length may prove difficult. With the development of cavity ring-down spectroscopy (CRDS) [6, 7], a technique with the capability of great sensitivity from a long effective pathlength (~1km) and a compact set up was achieved. Additionally, measurements of N_2O_5 using DOAS are limited due to the open pathlength where in situ measurements of NO_3 and N_2O_5 are possible by thermal decomposition of N_2O_5 to NO_3 at a temperature of 85 ^oC using a closed cell instrument such as CRDS. Using CRDS a zero baseline is obtained by titrating NO_3 with NO to form NO_2 where the cross section of NO_2 is negligible compared to NO_3 at the probe laser wavelength of 662 nm. Another detector developed for the NO_3 measurements is off-axis cavity ring-down spectroscopy (OA-CRDS) [8], which uses a narrow bandwidth laser aligned off-axis to activate the cavity modes in the cell. This technique uses the same method of NO titration to obtain zero baseline values. A CRDS based NO_3 detector requires a complex setup inculding a laser, which can be considerably bulky and expensive.

The trend of instrumentation for NO_3 detection has been towards portable and robust analyzers. Here a sensitive and portable instrument based on Broadband Cavity Enhanced Absorption Spectroscopy (BBCEAS) has been developed for the measurement of NO_3. A detailed introduction to the BBCEAS technique has been provided in Chapter 3. Briefly, the absorption coefficient of the sample can be determined from the measurement of continuous light transmitted into a cavity composed of highly reflective mirrors using the equation:

$$\alpha(\lambda) = \frac{1}{d}\left(\frac{I_0(\lambda)}{I(\lambda)} - 1\right)(1 - R(\lambda)) \qquad \textbf{[5.1]}$$

where I is the intensity of transmitted light with an absorbing medium present and I_o is the intensity of transmitted light without an absorber, R is the mirror reflectivity and, d is the length of the cavity. BBCEAS has the advantage of a long effective absorption pathlength in a compact setup (~1m), and sensitivity (ppt level) and the use of an inexpensive light emitting diode as a broadband light source and a CCD detector allows for the simultaneous analysis of multiple absorbers.

The NO_3 detector presented here is based on previously developed methods. The first use of BBCEAS to measure NO_3 was an LED based instrument [9]. The spectrum of the nitrate radical at a concentration of 40 ppt $\pm$ 2.5 ppt was obtained assuming a mirror reflectivity of 99.99 % over a 255 second acquisition time. To obtain a more accurate mirror reflectivity broadband cavity ring-down spectroscopy was used, providing a reflectivity of 99.9945 % at 652 nm to 99.9965 % at 670 nm. Another incoherent BBCEAS NO_3 detector employed an arc lamp as the source and a cell having a 4.5 meter open path length and a mirror reflectivity of 99.775 % at 665 nm, which was determined using a known concentration of NO_2 and provided a limit of detection for NO_3 of 4 ppt/1 min [10]. A NO_x analyzer was developed using an LED with an emission at 643 nm and although NO_3 was not directly measured, an estimated limit of detection for NO_3 of a few ppt (~2 ppt) at its 623 nm peak was extrapolated from NO_2 data [11]. Mirror reflectivity data was obtained using a commercial spectrophotometer (99.92 % at 630 nm). Another broadband spectrometer for NO_3 was developed with a limit of detection of 0.25 pptv/10 seconds calibrated using a mirror reflectivity of 99.9907 % from an intercomparison using broadband cavity ring-down spectroscopy and a variation known as phase shift

cavity ring down spectroscopy using 50 to 350 ppbv NO_2 [12]. This is the only BBCEAS setup that has demonstrated ambient sampling of NO_3 and has discussed the treatment of ambient data containing humid air. A follow up paper by the same group demonstrated the instrument's ability to monitor NO_3 from a tower[13]. The sum of NO_3 and N_2O_5 was measured up to levels of 800 ppt with a mirror reflectivity of 99.98 %. A cavity enhanced spectrometer for NO_3 was also developed by Schuster et. al. by using a continuous laser emission, which can be alternated between cavity enhanced mode and cavity ring-down mode. A mirror reflectivity (99.998 %) close to the peak NO_3 absorption at 662 nm was obtained using the CRDS mode. It should be noted that this instrument was only capable of probing NO_3 at the peak emission of the laser diode and lacked the broadband capability and the potential to measure multiple absorbers simultaneously that previous analyzers were capable of. Regardless, a limit of detection of 1 ppt in less than a second is proposed. A hybrid technique known as CE-DOAS, based on similar principles as BBCEAS has also been developed, which uses an open path cell composed of two high reflective mirrors and the treatment of spectra is analyzed using DOAS analysis [14]. No characterization of mirror reflectivity is taken and the reflectivity is assumed to be that reported by the manufacturer, R = 99.9985 % at 655 nm. NO_3 measurements were carried out in the SAPHIR chamber in that study.

5.3 Generating NO_3 for Laboratory Tests

NO3 is produced from the thermal decomposition of Dinitrogen pentaoxide (N_2O_5). The N_2O_5 precursor was generated by the reaction of pure NO_2 and excess ozone[15, 16]. High levels of ozone (a few % in O_2) were generated using an ozonator and the ozone was flowed through a U-tube packed with P_2O_5 to reduce moisture. The presence of moisture leads to the formation of nitric acid in the trap. The ozone was then reacted with high concentrations of $NO_2$to generate N_2O_5. The N_2O_5 was then collected by flowing through a trap submerged in an acetone and dry ice bath. The N_2O_5 crystals were collected at the bottom of the trap. To ensure that a maximum amount of N_2O_5 is trapped and to reduce the amount of NO_2 collected in the trap, the ozonator is continued to flow to flush the trap with ozone and convert any remaining NO_2 and form N_2O_5. The trap is covered from sunlight to prevent NO_3 decomposition into NO_2 by photolysis. The final product was pure N_2O_5 and not NO_2 by the absence of any brown colored crystals remaining in the trap. The crystals were subsequently transferred off-line to the BBCEAS instrument where the N_2O_5 was thermally decomposed to NO_3 and was introduced into the sample cell by diffusion. It is important to maintain the cold temperatures to prevent the N_2O_5 degradation into NO_2.

5.4 Instrument Design

Cavity ring-down and cavity enhanced spectroscopy are still relatively new techniques and much of the instrument must often be designed and constructed in house.

The selection of light emitting diodes (LED), the design of mirror mounts, sampling cell, and the detector must be considered. When designing a cell it is important to consider mirror mounts that will house the high reflective mirrors while still providing a leak tight seal to the surrounding environment. The most common designs for CRDS/CEAS mirror mounts are based on an o-ring seal[8] and flexible bellows.[7, 12, 17, 18] The o-ring design is the easiest and most inexpensive design to employ, where the o-ring serves the purpose of providing a seal while at the same time offering a few degrees of play for alignment purposes. In fact, the most popular commercially available mirror mount is based on an o-ring design (Los Gatos). The disadvantage of the commercial design is that the mirror window is designed for laser based experiments and not for use with an LED as the light source. Typically, for laser based systems, the beam profile is on the order of a few millimeters (~2 mm) but for an LED the profile can be around 10 times wider depending on how the light has been collimated. For BBCEAS experiments, it is important to maximize the light intensity entering the cavity to increase the signal intensity. Also, once inside the cell further losses of light can be expected as the light travels within the cell between each mirror. Thus, it is valuable to use mirror mounts that can maximize the clearance area of the mirror to be used. The flexible bellows design is an alternative design and offers a better seal for the cell and provides better translational motion for optimal optical alignment. When sampling at ambient pressure the o-ring design will suffice since leaking of the cell will be unlikely. In the design described here, a modified o-ring design is used. A schematic of the side profile of the mirror mount is shown in Figure 5.1. The schematic highlights the maximized window room for the mirror. A

photograph of the entire instrument is shown in Figure 5.2a. The photograph shows that the CEAS cell, detector, controls, and optics are all mounted on a portable laser table (Thorlabs). The laser table is 4 ft x 2 ft and is made of vibration dampening material for better instrument stabilization. The laser table is mounted on a portable frame which has a set of four wheels at the bottom, which allow for transportation of the setup to different parts of the lab. The permanent location for the instrument is in the College of Engineering – Center for Environmental Research and Technology (CE-CERT) environmental chamber where there are multiple chambers so portability is important. To stabilize the instrument, the wheels can be fastened and the legs can be stabilized to the floor.

The goal of the cell design was to have an instrument cell that was home built using commercially available vacuum fittings to have an easily reproducible cell to reduce the amount of machining in the future and to have mirror mounts machined based on an o-ring design to maximize the window area to increase the signal intensity entering the cell. The home built mount is displayed in the photograph shown in Figure 5.2b. The base of the mirror mount was machined from a 2-3/4 inch conflat flange (275-100NT, Norcal). A 1.92 inch diameter was bored out 0.3 inches deep to insert the mirror mounting plate. A 0.040 inch groove is cut into the base for an o-ring (1/16 inch thickness) used for making fine adjustments and maintaining a proper seal with the custom mirror mount holder. The high reflectivity mirror sits inside of the stainless steel mounting plate having a thickness of 0.3 inches, with the center bored out to maximize the window size of the mirror. The front of the mirror is held in place using a thin disk

(1.4 inch diameter) mounted directly on top of the mirror cover using three screws (4/40) equally spaced. This inner mirror mount housing is held in place by a 2.75 inch front mount cover. Three ¼ inch fine adjustment screws (F3SS25, Thorlabs) mounted through threaded bushings equally spaced are used for fine adjustments for alignment of a few degrees on the o-ring by adjusting the mirror mounting plate and to secure a leak tight seal of the cell.

The 2-3/4 inch CF flange is mounted to a 2.75 inch double side-ported flange with 1/8 inch NPT holes (FD-275150-2H, Duniway), which are used as the inlet ports for the nitrogen purge gas used to protect the mirrors from dust, debris, and contamination during sampling, which can degrade the mirror reflectivity. The purge gas flow enters a glass cell and flows out the exhaust port. The flow of the purge gas must be taken into account to account for any dilution of the sample. A 1 inch CF flange quick disconnect adapter (275-1QD, Norcal) is used to connect the mirror mounts to a glass cell.

The advantage of using the quick disconnect adapter to couple the glass cell is that the length of the cell can easily be modified by interchanging the glass tubing. In the arrangement used in this setup the glass cell uses 3 inlet ports but the glass cell can easily be interchanged if more inlet ports are needed. The glass cell can easily be customized depending on the needs for the experiment. In addition the glass cell reduces the amount of metal surface that the nitrate radical will come in contact with. The glass cell described here is approximately 65 cm long, 2.54 inches in diameter, with a wall thickness of 1/16 inches. Three inlet tubes (3/8 inch diameter, 1/16 inch thick) are

constructed along the glass cell, which are used as an inlet port, an outlet port and as a port used to connect a pressure gauge (Cole Parmer). The cell has an approximate volume of 400 cm^3. Minimizing the volume of the cell decreases the residence time of the nitrate radical in the cell. The residence time is minimized in order to prevent lower concentration readings from possible radical termination when the nitrate radical comes in contact with the walls of the cell. Additionally, the glass cell was coated with halocarbon wax (Halocarbon Wax) to prevent radical termination from wall reactions. The halocarbon wax is prepared by mixing with dichloromethane solvent. The solution is then poured into the glass tube until the entire inner wall of the glass tube has been coated. The solution is left to dry overnight.

The transmitted light exiting the back mirror of the cell was refocused using a lens (1 inch diameter, f= 0.35 in) onto fiber optics attached to an SM1 converter (SM1SMA, Thorlabs). The SM1 converter is mounted onto an x-y translation stage (LM1XY, Thorlabs) used to align the fiber optic cable to the focal point of light exiting the cell. This allows for the maximum amount of light to be collected. The rear of the CEAS device is shown in Figure 5.2c to display the fiber optic alignment setup. The fiber optic from the translation stage is connected to the combined monochromator (SR-163, Andor Technology) and CCD (Idus, Andor Technology). The Andor spectrometer is equipped with a "round to line" fiber optic cable to maximize the light going through the entrance slit where the fibers are all aligned vertically for direct injection into the monochromator. The grating on the monochromator is 1200 lines/mm and the slit width on the monochromator is 25 μm, which provides a resolution of 0.46 nm fwhm. This is

consistent with the resolution of the spectrometer obtained using the HeNe line at 638 nm. The CCD is calibrated using the 638 nm HeNe line and the 579 nm line from a mercury lamp.

Many previous incoherent broadband cavity enhanced absorption arrangements have employed xenon arc lamps as their light source. However, over the past few years the performance of LEDs has improved with higher powered LEDs now available on the market. LEDs with an emission spectrum of a few tens of nanometers having a spectral range similar to that of the high reflectivity mirrors used for BBCEAS have become an alternative option to the more expensive and bulkier xenon arc lamps. Additionally, xenon arc lamps tend to suffer from a constant fluctuating light intensity, which is more difficult to control compared to an LED. An LED is used in the experimental setup described here. The incoherent light was provided by a red LED (JET-655-10, Roithner Lasertechnik) in the 662 nm region. The LED provided an emission at 655 nm, close to the absorption feature of NO_3 at 662 nm. The LED was mounted to an aluminum block that was temperature stabilized using a thermoelectric cooler (TEC) (TEC3-2.5, Thorlabs) mounted between the aluminum block and a heat sink. The temperature was monitored using a temperature controller via a temperature transducer (TH10K, Thorlabs) which was mounted on the aluminum block on the opposite end of the TEC to help maintain a uniform temperature throughout the aluminum block housing the LED. A schematic of the LED setup is shown in Figure 5.3. The temperature was stabilized to about 25 ^{o}C $\pm$ 0.001 ^{o}C by keeping the temperature controller to 10 kohm resistance. To aid the TEC in cooling, a cooling fan typically used in computers was mounted adjacent

to the LED. Without the temperature stabilization the emission peak of the LED shifts to higher wavelengths and the LED tends to suffer from fluctuations in light intensity. These shifts and fluctuations will cause the background to be inconsistent and will result in altered spectra typically having broad backgrounds, which must be accounted for in the spectral fitting procedure. The LED was operated from 500 to 700 mA, supplied by a combination laser diode driver/temperature controller (ITC500, Thorlabs). The electrical components including the LED, TEC, and temperature transducer were wired in house to the specifications of the diode driver and temperature controller.

Light from the LED was coupled directly from the mounted LED to the cell using two lenses, which is shown in Figure 5.2b to collimate the incoherent light through the first high reflectivity mirror. Previous methods have used a fiber optics cable[12] to transfer light from the LED directly into the cell through the front mirror but for our purpose it is unnecessary since the instrument will remain stationary for chamber measurements. Using fiber optics is ideal for situations in which measurements will be made during field campaigns where there is more of a need for instrument robustness as in measurements conducted from an aircraft. The fiber optic setup does have the advantage of being able to house the light source in a different location from the BBCEAS cell and simplifies the alignment procedure. The first lens (1 inch diameter, f= 0.35 in) was mounted in front of the LED to collect the majority of the uncollimated light as possible. This light was focused onto the front mirror using a second lens (2 inch diameter, f=1 inch). The coupling efficiency has been previously discussed. The key to

having good coupling efficiency is to have an LED with good surface luminance opposed to high power from the LED.

Alignment of the light within the cell is fairly straightforward. The first lens is placed close to the LED to collect the majority of the uncollimated light and the 1 inch lens is used to collimate the light onto the front of the cell. A key indicator to maximizing light intensity through the cavity is a profile of the LED that should be focused onto the lens placed behind the back mirror. This profile ensures that the LED has been collimated and focused and there will be maximum light intensity from the LED. Focusing the LED to the midpoint of the cell was also attempted and although this would be expected to be the best alignment of the light within the cavity, more light was collected if the LED was focused onto the rear mirror of the cell. The back mirror is then mounted and the back reflection is redirected back towards the LED to guarantee the light is on axis within the cavity and to reduce losses from stray light. This typically requires very little adjustment. The front mirror is then mounted and the back reflection is directed to the LED. As soon as the mirrors are properly aligned, the transmission signal from the cavity enhancement should become visible on the data collection software provided by Andor. Removal of the background is necessary when the instrumental software is operated to reduce excess noise from the surrounding room light leaking into the detector. The signal is optimized with fine adjustments on the o-ring mirror mounts until the signal intensity reaches a maximum.

5.5 Data Analysis

Data was acquired using the software provided by the Andor CCD detector. Data was then saved in ASCII file format for analysis offline using a custom program written in the laboratory using the Labview software. Spectra are obtained using the BBCEAS equation, which requires the transmission spectra without, I_o, and with, I, absorber and the mirror reflectivity at the 662 nm region. Fitting of the spectra obtained is similar to that used by Heitman et. al.[19] The spectral region containing the strong absorption feature of NO_3 at 662 nm is fitted using the NO_3 cross section from 655 nm to 675 nm. In addition to NO_3, the absorption features of NO_2 and water are also included in the fit and the number density or concentration is extracted for NO_3. It should be mentioned that the chamber experiments are typically carried out without any humidity. The unknown parameters are extracted using a linear algebraic method known as the singular value decomposition (SVD) method. The equation for the nonlinear polynomial fit is shown below:

$$a(\lambda) = b_0 + b_1\lambda + b_2\lambda^2 + n_{H_2O}\sigma_{H_2O}(\lambda) + n_{NO_3}\sigma_{NO_3}(\lambda) + n_{NO_2}\sigma_{NO_2}(\lambda) \qquad \textbf{[5.2]}$$

where, $a(\lambda)$, is the wavelength dependent absorption coefficient, σ, is the cross section of the absorbing molecule and, n, is the number density of each absorber. The background signal is represented by b_0, $b_1\lambda$, and $b_2\lambda^2$. The best spectral fit will have minimized the residuals from the experimental data. The output data provides number density information for the absorbers in the spectral region of interest, typically a few nanometers (~10 nm) in the 662 nm region.

5.6 College of Engineering Center for Environmental Research and Technology (CE- CERT) environmental chamber

Large environmental chambers have seen increased use within the last few years to gather information about the atmosphere in a controlled environment. Some of the key studies of interest have been on secondary organic aerosol (SOA) formation and the evaluation of chemical mechanisms and using the data to develop atmospheric models. The use of large environmental chambers minimizes surface losses along the walls of the chamber. At the University of California Riverside, the Bourns College of Engineering Center for Environmental Research and Technology (CE-CERT) has developed a facility equipped with two 90 m^3 collapsible FEP Teflon reactors on a pressure controlled moveable framework [20]. Arc lamps and blacklamps are used to simulate incident solar radiation and a multitude of instrumentation is used to sample from the chamber and collect data. Addition of a detector capable of measuring nitrate radical data would prove beneficial to providing data used for models.

A 2.5 micron filter (Savillex, 450-47-3) is used at the sample inlet since the instrument will be used to monitor NO_3 concentrations from various reactions yielding secondary organic aerosol and particulates. Additionally, using a filter protects residue from condensing onto the mirror surfaces, which can lead to degradation of mirror reflectivity and a reduced sensitivity. A sample flow rate of 8 lpm, is controlled using an orifice (O' Keefe) connected to a diaphragm pump. The high flow rate is used to reduce the residence time of the nitrate radical within the cell and to minimize wall losses as the

NO_3 is transported through the Teflon tubing (3/8 inch o.d.). Filter losses have been characterized before with typical losses of NO_3 of about 80 % transmission. The results obtained from filter studies conducted at the chamber are consistent with previous results.[21] Typical transmission values of NO_3 at the high concentrations used in the CE-CERT chamber range from 75-80 % transmission. Regular changing of the filters is recommended as transmission efficiency drops over the span of an experiment. It is recommended that the filters be changed on an hourly basis.

5.7 Instrument Calibration

In the setup, the CCD collects transmission spectra using an exposure time of 0.5 seconds with 240 samples accumulated for an overall sampling time of around 2 minutes. An exposure time of 0.5 seconds was chosen to prevent saturation of the signal at the peak LED emission spectrum at a maximum operating power of 500 mW. The CCD of the spectrometer saturates at a maximum count number of ~65,000 counts. To prevent saturation a shorter exposure time is used. Increasing the accumulation time will compensate for the shorter exposure time. To improve the signal to noise, 240 samples are accumulated. The background signal under the same acquisition conditions is collected with the LED off and the background is subtracted from the transmission spectra. A low intensity LED emission spectrum is shown in Figure 5.4.

To test the instrument, initial experiments were conducted using NO_2 considering the nitrate radical is more difficult to work with and difficult to generate. An easy system

to demonstrate the capability of the instrument is NO_2. The NO_2 spectrum (Voigt) exhibits sharp spectral features between 610 to 620 nm, with the most intense peak at around 612 nm (4.49×10^{-20} cm2/molecule) and at 641 and 646 nm. Typical cross sections of NO_2 in the 660 nm region are in the order of about 4×10^{-21} cm^2/molecule. This is four orders of magnitude smaller than the peak absorption of NO_3 at 662 nm (2.0×10^{-17} cm^2/molecule). Although NO_2 is being used here to characterize the instrument, the cross section of NO_2 is orders of magnitude smaller than NO_3 and should not interfere with measurements obtained in ambient air or the environmental chamber. With the LED used to provide the broadband light and the mirrors in the selected region, the spectrum ranges for about a few tens of nanometers from 600 to 680 nm.

To obtain the absorbance spectra, treatment of the spectral data must include wavelength dependent mirror reflectivity information. In previous studies, measurement of the mirror reflectivity has varied from using commercial spectrophotometers, offline using CRDS or variations of CRDS (PS-CRDS), using a known concentration of an absorber in the region of interest, or simply assuming a reflectivity based on commercial specs. Typically molecular oxygen bands or NO_2 are used to extrapolate mirror reflectivity data if the concentration is known. For this study, the mirror reflectivity obtained using off-line CRDS measurements yields a higher reflectivity than that from a BBCEAS measurement of NO_2 and/or using the water lines from humid air. The mirror reflectivity obtained using CRDS is approximately R= 99.994 % at 655 nm and is constant throughout the span of a few tens of nanometers. The typical ring-down time corresponding to this mirror reflectivity is ~ 43 μs. A sample spectrum using these high

reflectivity mirrors in an open path configuration is shown in Figure 5.5 and shows sharp water lines. The reflectivity obtained using the off-line CRDS measurement is much higher than using a known absorber to calibrate. Using NO_2, the typical reflectivity at 662 nm is about R=99.98 %. NO_2 from a gas cylinder (4.5 ppm) was diluted with nitrogen using a span gas calibrator to a few hundred ppb and then introduced into the BBCEAS cell. The reflectivity curve is shown in Figure 5.6. The reflectivity drops significantly as the wavelength decreases. However, the region of interest lies at 662 nm where NO_3 exhibits peak absorbance. In this region the mirror reflectivity is constant. As a comparison, the mirror reflectivity data is also extracted using the water vapor concentration present in the room. The water vapor concentration was determined using a hygrometer displaying relative humidity. The relative humidity in the room ranged from 34 % RH to 41 % RH. A relative humidity of 41 % corresponds to a number density of 2.66 x 10^{17} molecules/cm^3 for water. However, using a known NO_2 concentration as the calibration method is more reliable than using the water lines from humid air because of the broadening of the water spectrum under the sampling conditions of the spectrometer. The spectrometer does not possess the resolution to resolve the water spectral features and thus, the cross section must be deconvoluted for measurement purposes.

Using a calibration gas with a known concentration is expected to be a more reliable calibration method than CRDS because the different modes excited using CRDS might not be the same as those of the LED, which can yield a different reflectivity. Additionally, fewer losses are expected for CRDS than BBCEAS which results in a

higher reflectivity. The mirror reflectivity measured using both methods are unexpectedly lower than the manufacturer (Los Gatos) quoted reflectivity. In addition, the manufacturer reflectivity quotes a peak reflectivity at 635 nm, but from the measured reflectivity using NO_2 it seems the peak reflectivity plateaus at a constant reflectivity of 99.98 % at around 662 nm.

With the reflectivity data, absorbance spectra can be obtained. To demonstrate this, approximately 1 ppm of NO_2 is introduced into the BBCEAS cell. The typical cavity transmission spectrum is shown in Figure 5.7a, where both the transmission spectrum without absorber, I_o and with NO_2, I, is shown. The shape of the transmission signal observed is from a combination of the high reflectivity mirrors and the emission of the LED. In these spectra one can observe the dips in the signal corresponding to the absorption bands of NO_2. After the analysis of the transmission spectra using equation 5.1, the corresponding spectrum of NO_2 is shown in Figure 5.7b. The spectrum of NO_2 is plotted by its absorption coefficient and compared to the literature NO_2 spectrum. Similarly, NO_3 is generated and analyzed using BBCEAS to yield an absorbance spectrum of NO_3. Figure 5.8a shows the transmission spectrum without absorber, and the transmission spectrum below displays the dips in signal that indicate NO_3 is present in the cell. As in the sample NO_2 spectrum, the NO_3 absorbance spectrum is obtained by incorporating the wavelength dependent mirror reflectivity and is shown in Figure 5.8b. The concentration of the NO_3 spectrum is 1.28 ppb, well above typical ambient concentration levels to show the prominent absorbance bands of NO_3. The absorption features are consistent with the literature NO_3 spectrum in red.

5.8 Instrument Stability and Allan Variance

When performing high sensitivity measurements, it is important to consider the instrument stability. In theory, increasing the averaging of the signal will improve the sensitivity of the instrument. Typically the signal to noise ratio improves by $\sqrt{N}$ where N is the number of spectra that have been averaged. However, in real systems there are limitations due to signal drift from fluctuations in temperature, decreasing LED intensity, and fluctuations in background spectra, in addition to other factors. There is an optimum point in the averaging of signals where averaging more spectra will not improve the signal any more. To determine the optimal integration time for the instrument a statistical analysis known as the Allan variance is performed[22]. The Allan variance is also another way of predicting the limit of detection for an instrument.

To determine the instrument performance and stability a collection of baseline measurements for a BBCEAS cavity flushed with nitrogen is obtained. A BBCEAS data set of 1224 sample transmission spectra (I) is collected with an integration time of 2 seconds per data point. A transmission spectrum of 60 spectra (equivalent of 120 seconds integration time) flushed with nitrogen is used as the background transmission spectrum without absorber present within the cell, I_0. The data is processed using the SVD method used to retrieve the NO_3 concentration. The data represents baseline values without any NO_3 present in the cell. The baseline data set is then analyzed to obtain spectra with integration times ranging from 4 to 1200 seconds. The Allan variance is calculated using the equations below:

$$\left\langle \sigma^2{}_A(k) \right\rangle_t = \frac{1}{2m} \sum_{s=1}^{m} \left[A_{s+1}(k) - A_s(k) \right]^2 \quad \textbf{[5.3]}$$

$$A_s(k) = \frac{1}{k} \sum_{l=1}^{k} x_{(s-1)k+l} \quad \textbf{[5.4]}$$

$$s = 1,\ldots,m, m = m'-1$$

where the time average, $<\sigma^2{}_A(k)>_t$, is calculated from, m, the set of independent measurements, s, the subensemble number, and, k, the "binsize". In terms of the integration time, $\tau = k\Delta t$, where Δt, is the constant time interval of each k, which is 2 seconds in the study described here. Calculating $<\sigma^2{}_A(k)>_t$, and plotting against the integration time on a log-log plot gives the Allan-plot shown in Figure 5.9.

From the Allan plot, it can be seen that averaging of the signal improves the limit of detection up to about 200 to 300 seconds until further averaging does not improve the sensitivity any more. The Allan plot appears to stabilize between 10 and 100 seconds of integration time until it continues its downward trend towards a minimum. The minimum point along the Allan plot estimates that integrating the spectra over an integration time of 200 to 300 seconds will yield the best limit of detection for the instrument. The Allan variance (σ^2) is reported in units of ppb with the minimum of the Allan variance of $\sim 10^{-6}$ corresponding to a value of 1 ppt (1σ) at the optimum integration time of 200 to 300 seconds. However, under normal sampling conditions the limit of detection is expected to be slightly higher when taking other factors into account such as fitting of spectra, additional absorbers, and aerosol that may be transported past the filter. An integration

time for this study was chosen to be 2 minutes (120 seconds), which is approximately half the amount of time from the optimum integration time predicted by the Allan plot. For measurements in the environmental chamber where concentrations are typically in the high ppt to ppb range, an integration time of 2 minutes is a sufficient amount of time to resolve the NO_3 peak. For potential future ambient measurements, the optimal integration time of ~200 seconds should provide good time resolved data for the NO_3 radical at one sampling site. However for field measurements conducted in an aircraft, shorter integration times providing good instrument stability with low detection limits would be desired.

The study presented here using the Allan variance method helps to explain the BBCEAS instrument stability for measurements of NO_3. The measurements should be carried out at integration times of less than 200 seconds to ensure that instrumental drift does not affect the system's performance. A theoretical limit of detection of approximately 1 ppt is proposed under laboratory conditions.

5.9 Instrument Characterization at CE – CERT Chamber

To characterize the response of the BBCEAS detector, NO_3 was generated from the reaction of NO_2 and ozone inside a dark environmental chamber at CE-CERT. This is shown in Figure 5.10. Typical concentrations in the environmental chamber are carried out at higher levels than those observed in ambient air and thus the sensitivity is not critical for this experiment. In the chamber, the reaction levels out at a concentration

of around 4 ppb. N_2O_5 was then introduced into the environmental chamber producing NO_3 from thermal decomposition and a subsequent rise in signal is observed at around 200 minutes. The signal decreases over time signifying the radical is terminated from wall loss. Isoprene is then introduced into the chamber at around 310 minutes of the experiment and the NO_3 remaining becomes oxidized. Isoprene was selected for the model/demonstration as it is an important and relevant reaction observed in the atmosphere.[3, 23] Isoprene is considered one of the most abundant non methane hydrocarbons in the troposphere and its high reactivity to oxidants in the atmosphere such as NO_3 makes this a good test. The products from the oxidation of isoprene by NO_3 include alkyl nitrate formation and secondary organic aerosol.

Another experiment that is ongoing at CE-CERT involves the reaction of NO_3 with aldehydes and characterizing the products formed. The kinetics of NO_3 with aldehydes in the gas phase has been previously studied.[24-26] In addition, the solution phase kinetics of the nitrate radical in aqueous solutions have also been investigated[27]. A reaction of interest is the reaction of NO_3 with diethylamine (DEA). The typical reaction profile of NO_3 with DEA is shown in Figure 5.11a. N_2O_5 is introduced into the chamber followed by introduction of DEA. Over the span of the 12 hour experiment the NO_3 signal decreases from a peak of ~ 1 ppb until the reaction undergoes completion by following the reaction profile. As the NO_3 is completely reacted a low concentration signal corresponding to a number density of 3.1×10^9 molecules/cm^3 is shown in Figure 5.11b. This corresponds to 100 ppt. The polynomial curve has a fit of 10 ppt (1σ). This was determined from the residual of the polynomial curve fit with the low concentration

signal, which is shown in Figure 5.11c. The residuals are in units of absorption coefficient, cm^{-1} and the sensitivity is calculated using the peak absorption cross section of NO_3 at 662 nm (2.0×10^{-17} cm^2/molecule). Thus the lowest detectable signal for the instrument is approximately 10 ppt per 2 minutes of integration time.

5.10 Ambient Sample

An ambient measurement was taken using the same sampling conditions as those used for sampling from the environmental chamber. A flow rate of 8 liters per minute was used to sample air from an access door located on the second floor of the CE-CERT environmental chamber building. Aside from this door there is no access to outdoor air. The ambient sample was collected during the night time, when NO_3 is expected to be present. Figure 5.12 shows a sample collected over a 2 minute integration time. In the figure, there is no NO_3 present but the spectrum exhibits the vibrational overtones from water vapor present in the air sample. The relative humidity was measured as 40 % using a hygrometer. The measurements were taken on a night in August 2010 that experienced some precipitation throughout the night and most likely terminated the radical present in the atmosphere. Water exhibits features from 627 nm to 632 nm (not shown) and 640 nm to 660nm. Figure 5.13 shows the spectrum with water features from 650 nm to 660 nm. The water signal does not exhibit intense spectral features around the 662 nm region where NO_3 is expected. It should still be possible to distinguish the NO_3 absorption peak at 662 nm despite the presence of water. From the previous figure showing the low

concentration NO_3 signal, a concentration of 50 ppt would easily be discernible above the water signal. However, water is still considered an interfering species and its absorbance must be fit in order to extract the NO_3 concentration. The signal confirms the sensitivity of the BBCEAS spectrometer and suggests that the instrument is capable of measuring NO_3 with good sensitivity.

5.11 Conclusion

A sensitive and portable BBCEAS NO_3 detector using an inexpensive LED having a 10 ppt limit of detection over a sampling period of 2 minutes is presented. A detailed description of the construction and development of the NO_3 instrument based on BBCEAS is given. The instrument is based on an inexpensive LED and the cell was designed based on a simple o-ring design. The mirror mounts and sampling cell were machined in house as well as all the electrical components of the system. The instrument is similar to CRDS with the advantage of being able to extract spectral features to direct confirmation of the analyte of interest. The ability to measure multiple absorbers simultaneously is also possible. In the case of NO_3 measurements, NO_2 and water are two major absorbers in the region with NO_2 having a cross section three orders of magnitude smaller than NO_3 at 662 nm. The mirror reflectivity must be calibrated using a standard or known absorber with a known concentration in order to extract accurate concentration information for NO_3. NO_2 is the most common and reliable calibration gas to be used for mirror calibration. Laboratory measurements in addition to environmental

chamber measurements of NO_3 reacting with isoprene and diethyl amine are performed to demonstrate the instrument's capability. The reaction of NO_3 with amines continues to be an ongoing project at the CE-CERT environmental chamber. Ambient measurements were attempted and a sample spectrum shows the significance of water vapor during ambient sampling. The sensitivity is expected to improve with higher reflectivity mirrors. Future experiments can include measurements of N_2O_5 by thermal dissociation.

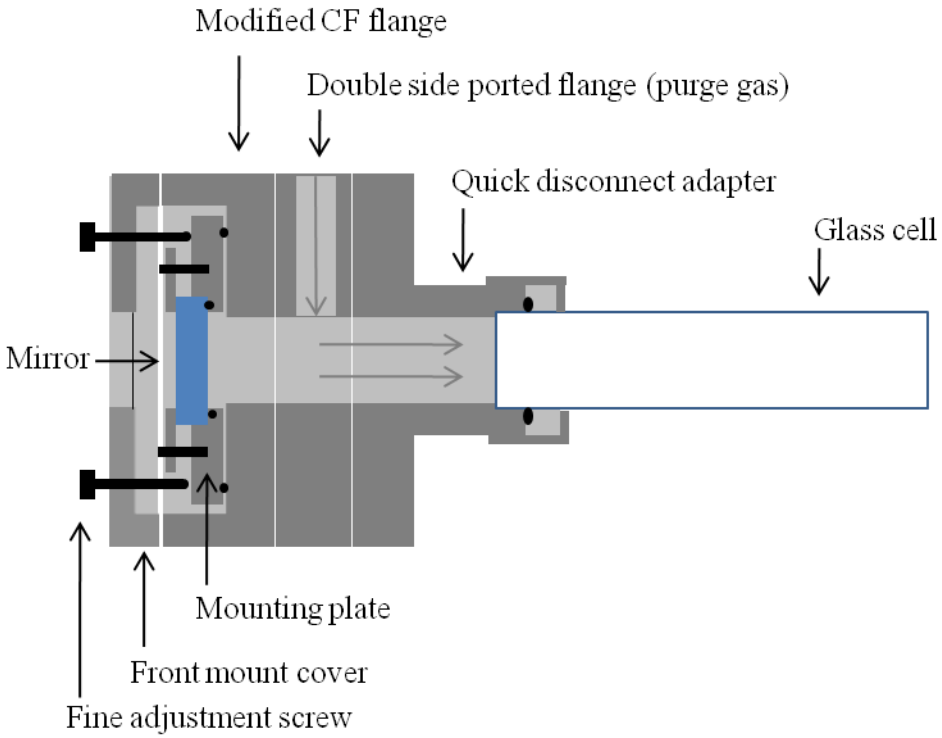

Figure 5.1: Schematic of the o-ring based mirror mounts used for NO_3 measurements. The mirror window area is maximized to allow the maximum intensity of light from an LED into the cell. The mount is designed to be used with commercial conflate flanges.

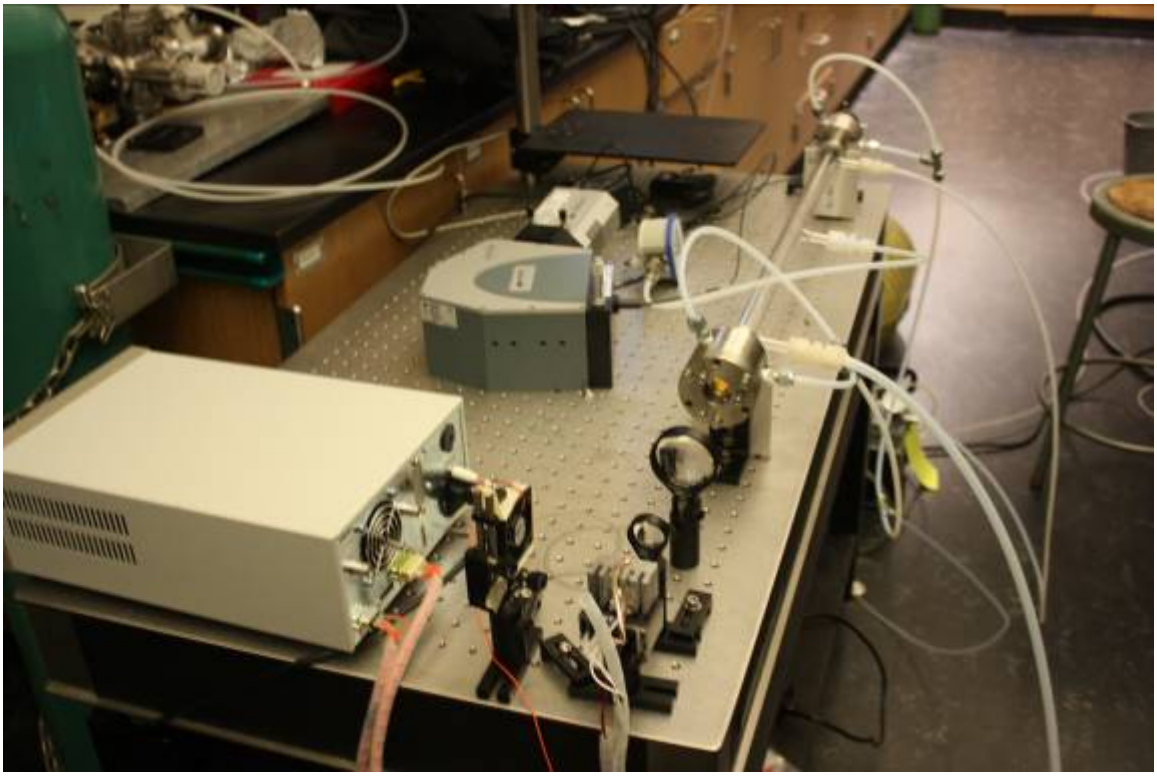

Figure 5.2a: Broadband Cavity Enhanced Absorption Spectroscopy (BBCEAS) of NO_3. The instrument is mounted on a portable laser table.

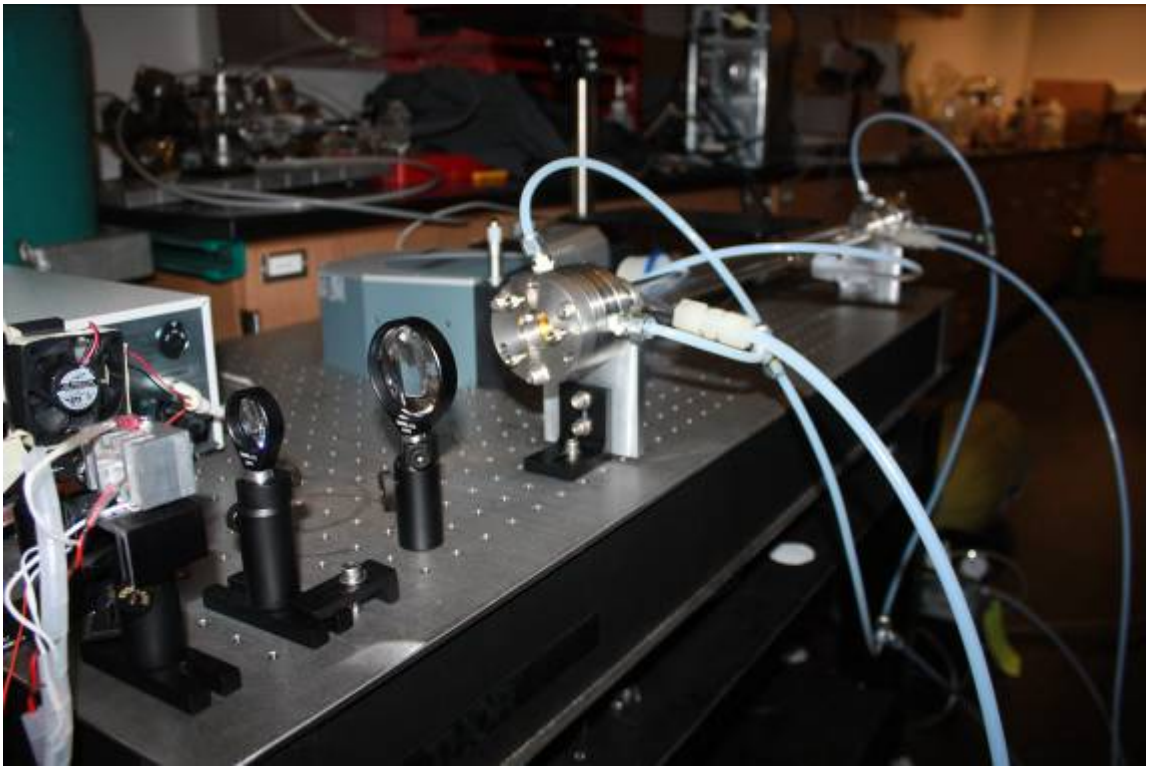

Figure 5.2b: Close up view of the BBCEAS instrument. The LED is mounted on a thermally controlled aluminum block. Two lenses are used to focus the light into the front mirror of the cavity.

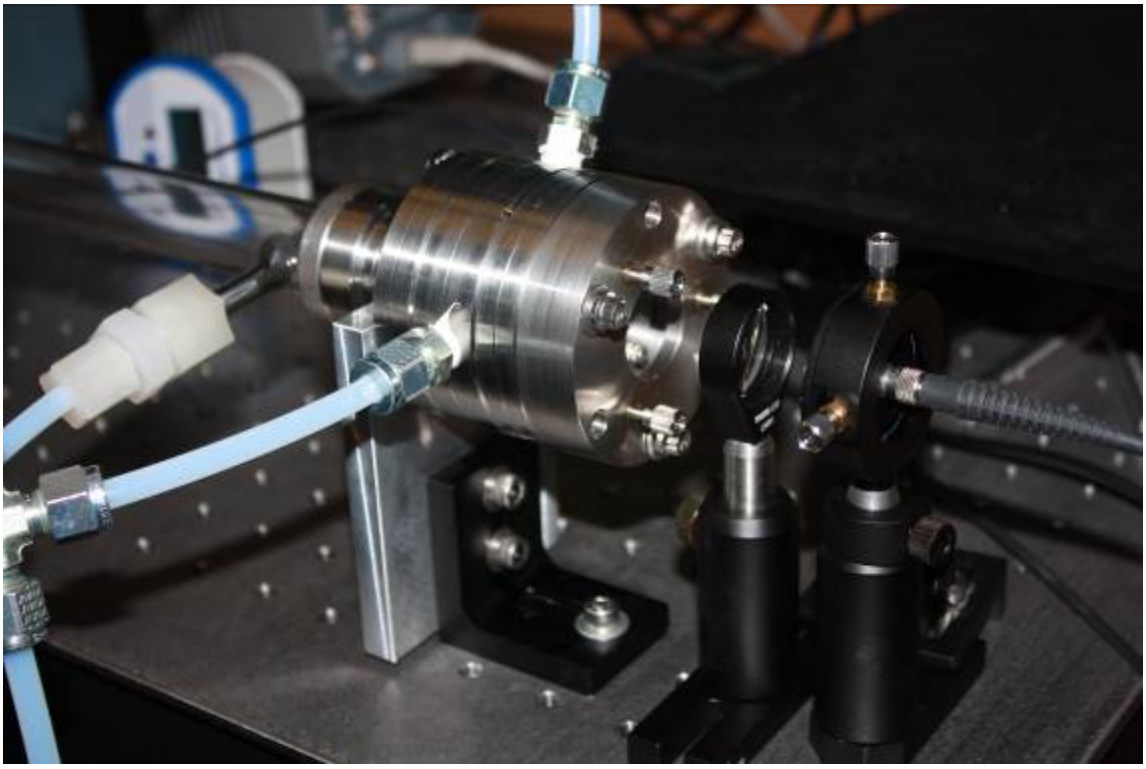

Figure 5.2c: Close up view from the back mirror of the cell. The light exiting the back mirror is refocused onto a fiber optic on a translational mount.

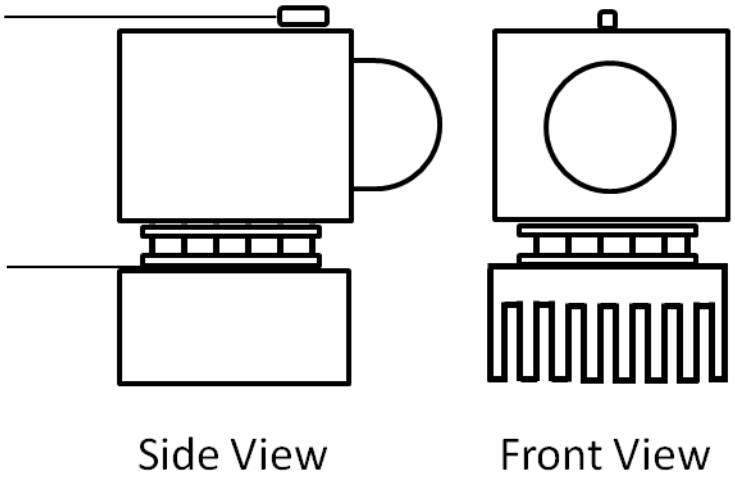

Figure 5.3: Schematic of the LED used for BBCEAS of NO_3. The LED is mounted to an aluminum block and the temperature is stabilized by the thermoelectric cooler (TEC) mounted to the bottom. The heat sink helps dissipate the heat released by the TEC. The temperature is measured using the temperature transducer mounted above the aluminum block.

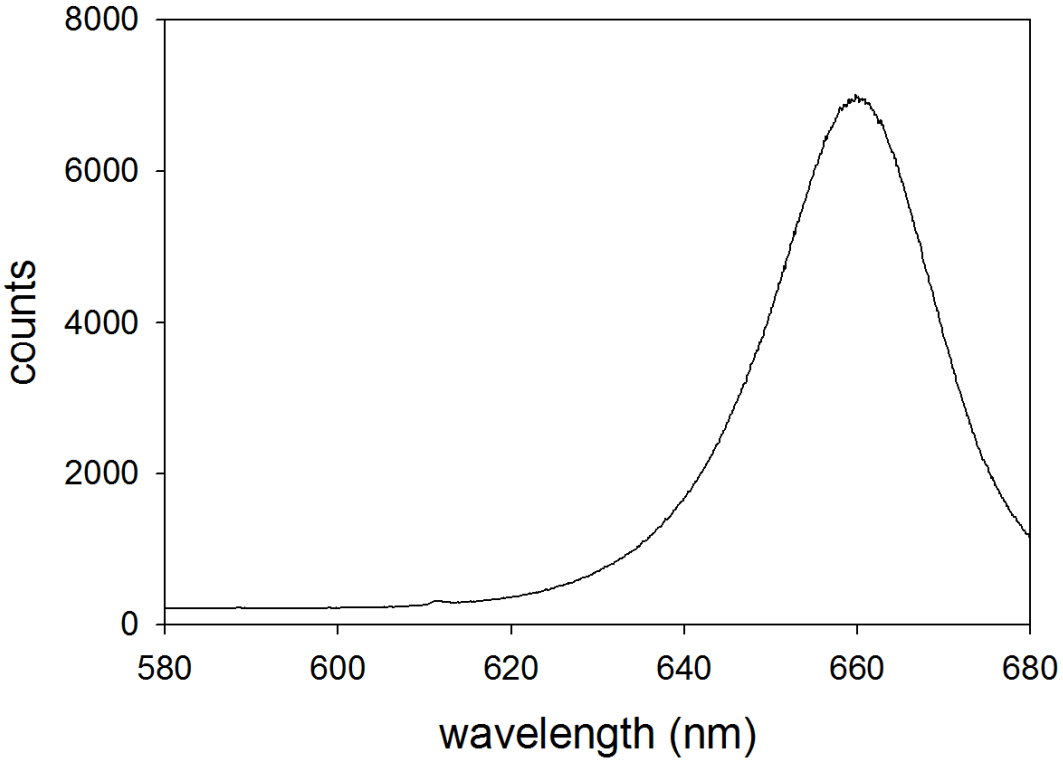

Figure 5.4: LED emission spectrum used for BBCEAS measurements of the NO_3 radical. LED emission peaks at ~660 nm, close to the NO_3 absorption peak at 662 nm.

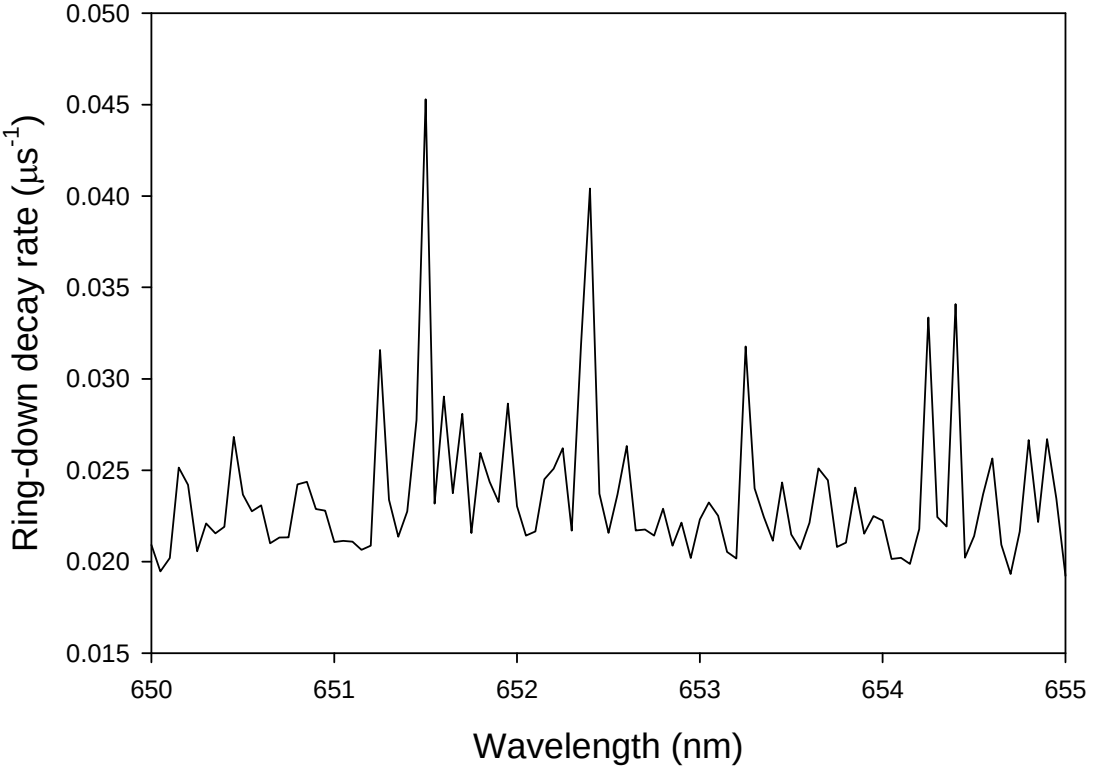

Figure 5.5: Mirror scan obtained using CRDS offline. The sharp peaks are due to water vapor in the room. The spectrum was obtained using an open path configuration. The reflectivity values obtained using CRDS are typically higher than using a standard.

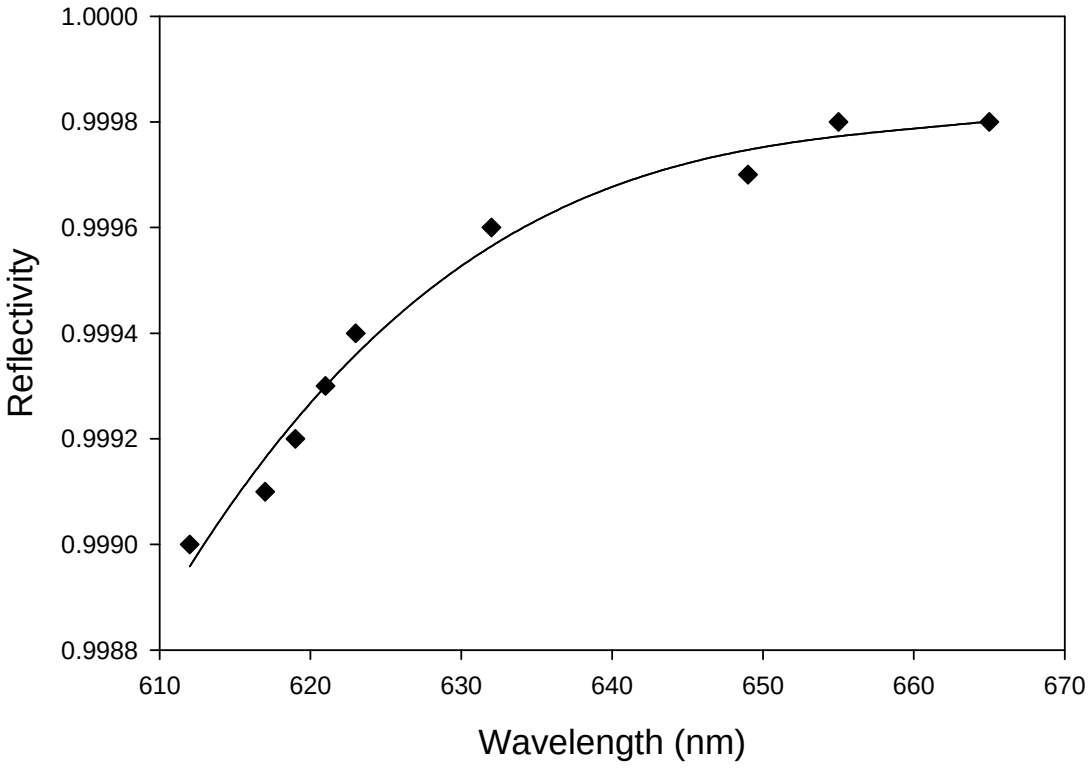

Figure 5.6: Mirror reflectivity calibrated using an NO_2 standard. The mirror reflectivity is R = 0.9998 at 662 nm, where NO_3 has peak absorbance.

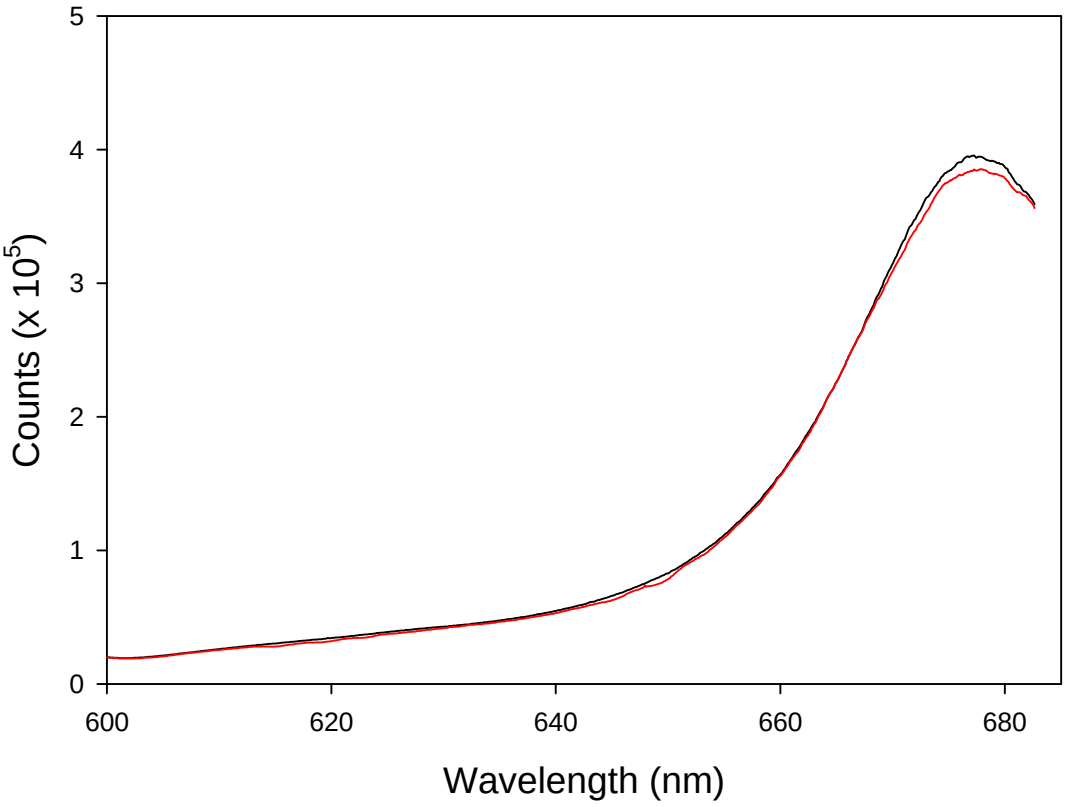

Figure 5.7a: Transmission spectra of IBBCEAS without absorber, I_0, and NO_2, I.

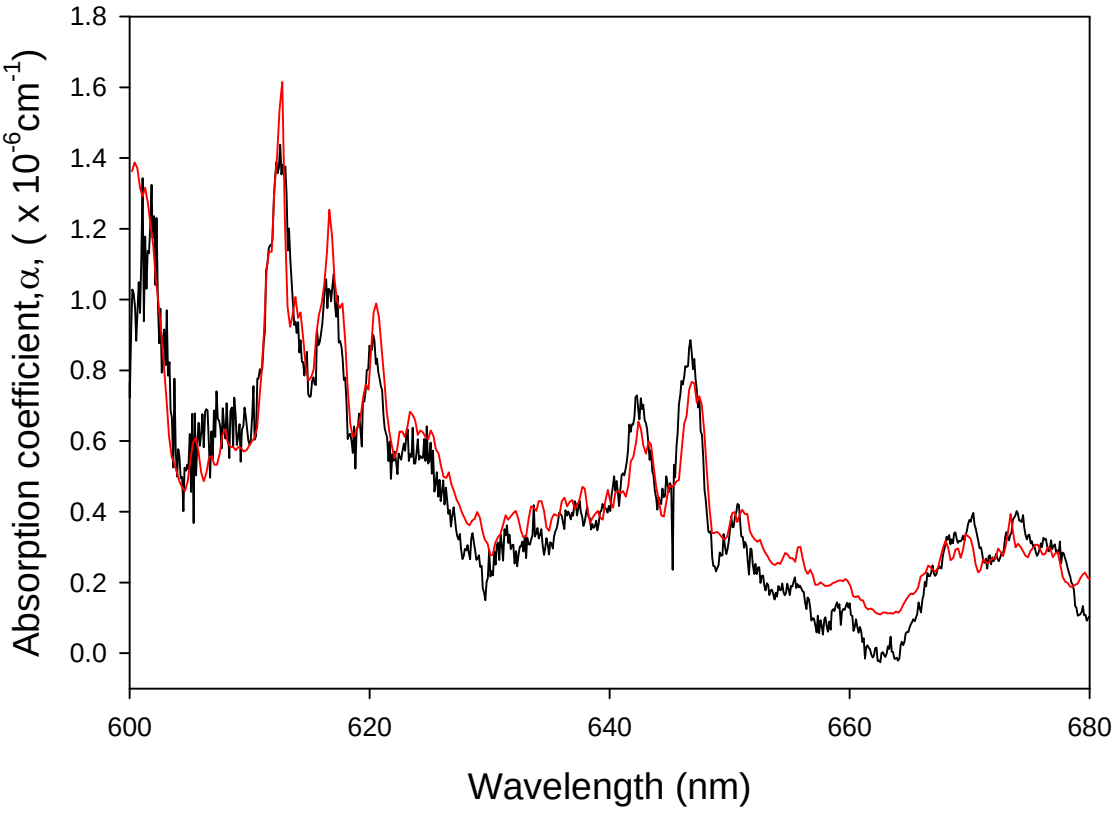

Figure 5.7b: IBBCEAS spectrum of NO_2 (black) and NO_2 reference spectrum from Voigt et. al. (red)

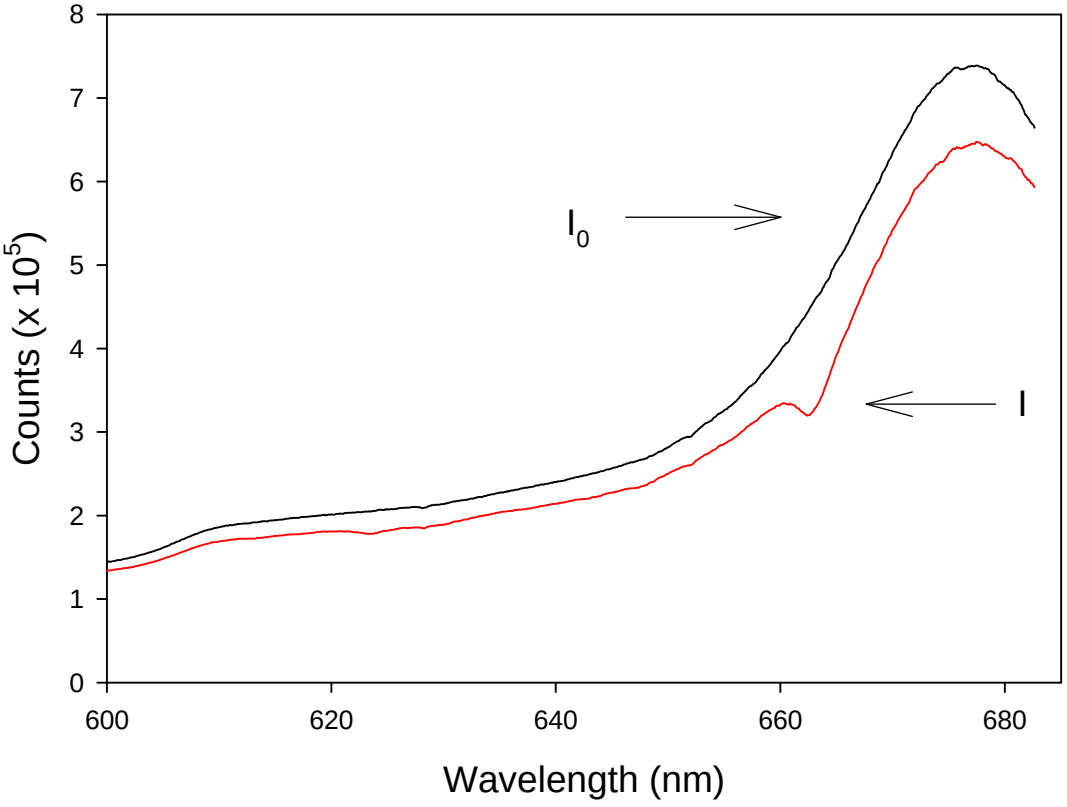

Figure 5.8a: BBCEAS transmission spectrum of high concentration (1.28 ppb) NO_3. The dips on the I spectrum signify NO_3 absorbance at 662 nm and 623 nm.

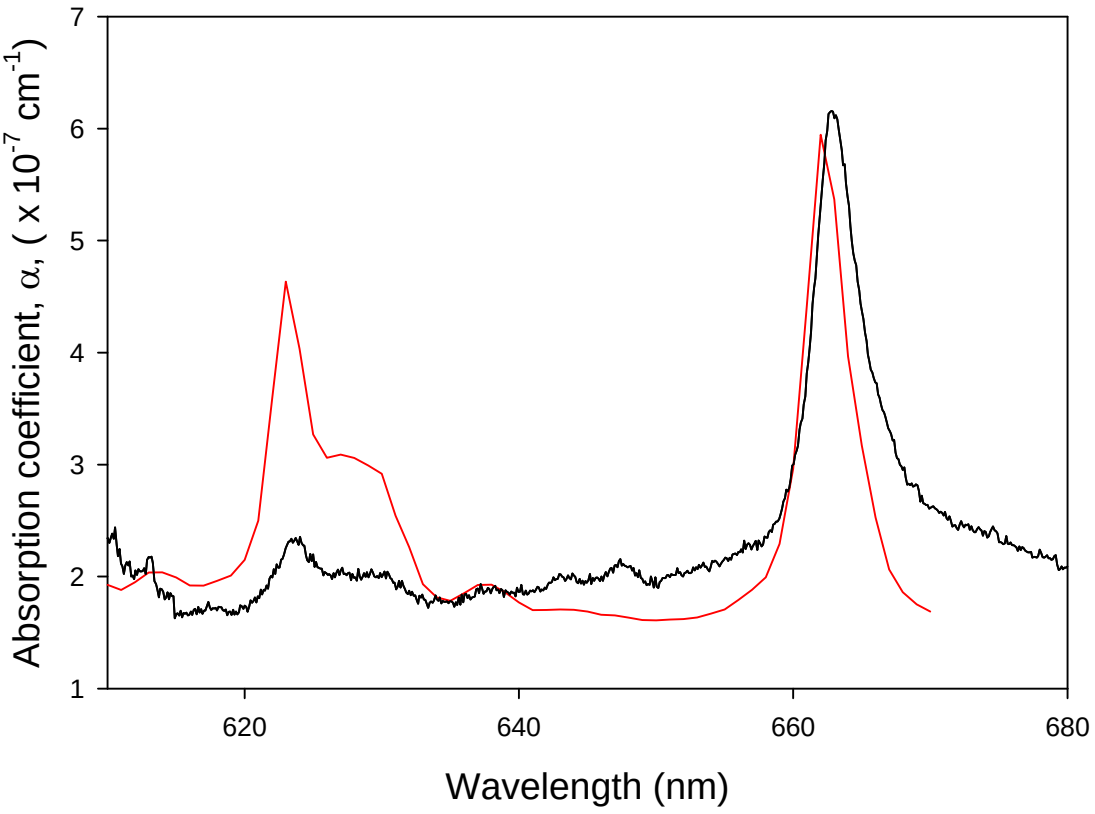

Figure 5.8b: BBCEAS absorbance spectrum (black trace) of high concentration (1.28 ppb) NO_3. NO_3 spectrum exhibits peak absorbance at 662 nm and 623 nm. The red trace is the literature NO_3 spectrum used for comparison.

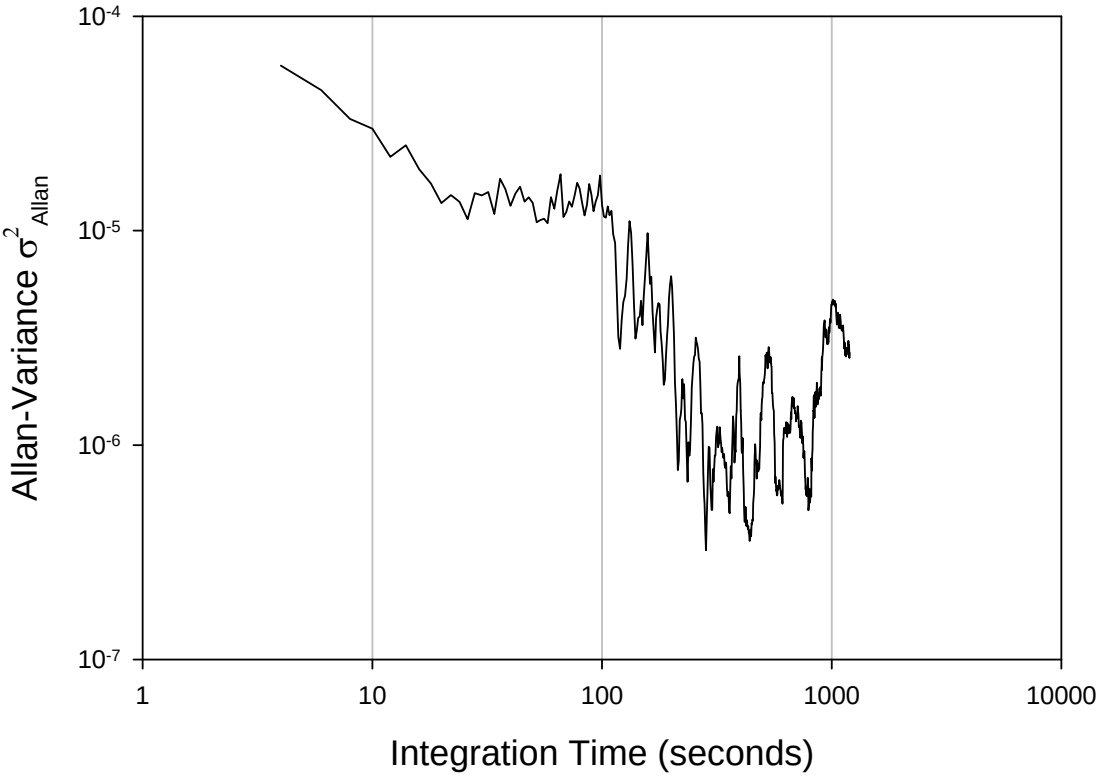

Figure 5.9: Allan-plot of the BBCEAS instrument for NO_3 measurements. 1100 baseline measurements with nitrogen gas in the cell are collected and using the Allan variance procedure an optimum integration time of ~200 seconds is predicted for the instrument. The optimum theoretical sensitivity for the instrument is predicted to be 1 ppt NO_3.

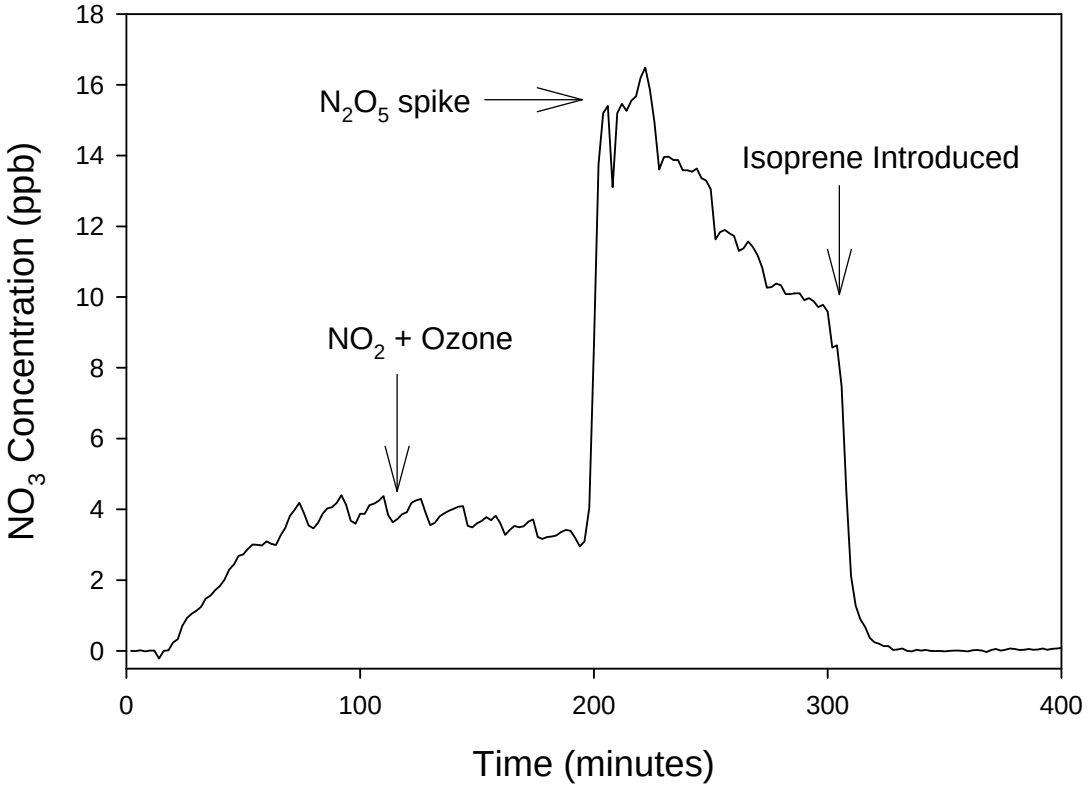

Figure 5.10: NO_3 measurement conducted at CE-CERT chamber.

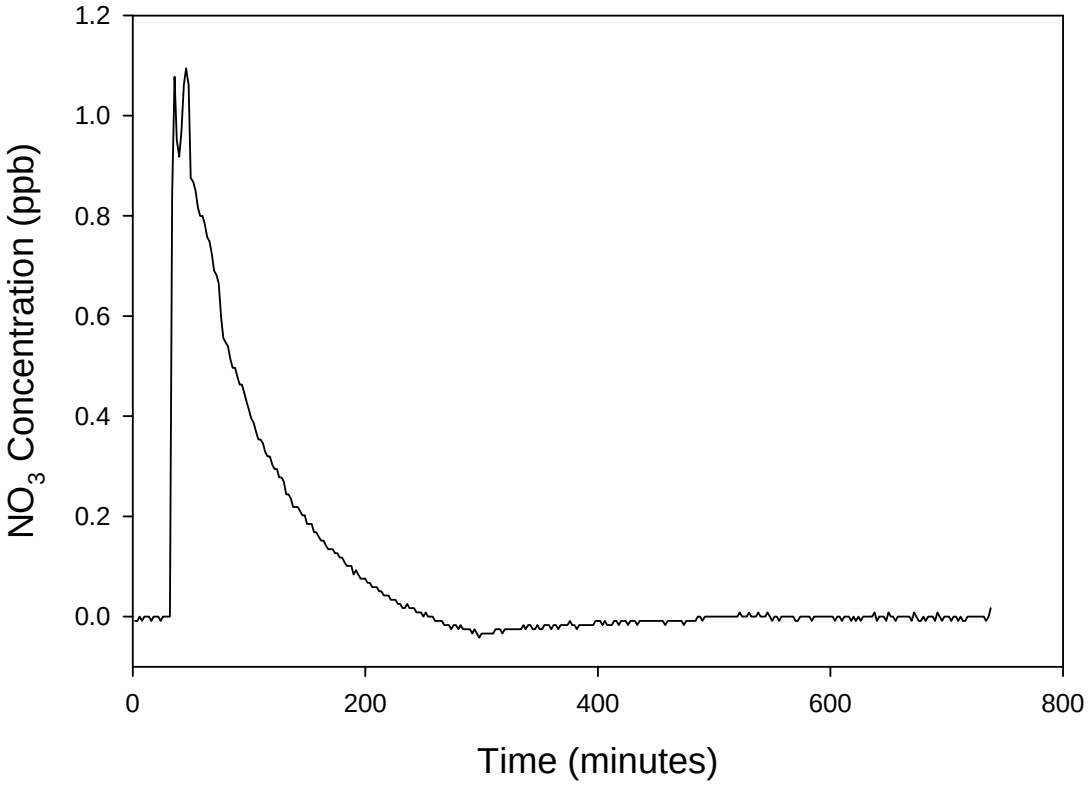

Figure 5.11a: NO_3 measurement conducted at CE CERT chamber. Signal disappears due to the reaction with an amine.

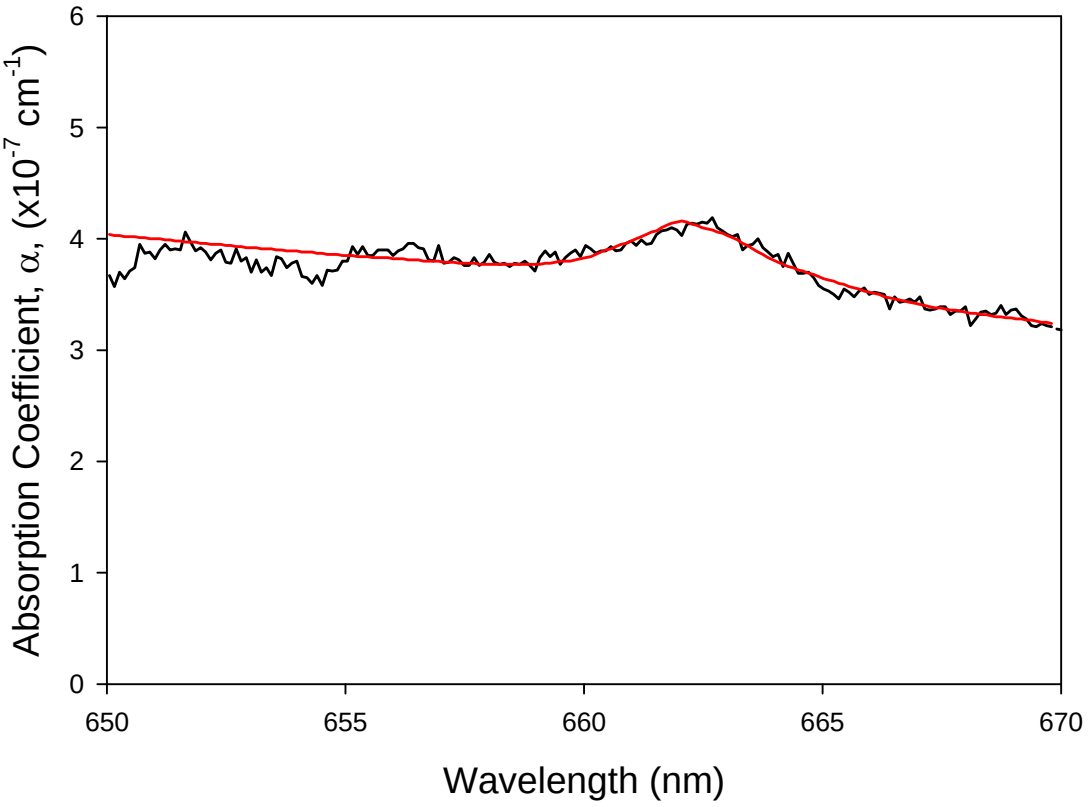

Figure 5.11b: Low concentration NO_3 signal at 662 nm from the amine chamber study at ~200 minutes of the run. The literature cross section of NO_3 is fit to the signal. The signal corresponds to a number density of 3.1 x10^9 molecules/cm^3.

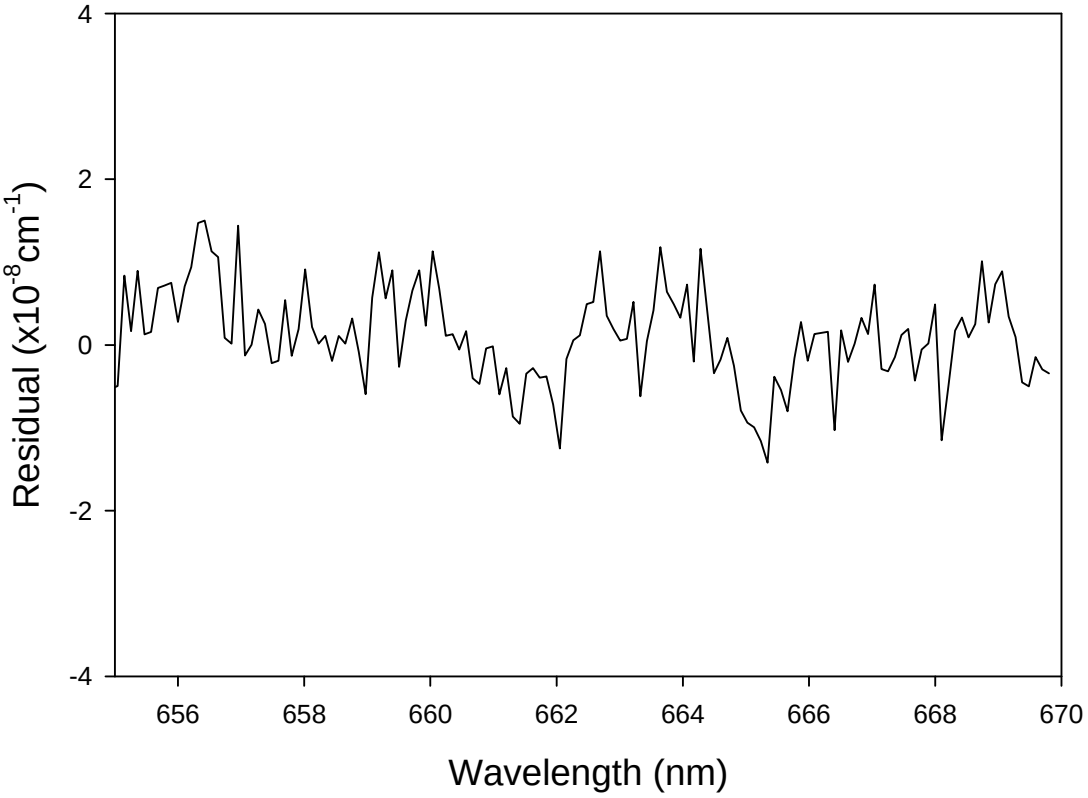

Fig 5.11c: Residual intensity from the polynomial curve fit from Figure 5.6b. The residuals correspond to a sensitivity of 11 ppt (1σ)

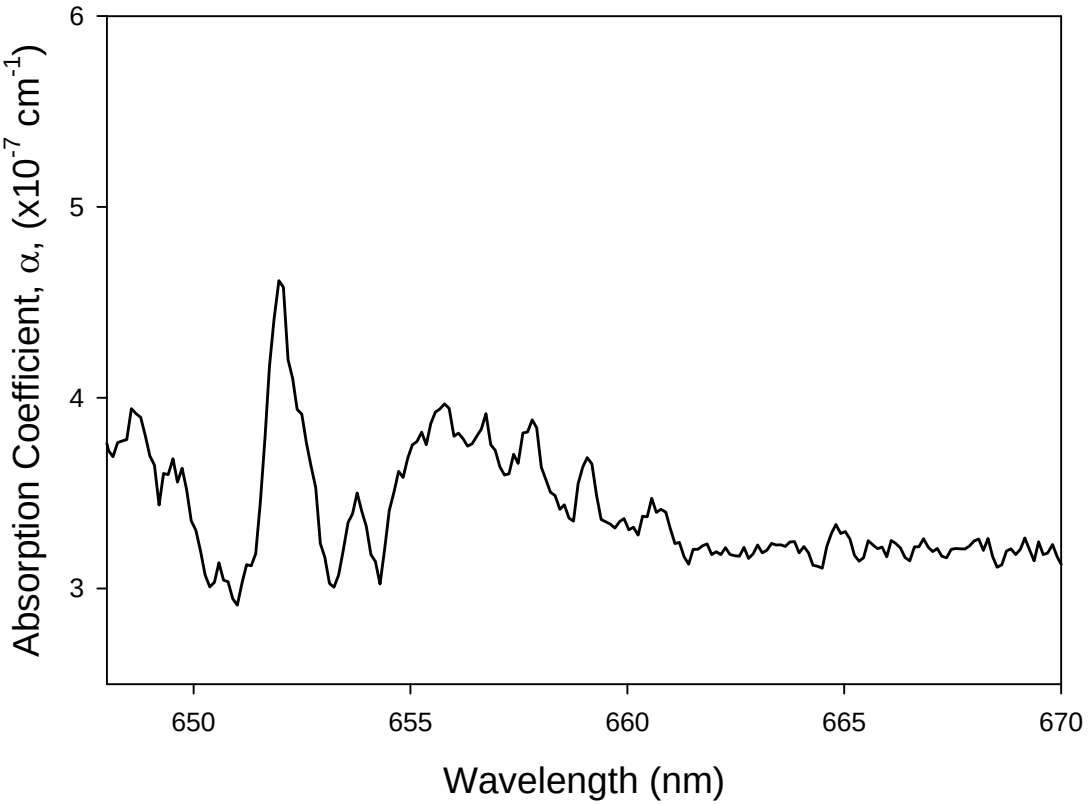

Figure 5.12: BBCEAS Ambient sample. The spectrum exhibits water features but no NO_3 is present.

5.12 References

1. Finlayson-Pitts, B. J.; Pitts, J. N., *Chemistry of the Upper and Lower Atmosphere*. Academic Press: 2000.

2. Brown, S. S.; Ryerson, T. B.; Wollny, A. G.; Brock, C. A.; Peltier, R.; Sullivan, A. P.; Weber, R. J.; Dube, W. P.; Trainer, M.; Meagher, J. F.; Fehsenfeld, F. C.; Ravishankara, A. R., Variability in nocturnal nitrogen oxide processing and its role in regional air quality. *Science* **2006,** *311* (5757), 67-70.

3. Rollins, A. W.; Kiendler-Scharr, A.; Fry, J. L.; Brauers, T.; Brown, S. S.; Dorn, H. P.; Dube, W. P.; Fuchs, H.; Mensah, A.; Mentel, T. F.; Rohrer, F.; Tillmann, R.; Wegener, R.; Wooldridge, P. J.; Cohen, R. C., Isoprene oxidation by nitrate radical: alkyl nitrate and secondary organic aerosol yields. *Atmospheric Chemistry and Physics* **2009,** *9* (18), 6685-6703.

4. Fry, J. L.; Kiendler-Scharr, A.; Rollins, A. W.; Wooldridge, P. J.; Brown, S. S.; Fuchs, H.; Dube, W.; Mensah, A.; dal Maso, M.; Tillmann, R.; Dorn, H. P.; Brauers, T.; Cohen, R. C., Organic nitrate and secondary organic aerosol yield from NO_3 oxidation of beta-pinene evaluated using a gas-phase kinetics/aerosol partitioning model. *Atmospheric Chemistry and Physics* **2009,** *9* (4), 1431-1449.

5. Platt, U.; Perner, D.; Winer, A. M.; Harris, G. W.; Pitts, J. N., Detection of NO_3 in the polluted troposphere by differential optical-absorption. *Geophysical Research Letters* **1980,** *7* (1), 89-92.

6. Brown, S. S.; Stark, H.; Ravishankara, A. R., Cavity ring-down spectroscopy for atmospheric trace gas detection: application to the nitrate radical (NO_3). *Applied Physics B-Lasers and Optics* **2002,** *75* (2-3), 173-182.

7. Brown, S. S.; Stark, H.; Ciciora, S. J.; McLaughlin, R. J.; Ravishankara, A. R., Simultaneous in situ detection of atmospheric NO_3 and N_2O_5 via cavity ring-down spectroscopy. *Rev. Sci. Instrum.* **2002,** *73* (9), 3291-3301.

8. Ayers, J. D.; Apodaca, R. L.; Simpson, W. R.; Baer, D. S., Off-axis cavity ringdown spectroscopy: application to atmospheric nitrate radical detection. *Appl. Optics* **2005,** *44* (33), 7239-7242.

9. Ball, S. M.; Langridge, J. M.; Jones, R. L., Broadband cavity enhanced absorption spectroscopy using light emitting diodes. *Chemical Physics Letters* **2004,** *398* (1-3), 68-74.

10. Venables, D. S.; Gherman, T.; Orphal, J.; Wenger, J. C.; Ruth, A. A., High sensitivity in situ monitoring of NO_3 in an atmospheric simulation chamber using incoherent broadband cavity-enhanced absorption spectroscopy. *Environmental Science & Technology* **2006,** *40* (21), 6758-6763.

11. Triki, M.; Cermak, P.; Mejean, G.; Romanini, D., Cavity-enhanced absorption spectroscopy with a red LED source for NOx trace analysis. *Applied Physics B-Lasers and Optics* **2008,** *91* (1), 195-201.

12. Langridge, J. M.; Ball, S. M.; Shillings, A. J. L.; Jones, R. L., A broadband absorption spectrometer using light emitting diodes for ultrasensitive, in situ trace gas detection. *Rev. Sci. Instrum.* **2008,** *79* (12), 14.

13. Benton, A. K.; Langridge, J. M.; Ball, S. M.; Bloss, W. J.; Osto, M. D.; Nemitz, E.; Harrison, R. M.; Jones, R. L., Night-time chemistry above London: measurements of NO_3 and N_2O_5 from the BT tower. *Atmos. Chem. Phys.* **2010,** *10*, 9781-9795.

14. Meinen, J.; Thieser, J.; Platt, U.; Leisner, T., Technical Note: Using a high finesse optical resonator to provide a long light path for differential optical absorption spectroscopy: CE-DOAS. *Atmospheric Chemistry and Physics* **2010,** *10*, 3901-3914.

15. Karagullan, F.; Santschi, C.; Rossi, M. J., The heterogeneous chemical kinetics of N_2O_5 on $CaCO_3$ and other atmospheric mineral dust surrogates. *Atmos. Chem. Phys.* **2005,** *5*, 10369-10408.

16. Canosa-Mas, C. E.; King, M. D.; McDonnell, L.; Wayne, R. P., An experimental study of the gas-phase reactions of the NO3 radical with pent-1-ene, hex-1-ene and hept-1-ene. *PCCP Phys. Chem. Chem. Phys.* **1999,** *1* (11), 2681-2685.

17. Muller, T.; Wiberg, K. B.; Vaccaro, P. H., An optical mounting system for cavity ring-down polarimetry. *Rev. Sci. Instrum.* **2002,** *73* (3), 1340-1342.

18. Schuster, G.; Labazan, I.; Crowley, J. N., A cavity ring down/cavity enhanced absorption device for measurement of ambient NO_3 and N_2O_5. *Atmos. Meas. Tech.* **2009,** *2* (1), 1-13.

19. Heitmann, U.; Ruth, A. A.; Varma, R. M.; Venables, D. S. *Air Pollution - Trace Radical Absorption through Cavity-Enhanced Spectroscopy (TRACES)*; 2008.

20. Carter, W. P. L.; Cocker, D. R.; Fitz, D. R.; Malkina, I. L.; Bumiller, K.; Sauer, C. G.; Pisano, J. T.; Bufalino, C.; Song, C., A new environmental chamber for evaluation of gas-phase chemical mechanisms and secondary aerosol formation. *Atmospheric Environment* **2005,** *39* (40), 7768-7788.

21. Fuchs, H.; Dube, W. P.; Cicioira, S. J.; Brown, S. S., Determination of inlet transmission and conversion efficiencies for in situ measurements of the nocturnal nitrogen oxides, NO_3, N_2O_5 and NO_2, via pulsed cavity ring-down spectroscopy. *Analytical Chemistry* **2008,** *80* (15), 6010-6017.

22. Werle, P.; Mucke, R.; Slemr, F., The Limits of Signal Averaging in Atmospheric Trace-Gas Monitoring by Tunable Diode-Laser Absorption Spectroscopy (TDLAS). *Appl. Phys.* **1993,** *B57*, 131-139.

23. Perring, A. E.; Wisthaler, A.; Graus, M.; Wooldridge, P. J.; Lockwood, A. L.; Mielke, L. H.; Shepson, P. B.; Hansel, A.; Cohen, R. C., A product study of the isoprene+NO_3 reaction. *Atmospheric Chemistry and Physics* **2009,** *9* (14), 4945-4956.

24. Carter, W. P. L.; Winer, A. M.; Pitts, J. N., Jr., Major atmospheric sink for phenol and the cresols. Reaction with the nitrate radical. *Environ. Sci. Technol.* **1981,** *15*, 829-831.

25. Atkinson, R.; Plum, C. N.; Carter, W. P. L.; Winer, A. M.; Pitts, J. N., Jr, Rate constants for the gas-phase reactions of nitrate radicals with a series of organics in air at 298 $\pm$ 1 K. *J. Phys. Chem.* **1984,** *88*, 1210-1215.

26. Cantrell, C. A.; Stockwell, W. A.; Anderson, L. G.; Busarow, K. L.; Perner, D.; Schmeltekopf, A.; Calvert, J. G.; Johnston, H. S., Kinetic study of the NO_3-CH_2O reaction and its possible role in nighttime tropospheric chemistry. *J. Phys. Chem.* **1985,** *89*, 139-146.

27. Osamu, I.; Akiho, S.; Iino, M., Kinetics for reactions of the nitrate radical (NO_3) with aldehydes in acetonitrile. *J. Phys. Chem.* **1989,** *93*, 4079-4083.

Chapter 6

Detection of Nitrous Acid (HONO) by Broadband Cavity Enhanced Absorption Spectroscopy

6.1 Abstract

The photolysis of nitrous acid is a major source of the hydroxyl radical (OH) in the troposphere. Currently, HONO formation in the atmosphere is not well understood but the heterogeneous hydrolysis of NO_2 is believed to be a major contributor. Instrumentation that can be used to provide insights into the formation of HONO is needed. Near-UV broadband cavity enhanced absorption spectroscopy (BBCEAS) has been developed to measure HONO in the 368 nm region using an inexpensive, high powered light emitting diode (LED). HONO and NO_2 are measured simultaneously and a limit of detection of 10 ppb (1σ) for an integration time of 2 minutes for HONO is demonstrated.

6.2 Introduction

The photolysis of nitrous acid (HONO) in the early morning is considered a major source of the hydroxyl radical (OH) in the troposphere[1]. The OH radical drives daytime chemistry in the troposphere by initially oxidizing volatile organic compounds (VOCs) which can further react to produce peroxyl radicals, leading to the formation of many atmospheric pollutants including, peroxy nitrates, alkyl nitrates and ozone. HONO is also a major indoor air pollutant and is known to react with amines to form carcinogenic nitrosamines[2]. HONO has been studied extensively, with the first ambient measurements of HONO made by Perner and Platt[3]. Typical ambient concentrations of HONO range from about 0.1 ppb to 10 ppb. Of major interest has been the mechanism for the formation of HONO in ambient air. The major source of HONO is believed to be the heterogeneous reaction of NO_2 with water on surfaces[4]:

$$2NO_2 + H_2O \xrightarrow{surface} HONO + HNO_3 \qquad \textbf{[6.1]}$$

The surfaces needed for this reaction include aerosol particles, glass, soil, foliage, and concrete among many others. There have been many studies investigating the heterogeneous hydrolysis of NO_2 [5, 6] and there is a need for future studies of the HONO system to better understand the mechanism for formation. Additionally, having

instrumentation that is capable of measuring HONO at the ambient level and improving our understanding of the atmosphere is important.

HONO has many spectroscopic features in the near UV and these absorption bands have been used for HONO measurements. The most commonly used spectroscopic instrument used for HONO measurements has been differential optical absorption spectroscopy (DOAS).[3, 7-9] DOAS has the capability of measuring multiple trace species in a wide spectral region. To achieve low limits of detection (ppt level over minutes of integration) a long optical pathlength is needed. Typically for DOAS measurements a pathlength of several kilometers is required. The disadvantage of this set up is that the measurement is an average over the entire column sampled. Additionally, when laboratory measurements are desired, the DOAS setup is not ideal. Instead, infrared spectroscopy is typically used for laboratory HONO experiments, notably heterogeneous hydrolysis experiments[5, 6] but lacks sensitivity. HONO has also been measured in the laboratory by cavity ring-down spectroscopy (CRDS) having a limit of detection in the range of ambient measurements of ~5 ppb in 15 seconds.[10] However, there are multiple absorbers in the near UV region and CRDS is not capable of distinguishing the signal contribution from a particular absorber. For instance, NO_2 absorbs in the same region as HONO and unless the CRDS is equipped with broadband capabilities or HONO is selectively removed using a denuder, measurements are difficult. CRDS is best suited for laboratory experiments without any NO_2 present. Photofragmentation/Laser induced fluorescence (PF-LIF) measurements of HONO by way of detection of OH from the photodissociation of HONO has also been used.[11]

HONO has also been measured by wet chemical methods. Annular diffusion denuders coated with sodium carbonate have been used to collect HONO where it reacts to form NO_2^-.[8, 12] The NO_2^- is then extracted and analyzed using ion chromatography. The annular denuder method lacks selectivity, and NO_2 and peroxy acetyl nitrate (PAN) are known interfering species resulting in a positive bias as they form NO_2^- along the walls of the denuder. The HONO data retrieved from the denuder method is a measurement over the entire period sampled and lacks the capability for real time monitoring. An in situ technique known as long path absorption photometry (LOPAP) measuring HONO by wet sampling of ambient air, conversion to an azo dye and subsequent photometric detection has been developed with detection limits ranging from 3 to 50 pptv/ 4 minutes[13].

Commercial chemiluminescent NO_x analyzers have also been used for HONO measurements[14]. The technique collects HONO through a scrubber made of alkaline solution forming NO_2^- and is then reduced to NO and measured using the NO_x analyzer. However, the method is susceptible to interference from NO_2 and PAN since these species also form NO_2^- in alkali solution.

Incoherent broad band cavity enhanced absorption spectroscopy (IBBCEAS) has recently been developed and allows for sensitive trace gas measurements providing a long pathlength in a compact setup [15]. The broadband light source from an arc lamp or LED allows for the capability for multiple absorbing species simultaneously. Most BBCEAS instruments developed have measured atmospheric pollutants in the visible

region, such as NO_2[16] and NO_3 [17-19]. Recently, high powered LEDs have become available in the near UV region and this has extended the technique towards another key atmospheric species, HONO [20]. The instrument described here is based on the method for simultaneous detection of HONO and NO_2 in the near UV region recently reported [20]. The goal is to design an instrument that is capable of measuring HONO during environmental chamber studies or laboratory studies aimed at studying sources of HONO formation such as in heterogeneous hydrolysis experiments.

6.3 Experimental

The near UV light was provided by a high powered UV LED (Nichia) in the 365 nm region. The LED had a Gaussian emission peak at 365, which covered two HONO absorption peaks at 354 nm and 365 nm. The LED was mounted to a temperature controlled aluminum plate and the temperature of the LED was stabilized using a thermoelectric cooler (TEC) (TEC3-2.5, Thorlabs), which is mounted onto a heat sink to maintain a stable temperature. The temperature was monitored using a temperature controller via a temperature transducer (TH10K, Thorlabs) also mounted on the aluminum block. The temperature was stabilized to about 25 ^{o}C $\pm$ 0.001 ^{o}C by keeping the temperature controller to 10 kohm resistance. The LED was operated at 10 mA, supplied by a combination laser diode driver/temperature controller (ITC500, Thorlabs). The maximum current for the LED is 700 mA but saturation of the signal is observed at currents above the set current. Saturation of the signal will result in distorted spectra. Light from the LED was coupled directly from the mounted LED to the BBCEAS cell

using two lenses (2 inch diameter, f = 1 inch) to collimate the incoherent light. The set up is similar to the BBCEAS NO_3 based instrument described in the previous chapter. The sample cell is also based on a similar design. The high reflectivity mirrors used had a reflectivity of 99.99 % (Los Gatos) and are separated a distance of 1 meter. The transmitted light exiting the cell is refocused with a lens (1 inch diameter, f= 0.35 in) onto fiber optics attached to an SM1 converter (SM1SMA, Thorlabs) mounted onto an x-y translation stage (LM1XY, Thorlabs) leading to the combined monochramtor (SR-163, Andor Technology) and CCD (Idus, Andor Technology).

6.4 Generation of HONO

HONO was generated using the design of Febo et. al. [21]and is the same method used in the detection of HONO using CRDS[10]. An illustration of the HONO generation setup is shown in Figure 6.1. HCl gas permeated through the walls of Teflon tubing (0.2 mm thickness, ~50 cm in length) submerged in hydrochloric acid (12 M) into a stream of humidified argon carrier gas. The gas flow was directed into a temperature stabilized oven (~40 ^{o}C) housing a glass vessel containing the $NaNO_2$ powder. The $NaNO_2$ powder sits on a frit, which is a part of the design of the glass vessel. The $NaNO_2$ powder was constantly stirred using a magnetic stir bar in the glass vessel, which was placed above a magnetic stir plate. The resulting HONO generated was diluted using argon gas and introduced into the CEAS cell. A filter was placed on the outlet of the generator leading to the CEAS cell to prevent any $NaNO_2$ powder from entering the cell.

6.5 Results and Discussion

Typically, carrying out measurements of atmospheric species that absorb in the near UV is difficult because they often interfere with one another. Measuring the HONO system is a good example. The absorption cross sections for both HONO and NO_2 from 350 nm to 380 nm are shown in Figure 6.2. HONO has two strong absorption bands. One of the absorption bands lies at 354 nm with an absorption cross section of 4.9×10^{-19} cm^2/molecule and the other absorption band lies at 368 nm with an absorption coefficient of 4.4×10^{-19} cm^2/molecule. However, NO_2 has a consistent absorption of 4×10^{-19} to $6 \times x\ 10^{-19}$ cm^2/molecule sitting above the HONO absorption spectrum. From this region the peak used for monitoring HONO would be the 354 nm peak since it approaches the same cross section as NO_2 at 354 nm. In fact, this was the region probed using CRDS previously in our lab.[10] However, since the source of near UV light used in this study has a peak LED emission at 365 nm, the HONO peak best suited for measurements is the 368 nm peak. One advantage to using the 368 nm peak for HONO measurements is that it is easier to distinguish HONO from an NO_2 background because NO_2 does not peak in the same region, whereas, in the 354 nm region both HONO and NO_2 have a peak.

When measurements of the atmospheric HONO and NO_2 system is of interest, the typical concentrations for both species should be considered. Typically HONO arises in the early morning and is photolyzed quite rapidly in the presence of sunlight and can often reach concentrations of ~ 5 ppb. NO_2 can vary and often reaches concentrations as high as 80 ppb in highly polluted environments. In the early morning when HONO might

be present, typical NO_2 concentrations may be around ~40 ppb. Therefore, if ambient measurements are of interest, this typical ratio of NO_2 to HONO must be considered. For instance, Figure 6.3a illustrates the 354 nm HONO region as a model with varying NO_2 concentrations. This region is shown because of the similar magnitude cross section as NO_2. If the HONO concentration is 100 times smaller than the NO_2 concentration, then it becomes difficult to differentiate from the NO_2 absorption spectrum. This is depicted in the lower red trace of Figure 6.3a. The sum of the spectra is dominated by the NO_2 spectrum. The HONO peak becomes more evident once concentrations of HONO are a tenth of NO_2 concentrations (for instance, 5 ppb HONO and 50 ppb NO_2), which is depicted in the middle, blue trace. The upper black trace represents a spectrum when HONO concentration is a fifth of the NO_2 concentration. However, using the model it is difficult to distinguish the HONO peak from NO_2 absorption features even in the case having a high HONO concentration. Therefore, it is better to use the 368 nm peak for HONO measurements. This is shown in Figure 6.3b. The trend follows that of Figure 6.3a but in the 368 nm region. As the HONO concentration increases it is easier to distinguish between HONO and NO_2 features.

For the system of interest in this study, both the HONO and NO_2 cross section must be taken into account. The wavelength dependent absorption coefficient accounts for multiple absorbers in the same region using the equation below:

$$\alpha(\lambda) = n_{HONO} \cdot \sigma_{HONO}(\lambda) + n_{NO_2} \cdot \sigma_{NO_2}(\lambda) + a_1 \cdot \lambda + a_2\lambda^2 + a_3\lambda^3 + b \qquad \textbf{[6.2]}$$

where α is the wavelength dependent absorption coefficient, n_{HONO}, is the number density for HONO, σ_{HONO}, is the wavelength dependent cross section of HONO, n_{NO2} is the number density of NO_2, σ_{NO2} is the wavelength dependent cross section of NO_2, λ is the wavelength, and a_1, a_2, a_3 and b account for the background observed in the spectra that usually arise from fluctuations in LED intensity.

The manufacturer reflectivity data is reported to have a reflectivity of R=0.9999 at 370 nm. However, as discussed in the previous chapter, the reported reflectivity cannot be assumed because the BBCEAS set up will have more losses compared to laser based arrangements due to uncollimated stray light. To calibrate the mirror reflectivity a known absorber is used. For this absorption region NO_2 is the best standard since it is easier to handle compared to HONO and the absorption cross section is comparable. The concentration of the NO_2 used to calibrate the mirror reflectivity was 540 ppb from an NO_2 gas cylinder. The transmission spectrum is shown in Figure 6.4. The upper trace is the transmission signal without absorber, I_0, and the red lower trace is the transmission signal with 540 ppb of NO_2, I. The data is then fit to the NO_2 literature spectrum, shown in Figure 6.5. The mirror reflectivity is then extracted using the wavelength dependent BBCEAS equation. The mirror reflectivity curve is shown in Figure 6.6. The mirror reflectivity peaks at 370 nm with an R = 0.992. The peak reflectivity is constant for about ten nanometers including the region that would cover the HONO absorption peak at 368 nm. The reflectivity drops to 0.980 nm at 350 nm.

Uncertainty with the mirror reflectivity can arise from knowing the exact concentration of the NO_2 calibration gas. Over long periods of time the sample degrades, which can lower the concentration of NO_2 and, thus, the mirror reflectivity can in fact be higher than reported here. Higher reflectivity corresponds to having a lower detectable signal. If the concentration of the calibration tank of NO_2 was 400 ppb, the mirror reflectivity at 365 nm would be R = 0.995. This reflectivity would be approaching the reported reflectivity of a previous study measuring HONO using BBCEAS. By using the equation to determine the absorption coefficient the (1-R) term for the higher reflectivity (R = 0.995) would have an absorption coefficient that is approximately 1.6 times smaller than using the lower reflectivity (R = 0.992). In conclusion, the limit of detection reported here is a slight underestimation of the technique's sensitivity given a mirror reflectivity of R= 0.992.

All BBCEAS data is collected over a CCD acquisition time of 0.5 seconds over an accumulation of 240 samples for an overall integration time of 2 minutes. Figure 6.5 reflects the BBCEAS spectra obtained. The spectrum is in good agreement with the literature absorption spectrum of NO_2. The spectrum contains more noise at the region where the reflectivity of the mirrors decreases and exhibits a lower intensity output from the LED. The increased noise around the 350 to 360 nm region makes the peak HONO absorption at 368 nm the ideal region to probe HONO as opposed to using the peak HONO absorption at 354 nm. Similarly, from 380 to 400 nm the noise follows a similar trend and experiences an increased amount of noise. However, from 360 to 380 nm the

reflectivity of the mirrors is highest and the intensity of the LED is the greatest, making the 368 nm HONO peak the best peak of the HONO spectrum to monitor.

A BBCEAS spectrum of HONO is shown in Figure 6.7. The spectrum is consistent with the literature spectrum of HONO displayed in Figure 6.1. Clearly, the 354 nm and 368 nm peaks indicate that HONO is present. The HONO spectrum also has a slight NO_2 background since the Febo et. al. source produces a slight amount of NO_2 which accounts for the rising background consistent with background NO_2 absorbance. To account for the NO_2 and background, the spectrum is fit using the third order polynomial shown in equation 6.1. Figure 6.7 is a close up of view of the 368 nm HONO peak covering 364 nm to 374 nm that has been fit using equation 6.2. In Figure 6.7, the main HONO feature at 365 nm is shown in addition to NO_2 absorption features. In Figure 6.8, the red trace is the polynomial fit of the experimental spectrum. The number density extracted for the contribution from HONO is 5.0×10^{12} molecules/cm^3 (203 ppb HONO). Similarly, the contribution from NO_2 is 3.1×10^{12} molecules/cm^3 (126 ppb NO_2). Below the experimental spectrum and its fit the HONO and NO_2 contribution are shown as the dotted traces. The rising background is also shown below the spectrum in the solid black line.

HONO and NO_2 have similar cross sections in the 354 nm region (Figure 6.1). However, both the combination of low mirror reflectivity and weak LED intensity contribute to the increased noise level at that region of the BBCEAS spectrum. The 354 nm HONO peak is also used to extract concentration information and compare with the

results from the polynomial fit of HONO and NO_2 in the 365 nm region. Figure 6.9 shows the close up of the 354 nm HONO peak that has been fit to extract concentration information. The red trace is the polynomial fit of the experimental spectrum. The fit calculates that the contribution from HONO is 3.80×10^{12} molecules/cm^3 (150 ppb HONO). The contribution from NO_2 in the spectrum is 2.35×10^{12} molecules/cm^3 (100 ppb). The individual HONO and NO_2 spectra are shown below (dotted trace) along with the rising background (solid line).

The fit of the 368 nm peak yields a concentration for both HONO and NO_2 that is approximately 20 % higher than the concentration for both HONO and NO_2 at the 354 nm region. One potential source for the discrepancy between the two fits could be that the mirror reflectivity is slightly worse in the 354 nm region than reported. Based on the calibrated reflectivity curve the reflectivity at 354 nm is R=0.984. However, the reflectivity should be R=0.98 in the 354 nm region to have a similar concentration obtained from the fitting at around 368 nm. The reasoning for the discrepancy is that the intensity of the LED at around 354 nm decreases significantly compared to the peak emission at 365 nm. In addition, the high reflectivity region of the mirrors also tails off at around 354 nm. The low intensity overlapped with a lower reflectivity means that any mis-alignment of the mirrors will become magnified in this region. In other words, more light will leak out of the cavity and there will be fewer reflections within the cavity which corresponds to having a lower calibrated mirror reflectivity. This results in a shorter effective pathlength and a smaller enhancement signal and would explain why the peak height at 354 nm is slightly smaller than the 368 nm peak. However, when future

measurements are carried out, the 368 nm peak will be chosen over the 354 nm region because of the higher signal to noise ratio from higher LED output and higher mirror reflectivity.

To obtain a limit of detection for HONO using the 368 nm peak, the residual noise from the polynomial fit to the experimental data is used. The residuals correspond to a limit of detection of 10 ppb (1σ)/ 2 minutes of integration for HONO (not shown). Previous measurements of HONO using BBCEAS have reported a limit of detection of 0.13 ppb over an integration time of 10 minutes using a pathlength of 4 meters. In the study only the 368 nm HONO region was used for measurements. A longer integration time of 10 minutes using this instrumental setup should improve the limit of detection by approximately 2 times taking into account an improvement in the signal by $1/\sqrt{N}$. Further improvements in sensitivity can be achieved if the mirror reflectivity is in fact higher than reported here. Increasing the length of the cavity to 4 meters should also increase the sensitivity. Again, if the NO_2 calibration sample is 400 ppb this would correspond to a reflectivity around R=0.9995 and would further improve the sensitivity by 2 fold. Accounting for these improvements the sensitivity can be as low as 1.25 ppb HONO at 368 nm.

6.6 Conclusion

In this study, BBCEAS is demonstrated to be a method capable of measuring HONO and NO_2 in the near UV region. The instrument is best suitable for higher

concentration laboratory experiments or environmental chamber studies. A potential system that this instrument would be ideal to provide more insights would be heterogeneous hydrolysis of NO_2 experiments. The broadband nature of the device allows for multiple absorbers to be probed simultaneously. A third order polynomial fit is used to extract concentration information for both HONO and NO_2. This technique can also extend to measure HONO using the 354 nm peak. The concentration extracted from the 368 nm peak is compared to the HONO peak at 354 nm. Discrepancies were present in the concentration reported with the concentration of HONO and NO_2 in the 365 nm region being twice that of the 365 nm region. This is most likely due to a reduced mirror reflectivity in that region. A limit of detection of 10 ppb/2 minutes (1σ) using the 368 nm HONO peak is proposed with the potential to improve sensitivity with longer integration times, longer cell pathlength, and a higher mirror reflectivity.

The demonstration of near UV BBCEAS experiments will lead to the future development of deep UV BBCEAS instruments capable of measuring atmospheric pollutants such as SO_2. As was discussed in chapter 3, SO_2 exhibits strong absorption bands in the deep UV region. Recently, high powered UV LEDs have become available and would provide the incoherent light needed for BBCEAS analysis of atmospheric species extending in this region. This could potentially provide an inexpensive and portable analyzer for SO_2.

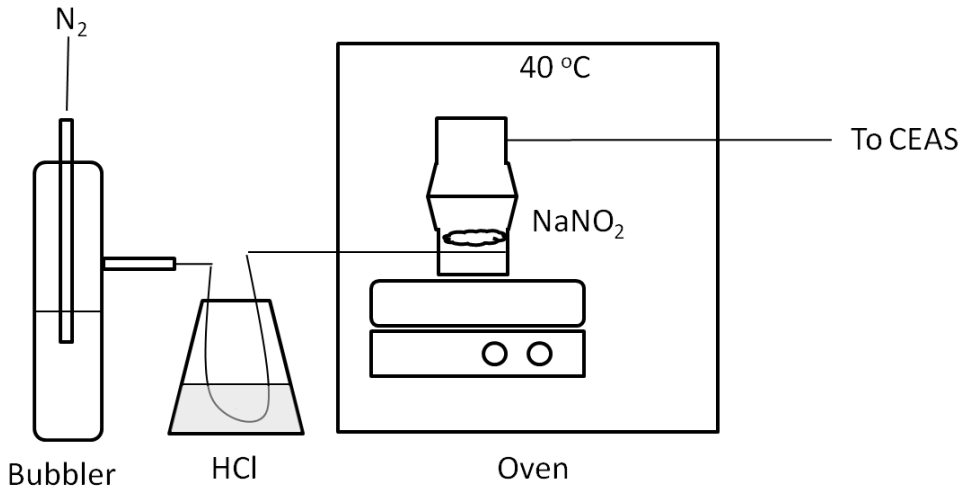

Figure 6.1: Illustration of the HONO generation setup. HONO is generated based on the Febo et. al. method. Nitrogen is introduced into a bubbler containing water to provide humidified air, which flows into an Erlenmeyer flask containing HCl. The HCl is transferred into the air stream through the semipermeable tubing and reacts with $NaNO_2$ in the glass vessel held at a constant temperature of 40 ^{o}C to generate HONO.

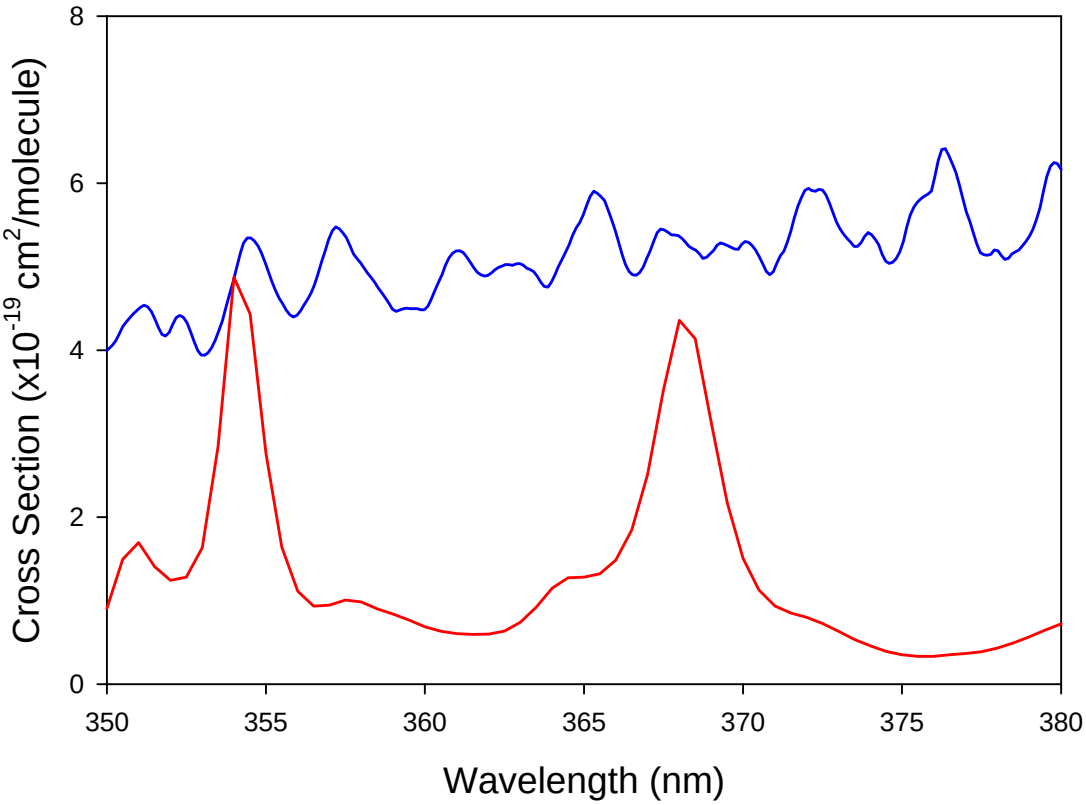

Figure 6.2: Cross section data of HONO (red) and NO_2 (blue) in the region of interest. HONO exhibits a peak at 354 nm and 358 nm.

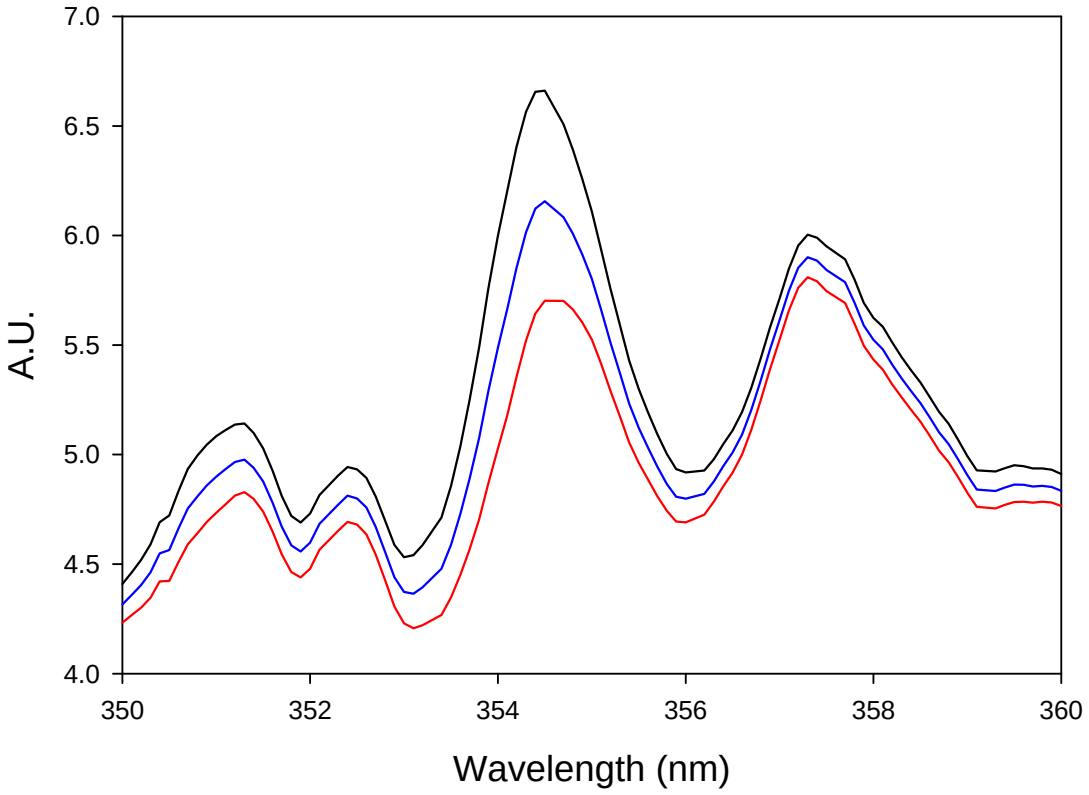

Figure 6.3a: Model of overlapping HONO and NO_2 signal at varying concentrations at around 354 nm. The red trace represents a spectrum when the NO_2 concentration is 100 times larger than HONO. The blue trace represents NO_2 at 10 times higher concentration than HONO and the black trace represents NO_2 at 5 times the concentration of HONO.

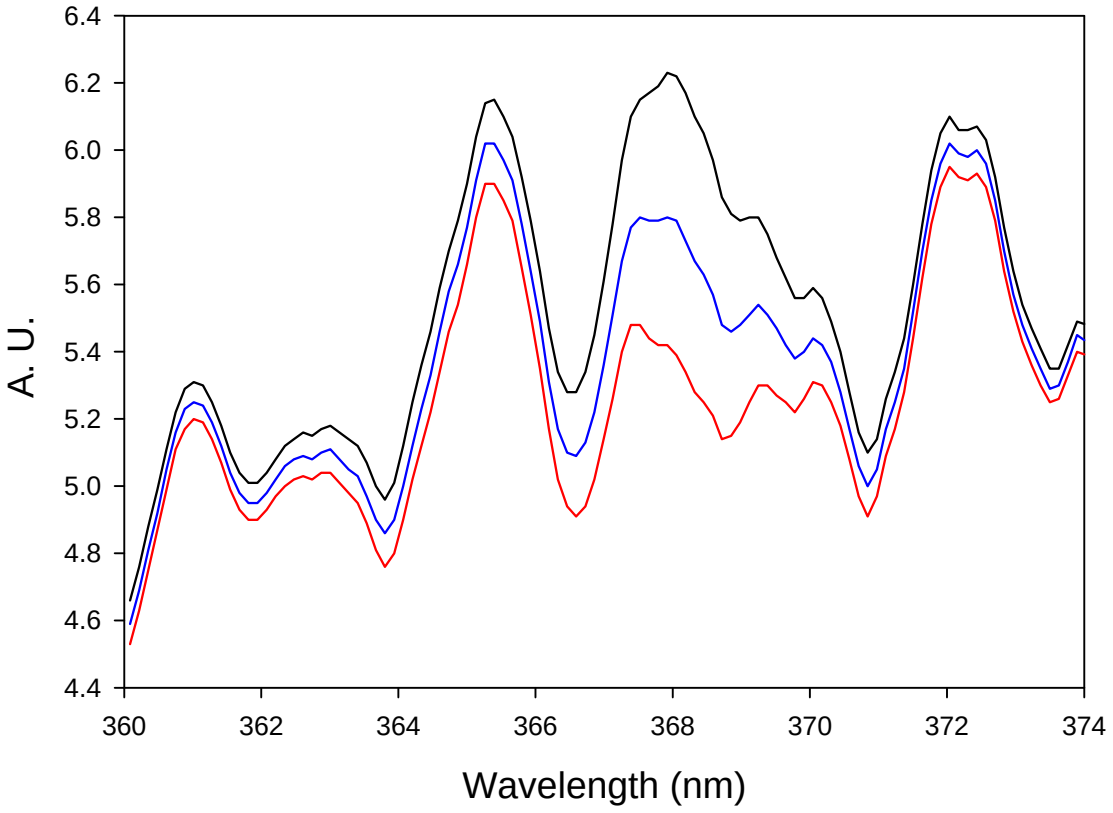

Figure 6.3b: Model of overlapping HONO and NO_2 signal at varying concentrations at around 368 nm. The red trace represents a spectrum when the NO_2 concentration is 100 times larger than HONO. The blue trace represents NO_2 at 10 times higher concentration than HONO and the black trace represents NO_2 at 5 times the concentration of HONO.

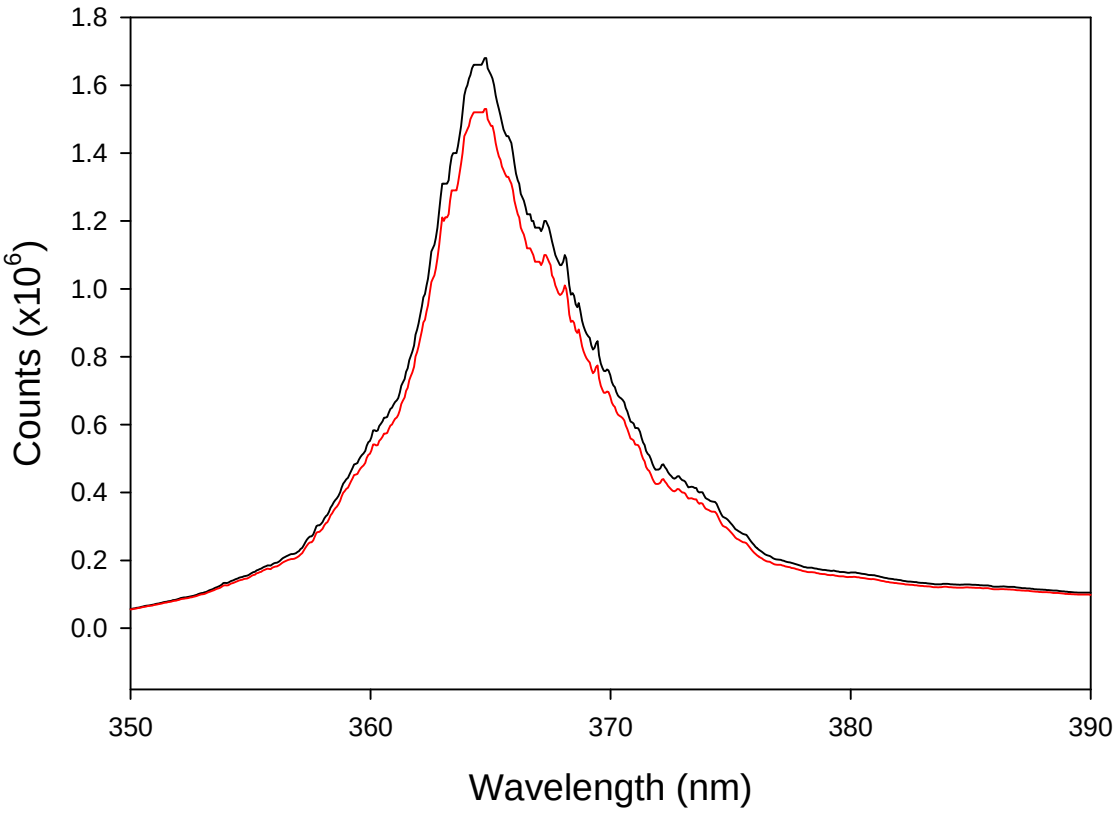

Figure 6.4: BBCEAS transmission spectrum without NO_2 absorber is depicted in the black trace and with 540 ppb NO_2 present in the cell in the red trace.

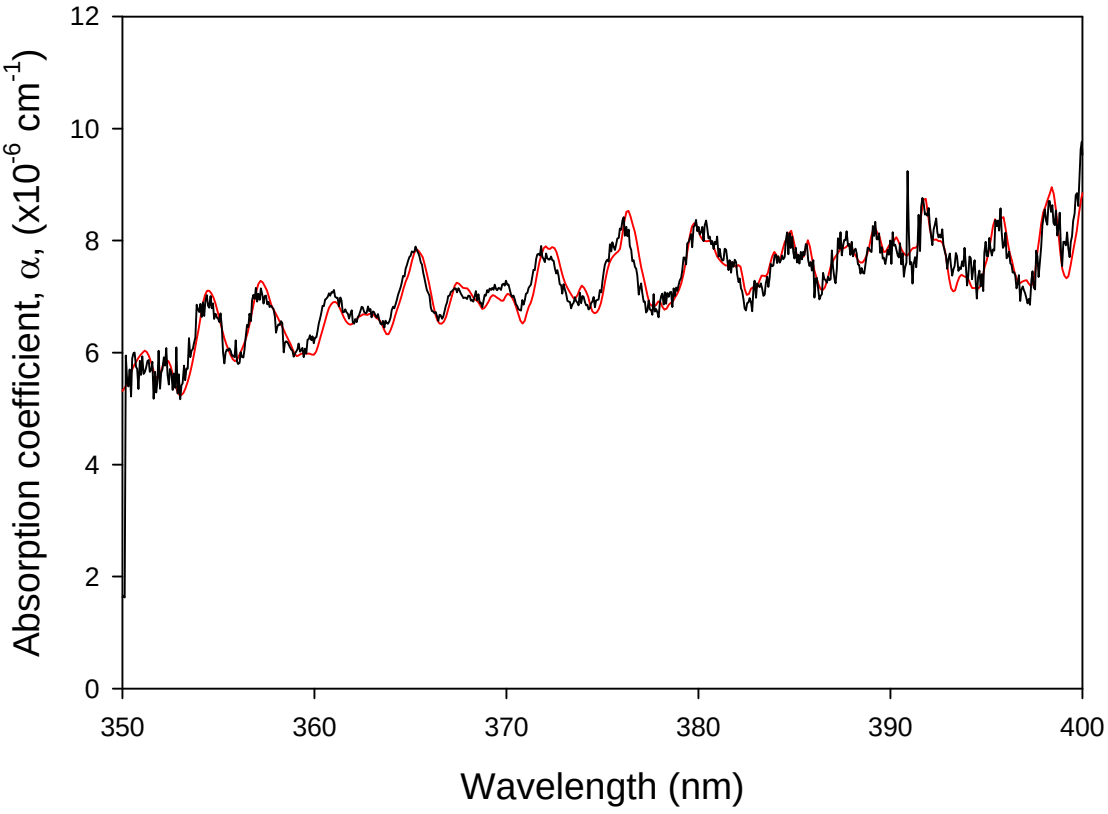

Figure 6.5: NO_2 overlap spectrum. 540 ppb of NO_2 is overlapped with reference NO_2 spectrum. The spectrum is used to extract mirror reflectivity data. Increased noise from 350 nm to 360 nm and 380 nm to 400 nm is a result of lower mirror reflectivity and lower LED intensity.

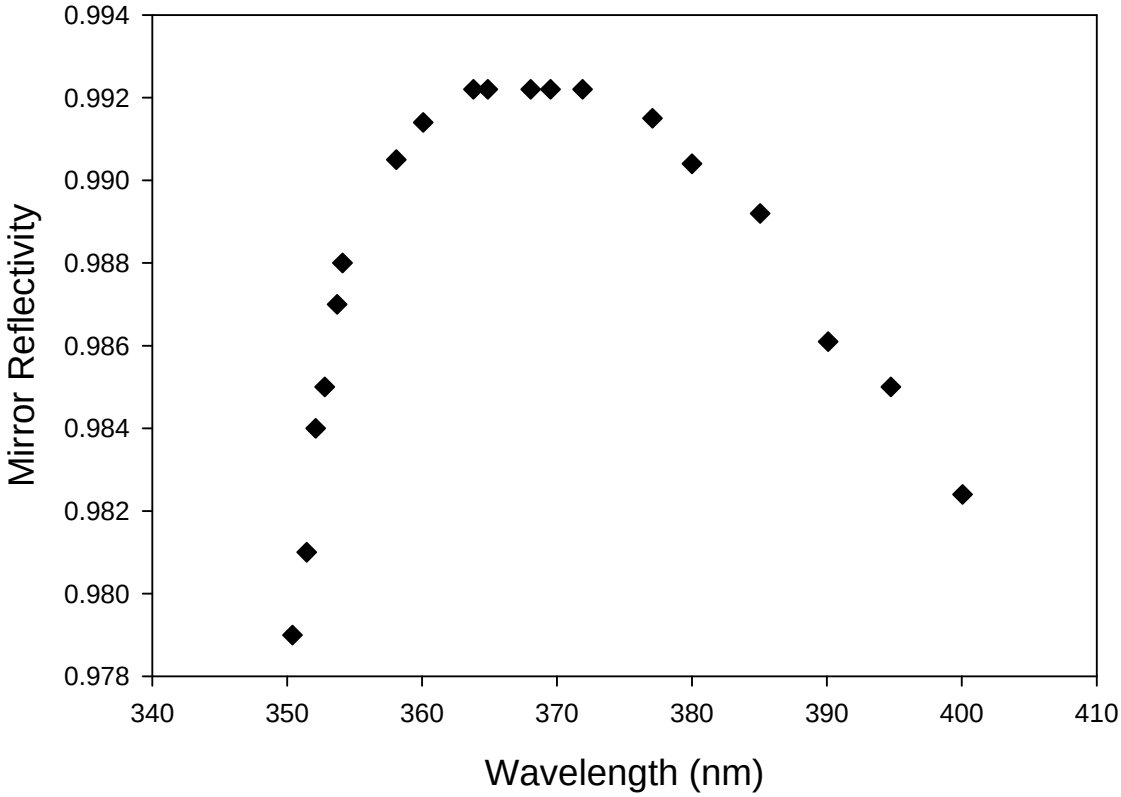

Figure 6.6: Mirror reflectivity curve. The points are extrapolated from fitting the NO_2 literature spectrum with 600ppb NO_2 calibration gas. The peak reflectivity in the region of interest 368 nm is R=0.992.

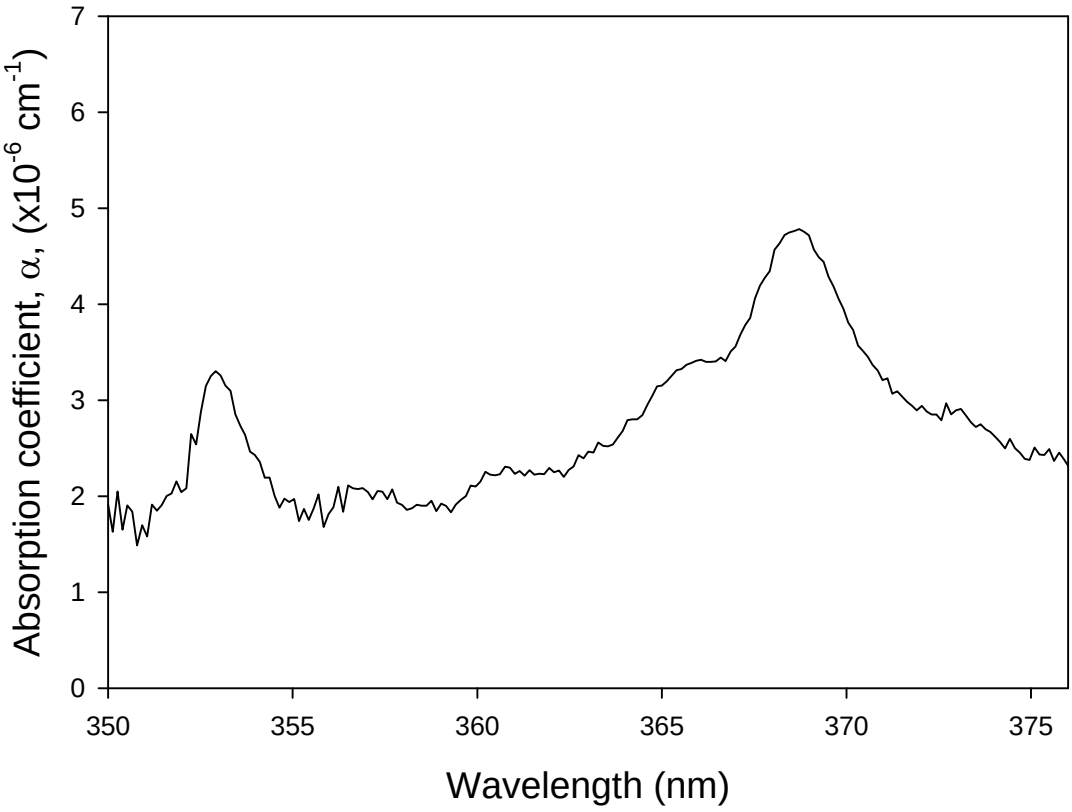

Figure 6.7: BBCEAS spectrum of HONO produced from the Febo et. al. reaction. The concentration of HONO is 203 ppb. HONO has two absorption peaks between 350 nm and 375 nm, the 354 nm peak and the 368 nm peak. The spectrum of HONO sits on an NO_2 background.

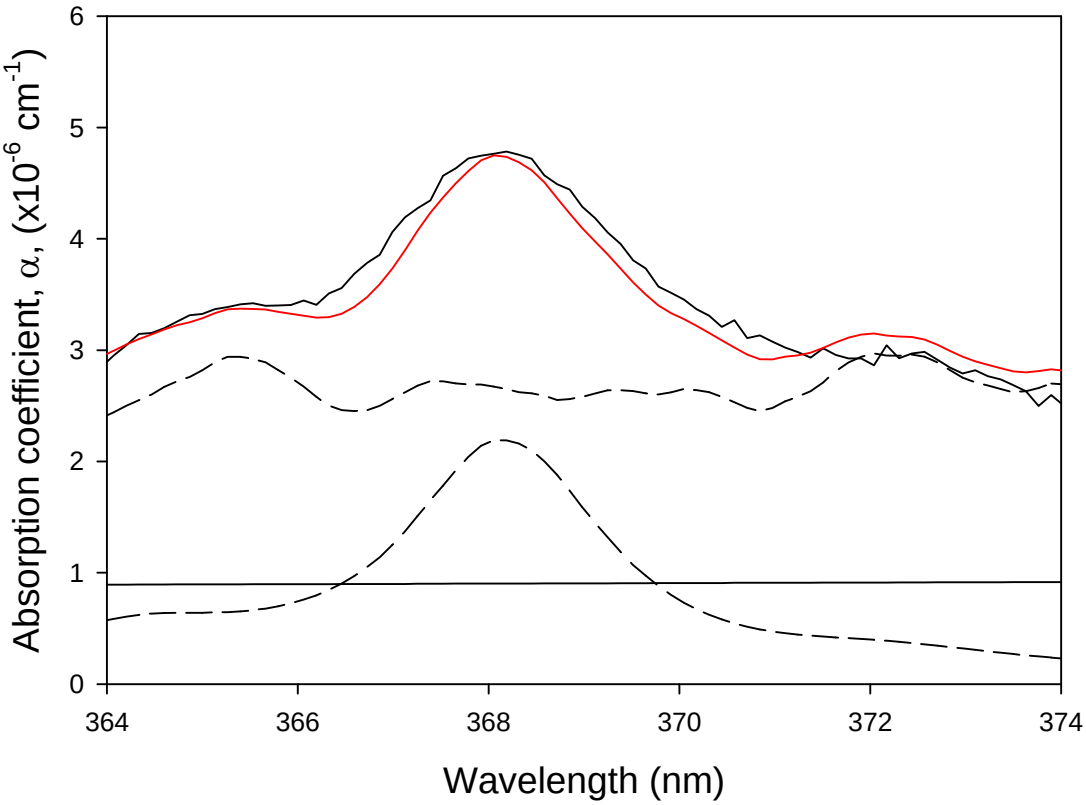

Figure 6.8: Simultaneous measurement of HONO and NO_2 using BBCEAS (black trace) is fit using a third order polynomial (red trace). The HONO and NO_2 contribution to the experimental spectrum are depicted in the dotted traces. The background is shown as the black line.

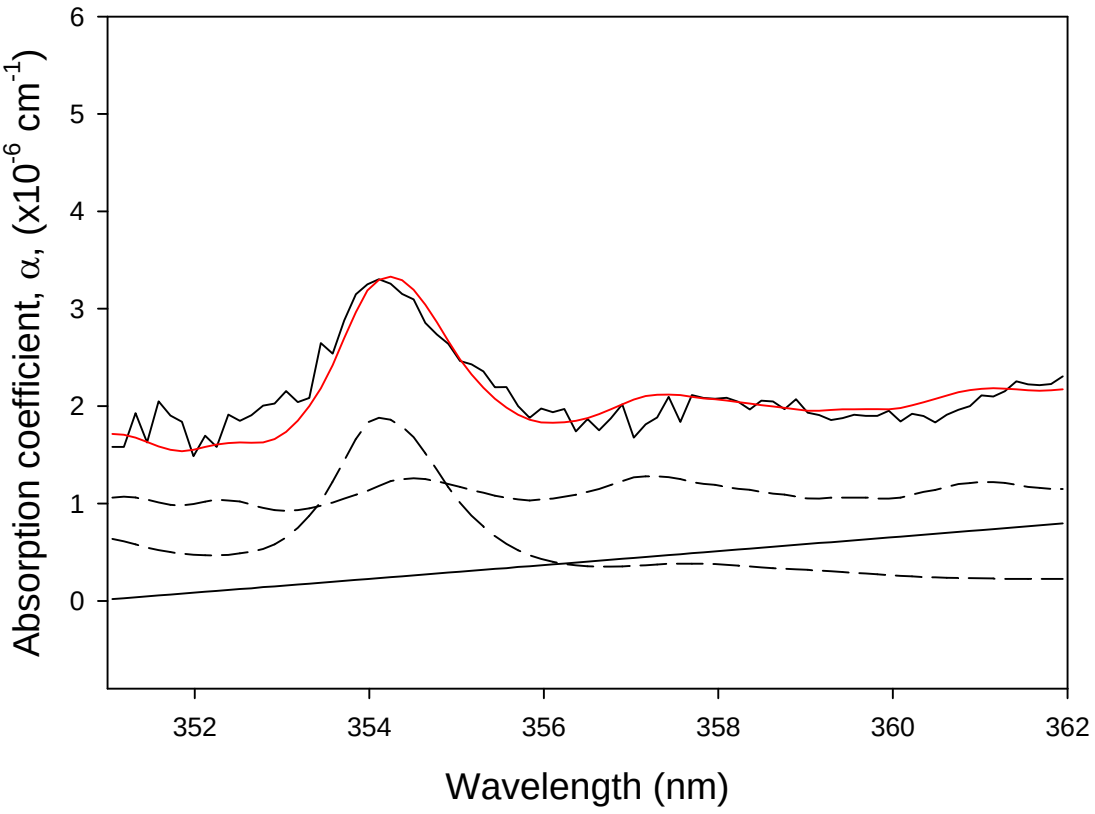

Figure 6.9: Simultaneous measurements of HONO and NO_2 using BBCEAS in the 354 nm region (black trace) is fit using a third order polynomial (red trace). The HONO and NO_2 contribution is shown in the dotted trace and the overall background observed is the straight black line.

6.7 References

1. Finlayson-Pitts, B. J.; Pitts, J. N., *Chemistry of the Upper and Lower Atmosphere*. Academic Press: 2000.

2. Pitts, J. N.; Grosjean, D.; Vancauwenberghe, K.; Schmid, J. P.; Fitz, D. R., Photo-oxidation of aliphatic-amines under simulated atmospheric conditions-formation of nitrosamines, nitramines, amides, and photo-chemical oxidant. *Environ. Sci. Technol.* **1978,** *12* (8), 946-953.

3. Platt, U.; Perner, D.; Harris, G. W.; Winer, A. M.; Pitts, J. N., Observations of nitrous-acid in an urban atmosphere by differential optical-absorption. *Nature* **1980,** *285* (5763), 312-314.

4. Finlayson-Pitts, B. J.; Wingen, L. M.; Sumner, A. L.; Syomin, D.; Ramazan, K. A., The heterogeneous hydrolysis of NO_2 in laboratory systems and in outdoor and indoor atmospheres: An integrated mechanism. *Phys. Chem. Chem. Phys.* **2003,** *5* (2), 223-242.

5. Ramazan, K. A.; Syomin, D.; Finlayson-Pitts, B. J., The photochemical production of HONO during the heterogeneous hydrolysis of NO_2. *Phys. Chem. Chem. Phys.* **2004,** *6* (14), 3836-3843.

6. Ramazan, K. A.; Wingen, L. M.; Miller, Y.; Chaban, G. M.; Gerber, R. B.; Xantheas, S. S.; Finlayson-Pitts, B. J., New experimental and theoretical approach to the heterogeneous hydrolysis of NO_2: Key role of molecular nitric acid and its complexes. *J. Phys. Chem. A* **2006,** *110* (21), 6886-6897.

7. Winer, A. M.; Biermann, H. W., Long pathlength differential optical-absorption spectroscopy (DOAS) measurements of gaseous HONO, NO_2 and HCHO in the California south coast air basin. *Res. Chem. Intermed.* **1994,** *20* (3-5), 423-445.

8. Febo, A.; Perrino, C.; Allegrini, I., Measurement of nitrous acid in Milan, Italy, by DOAS and diffusion denuders. *Atmos. Environ.* **1996,** *30* (21), 3599-3609.

9. Stutz, J.; Oh, H. J.; Whitlow, S. I.; Anderson, C.; Dibbb, J. E.; Flynn, J. H.; Rappengluck, B.; Lefer, B., Simultaneous DOAS and mist-chamber IC measurements of HONO in Houston, TX. *Atmos. Environ. 44* (33), 4090-4098.

10. Wang, L. M.; Zhang, J. S., Detection of nitrous acid by cavity ring down spectroscopy. *Environ. Sci. Technol.* **2000,** *34* (19), 4221-4227.

11. Rodgers, M. O.; Davis, D. D., A uv-photofragmentation laser induced fluorescence sensor for the atmospheric detection of HONO. *Environ. Sci. Technol.* **1989,** *23* (9), 1106-1112.

12. Ferm, M.; Sjodin, A., A sodium-carbonate coated denuder for determination of nitrous acid in the atmosphere. *Atmos. Environ.* **1985,** *19* (6), 979-983.

13. Heland, J.; Kleffmann, J.; Kurtenbach, R.; Wiesen, P., A new instrument to measure gaseous nitrous acid (HONO) in the atmosphere. *Environ. Sci. Technol.* **2001,** *35* (15), 3207-3212.

14. Kanda, Y.; Taira, M., Chemiluminescent method for continuous monitoring of nitrous-acid in ambient air. *Anal. Chem.* **1990,** *62* (19), 2084-2087.

15. Fiedler, S. E.; Hese, A.; Ruth, A. A., Incoherent broad-band cavity-enhanced absorption spectroscopy. *Chem. Phys. Lett.* **2003,** *371* (3-4), 284-294.

16. Langridge, J. M.; Ball, S. M.; Jones, R. L., A compact broadband cavity enhanced absorption spectrometer for detection of atmospheric NO2 using light emitting diodes. *Analyst* **2006,** *131* (8), 916-922.

17. Langridge, J. M.; Ball, S. M.; Shillings, A. J. L.; Jones, R. L., A broadband absorption spectrometer using light emitting diodes for ultrasensitive, in situ trace gas detection. *Review of Scientific Instruments* **2008,** *79* (12).

18. Ball, S. M.; Langridge, J. M.; Jones, R. L., Broadband cavity enhanced absorption spectroscopy using light emitting diodes. *Chem. Phys. Lett.* **2004,** *398* (1-3), 68-74.

19. Triki, M.; Cermak, P.; Mejean, G.; Romanini, D., Cavity-enhanced absorption spectroscopy with a red LED source for NOx trace analysis. *Appl. Phys. B-Lasers Opt.* **2008,** *91* (1), 195-201.

20. Gherman, T.; Venables, D. S.; Vaughan, S.; Orphal, J.; Ruth, A. A., Incoherent broadband cavity-enhanced absorption spectroscopy in the near-ultraviolet: Application to HONO and NO_2. *Environ. Sci. Technol.* **2008,** *42* (3), 890-895.

21. Febo, A.; Perrino, C.; Gherardi, M.; Sparapani, R., Evaluation of a high purity and high-stability continuous generation system for nitrous acid. *Environ. Sci. Technol.* **1995,** *29* (9), 2390-2395.

Chapter 7

Conclusion

Cavity ring-down spectroscopy (CRDS) and broadband cavity enhanced absorption spectroscopy (BBCEAS) are two useful methods based on absorption spectroscopy for measuring compounds important to the atmosphere. Three species measured using the cavity enhanced methods developed in the laboratory include SO_2, NO_3, and HONO. All three species play a major role in atmospheric pollution in major urban areas.

Emissions of SO_2 can pose a health risk to the population in urban areas because it is a known irritant. SO_2 can also be oxidized to harmful aerosol sulfate, which can contribute to negative feedback, or a net cooling effect on climate. Deposition of the aerosol sulfate contributes to increased acidity to the ecosystem and the formation of sulfate particulates is directly related to mortality rates. The technique used to measure SO_2 was based on CRDS in the UV region (308 nm). The atmosphere is known to have other major atmospheric pollutants that absorb in the UV region and can act as interfering species. Thus, the ferrous sulfate scrubber and a sodium carbonate denuder were used to reduce these interfering species and obtain quantitative measurements of SO_2. A limit of detection of 3.5 ppb/10 s (S/N =2) is demonstrated. SO_2 concentrations are typically higher in the eastern part of the United States than the sampling site (Riverside, CA) in

this study. As a result, ambient measurements indicate that the technique is best suited for more polluted environments. The low ambient concentrations of SO_2 are an indicator of the progress made with having stricter regulations on emissions imposed by the government over the last few decades. With some improvements in the instrumental set up including higher reflectivity mirrors, better mode matching of the laser coupled into the cavity, and incorporating a detector that is sensitive in the UV region could improve the sensitivity to compete with commercial SO_2 analyzers. Future advances in using multi reflection cells for absorption measurements include the development of an LED based CEAS spectrometer for SO_2 measurements. Advances in LED's in the deep UV region can extend cavity enhanced absorption measurements for SO_2. This would be potentially an inexpensive portable device used to measure trace SO_2 levels in the atmosphere and could compete with the commercial PFA.

The nitrate radical, NO_3, is the major oxidizing species found in the nighttime air. To study this major atmospheric pollutant, a new instrument based on broadband cavity enhanced absorption spectroscopy (BBCEAS) was developed for our lab. In this BBCEAS set up, an inexpensive, high powered LED was used to provide the broadband light and a CCD is used as the detector, which allow for analysis of multiple absorbers within the same region. A sensitivity of 40 ppt/2 min was achieved for NO_3 using BBCEAS. This sensitivity is approaching ambient levels but is best suited for environmental chambers where the concentration of NO_3 is typically higher. Measurements to demonstrate the technique's capabilities were carried out in a large (90 m^3) environmental chamber located at CE-CERT. The instrument was characterized

with the chamber reaction of NO_2 with ozone to generate NO_3, N_2O_5 was then spiked into the chamber, followed by the introduction of isoprene to eliminate any signal due to NO_3. The reaction of NO_3 with an amine is also shown to demonstrate the NO_3 BBCEAS method. Additionally, ambient measurements were attempted but the spectrum was dominated by water absorption features and no ambient NO_3 was visible.

Finally, measurements of HONO in the near UV were obtained using a UV LED and BBCEAS. HONO is a major source of the hydroxyl radical in the early morning and is the main daytime oxidizing species. Additionally, experiments leading to further insights into the formation of HONO are of interest. A limit of detection of 10 ppb (1σ) over an integration time of 2 minutes was proposed using the HONO absorption at 368 nm. This limit of detection makes the technique more suitable for studies in an environmental chamber. Longer integration times can improve detection sensitivities to those approaching ambient levels. Heterogeneous hydrolysis experiments could eventually be performed to gain further insights to the formation of HONO due to the techniques capability of measuring HONO and NO_2 simultaneously. This was demonstrated from the generation of HONO using a HONO generation system, which also contained some NO_2. Further improvements on sensitivity can be achieved with a higher mirror reflectivity, a longer pathlength, and longer integration times.

Overall, absorption spectroscopy using high finesse cavities (CRDS and CEAS) is a relatively simple technique to employ in the monitoring of atmospheric pollutants in laboratory studies, environmental chambers, and potentially ambient measurements.

Background interfering species can be eliminated by the denuder and scrubber method, titration, or by fitting the spectra obtained with cross section data. Having techniques that can provide insightful data in atmospheric processes can lead to a better understanding of the atmospheric system, which can eventually extend to environmental policy.